

DESIGN ASPECTS AND PERFORMANCE CHARACTERISTICS
OF RADIAL FLOW ENERGY DISSIPATORS

by

Khosrow Meshgin
Walter L. Moore

Research Report Number 116-2F

Performance of Circular Culverts on Steep Grades
Research Project 3-5-69-116

conducted for

The Texas Highway Department

in cooperation with the
U. S. Department of Transportation
Federal Highway Administration

by the

CENTER FOR HIGHWAY RESEARCH
THE UNIVERSITY OF TEXAS AT AUSTIN

PREFACE

The research work presented herein is the final report on Research Project No. 3-5-69-116, entitled "Performance of Circular Culverts on Steep Grades - Part III Exploratory Study of Energy Dissipator for Culvert Outlets." The authors wish to thank the Texas Highway Department and the U. S. Department of Transportation Federal Highway Administration for providing financial support, and The University of Texas Center for Highway Research for providing general assistance and advice. Special thanks go to Messrs. Samuel V. Fox, William J. Dallas, and Frank Johnson, staff members of THD and the Federal Highway Administration, who showed a continuing interest in the project throughout its duration. The authors wish to express their sincere appreciation to Dr. Frank D. Masch, Dr. Carl W. Morgan, Dr. E. Gus Fruh, and Dr. Paul A. Jensen, faculty members, The University of Texas at Austin, for their comments and critical review of the manuscript.

Special thanks go to Mr. Edward H. Bruce for his laboratory assistance and model construction. Sincere thanks is expressed to Engineering students Messrs. Phillip C. Cook, Emede Garcia, and Carlos Vargas for data collection and reduction, and for drafting assistance. Special acknowledgment is due to Mrs. Patricia L. Harris for typing and proof-reading the final manuscript. Finally appreciation is expressed to all individuals and agencies who were instrumental in the preparation and completion of this report.

The opinions, findings, and conclusions expressed in this publication are those of the authors and not necessarily those of the Federal Highway Administration.

Khosrow Meshgin
Walter L. Moore

ABSTRACT

The present investigation was undertaken to explore the feasibility and performance characteristics of a radial flow basin for use as a flow energy dissipator, and to develop design concepts applicable to highway culverts. The radial flow energy dissipator incorporated a vertically curved drop section which induced radial supercritical flow in a rapidly flared basin where an arc of a circular hydraulic jump was formed. High pressures were developed when the flow impinged on the beginning of the basin floor, thus forcing the flow to spread laterally and stay in contact with the flared wingwalls of the stilling structure.

Experimental investigations indicated the effectiveness of the radial flow energy dissipator in stabilizing the jump, reducing the energy of high-velocity flow, and spreading the flow within the basin. The sensitivity of the performance characteristics of the structure to variations in such parameters as the flaring angle of wingwalls, the ratio of the width of downstream channel to the culvert diameter, and the height of the drop from the culvert outlet to the horizontal basin floor were explored. Furthermore, the adaptability of the dissipator to rectangular as well as trapezoidal downstream channel was investigated.

Based on the experimental results and a semi-analytical treatment of the hydraulic characteristics of the radial flow basin a design procedure was developed which may be followed for the selection of the important dimensions of a radial flow dissipator under a given set of field conditions. A simplified form of the circular hydraulic jump equation was obtained which was the basis for the design procedure.

SUMMARY

This fourth report dealing with a new type energy dissipator for use at highway culvert outlets includes laboratory measurements of the hydraulic performance of the dissipator as well as concepts developed for the design of the culvert and dissipator using the new concept.

The dissipator uses basic physical principles in a new way to cause the flow from a relatively narrow culvert to be spread in width as it passes through the structure. The flow can be released at a depth and width corresponding closely with that of the downstream channel. The resulting reduction in potential for concentrated local scour that often occurs at culvert outlets will reduce or eliminate the need for expensive maintenance that often occurs at such locations. The stilling basin contains no obstructions which might catch debris or drift and clog the structure.

General concepts and procedures are described for determining the geometric design of the structure, but at the present time this requires a rather high level of competence in hydraulic theory and designs.

IMPLEMENTATION STATEMENT

The investigation has shown that the principle of the circular hydraulic jump can be incorporated into an energy dissipator for culvert outlets to produce a structure that appears to be practical and to have certain advantages over other types of energy dissipators. Its principle advantages are:

1. The relatively narrow flow as confined by the culvert can be spread to a width that is compatible with the downstream channel.
2. The radial flow between the flared walls of the stilling basin, which results in the formation of a segment of a circular hydraulic jump, provides stability of the jump over a range of tailwater elevations.
3. The structure is open at the top and has no barriers to catch drift or debris and clog the structure.

A one-third scale model of the radial flow energy dissipator designed for a four by four-foot box culvert operated satisfactorily and gave some confidence that the concepts and procedures developed for the design of the structure are valid. In order to implement the knowledge developed by the research, the following steps should be taken:

1. A site for a field installation should be selected and a structure carefully designed according to the principles developed. In building the field installation, provision should be made for gaining information about the performance

of the structure without the necessity of having an observer on the spot. For example, several piezometers located in the bottom along the centerline of the structure could be connected to transparent manometer wells treated with cork dust to record the maximum stage. A periodic check of these manometers would indicate the water levels obtained within the structure. Another suggestion would be to construct a longitudinal trench one or one-half foot wide and two to three feet deep immediately downstream from the structure and fill it with layers of materials selected to have increasing resistance to the scour. Periodic observations of this trench would indicate the degree of scour protection achieved by the structure.

2. The design procedures should be examined more carefully and more specific directions prepared so the structures can be designed by personnel with more limited hydraulic experience.
3. An economic study should be made to compare the total cost of the culvert dissipator system proposed here with that of alternate types of designs.
4. Under some situations it may be desirable to lead the flow from a short culvert under the highway into an open trapezoidal chute leading to an energy dissipation structure near the bottom of the embankment slope. For these conditions, it will be necessary to explore methods for utilizing the radial flow energy dissipator with the flow entering from a trapezoidal upstream channel.

It is believed that the employment of the type of energy dissipator developed here will result in reduced maintenance expense for correcting problems of local scour at culvert outlets and may result in less total cost for the culvert dissipator combination than experienced for other types of designs.

TABLE OF CONTENTS

	Page
PREFACE.	ii
ABSTRACT	iii
SUMMARY.	iiia
IMPLEMENTATION STATEMENT	iiib
LIST OF ILLUSTRATIONS.	vi
GLOSSARY OF SYMBOLS.	viii
CHAPTER 1 INTRODUCTION	1
Objective	2
Scope of Investigation.	3
CHAPTER 2 ENERGY DISSIPATION	5
Height and Length of Hydraulic Jump	5
Location of Hydraulic Jump.	7
Conjugate Depths for Different Channel Shapes	8
Energy Losses in Hydraulic Jump	12
Existing Energy Dissipators	13
Drop Structure - Stilling Basins	13
UngROUTED Rock - Lined Depression.	13
Bucket Type Dissipators.	15
Impact Type Energy Dissipators	18
Saint Anthony Fall Basin	20
Radial Flow Dissipator	22
Development of Radial Flow Surface Curve Equation	25

	Page
CHAPTER 3	
MODEL CONSTRUCTION AND EXPERIMENTAL RESULTS.	29
Model Construction.	29
Experimental Procedure.	35
Limiting Froude Number F_t for Valid Experimentation . . .	42
Rectangular Downstream Channel.	45
Stability of the Hydraulic Jump.	45
Velocity Distribution and Reduction.	52
Water Surface Profile.	68
Trapezoidal Downstream Channel.	74
Stability of the Hydraulic Jump.	76
Velocity Distribution and Reduction.	81
Water Surface Profile.	88
CHAPTER 4	
DESIGN PROCEDURE FOR PROTOTYPE RADIAL FLOW DISSIPATORS.	90
Hydraulic Design of Culverts.	91
Width, Height, and the Radius of Curvature of Entrance Channel	92
Stilling Basin Dimensions	101
CHAPTER 5	
CONCLUSIONS.	114
BIBLIOGRAPHY	118
APPENDICES	120

LIST OF ILLUSTRATIONS

Figure No.	Title	Page
2-1	Definition Sketch for the Circular Jump.	11
2-2	Vertical Drop Basin.	14
2-3	Solid Roller Bucket Type Basin	16
2-4	Slotted Roller Bucket.	17
2-5	Bradly-Peterka Basin	19
2-5	Contra-Costa Energy Dissipator	19
2-7	S. A. F. Stilling Basin.	21
2-8	Radial Flow Energy Dissipator.	23
3-1	Schematic Layout of Model with Trapezoidal Downstream Channel.	30
3-2	Sectional View of Rectangular Channel Basin.	32
3-3	Sectional View of Trapezoidal Channel Basin.	33
3-4	Photographic View of Entrance Channel and Stilling Basin Layout for Trapezoidal Downstream Channel.	37
3-5	Location of Velocity Measurements for Rectangular and Trapezoidal Channels	40
3-6	Location of Water Surface Measurements in Rectangular Channel for $\theta = 30^\circ$ and $\theta = 22.5^\circ$	41
3-7	Froude Number F_t vs. Pressure.	43
3-8 to 3-11	Plot of y_2/y_t vs. x/y_t for REC Arrangements.48 - 51
3-12	Plot of y_2/y_t vs. F_t for Arrangement REC 3	53
3-13 to 3-24	Velocities in Downstream Channel for REC Arrangements55 - 66
3-25 to 3-28	Water Surface Profile of Flow for REC Arrangements70 - 73

Figure No.	Title	Page
3-29	Water Surface Profile of Flow Along the Centerline of Trapezoidal Downstream Channel (Arr. TRAP 1, 2)	77
3-30	Water Surface Profile of Flow Along the Centerline of Trapezoidal Downstream Channel (Arr. TRAP 4)	78
3-31	Water Surface Profile of Flow Along the Centerline of Trapezoidal Downstream Channel (Arr. TRAP 5)	79
3-32 to 3-36	Velocities in Downstream Channel for TRAP Arrangements	82 - 86
4-1	Schematic Representation of Culvert Installation and Dissipating Structure.	94
4-2	A Typical Dissipating Structure with Trapezoidal Downstream Channel Indicating Flow Variables	97
4-3	Graph of F_t vs. y_t/R	100
4-4	Plot of y_o vs. F_1	103
4-5	Graph of m vs. r_o	106
1A	Flow Chart for Program Cube.	123
1B	Typical Highway Culvert Installation and Energy Dissipator	126
2B	Radial Flow Stilling Basin - Plan View	130
3B	Radial Flow Stilling Basin - Elevation View.	131
4B	View of the Transitional Section and the End Sill.	132
5B	Photographic View of the Model at Balcones Center.	139
6B	Relative Velocity Pattern in Downstream Channel.	142

GLOSSARY OF SYMBOLS

a_r	Normal component of acceleration directed toward the center of curvature
a'	Projected length of the edge of triangular converging walls on a horizontal plane
A_c	Critical cross sectional area of flow
A_1	Cross sectional area of flow before the jump
A_2	Cross sectional area of flow after the jump
b	Width or diameter of culvert, also width of entrance channel
b'	Average width of channel or culvert
B	Bottom width of the downstream channel
c	Base length of triangular converging walls, also a constant
C	Chezy coefficient
D	Circular pipe diameter
D_s	Hydraulic depth on end sill
E	Specific energy of flow
E_L	Energy loss through hydraulic jump
E_1	Energy of flow upstream of hydraulic jump
F	Froude number in a channel
F_{pt}	Froude number at the point of tangency of entrance channel
F_t	Froude number at the top of entrance channel
F_1	Froude number before hydraulic jump
g	Acceleration of gravity
h	Piezometric head
h_j	Height of hydraulic jump

H	Height of drop in drop structure stilling basin
H_L	Transitional loss from the radial flow basin to the downstream channel
H_s	Height of end sill
K	Proportionality constant
K_1'	Proportion of the depth of flow to the center of gravity before the jump
K_2'	Proportion of the depth of flow to the center of gravity after the jump
L_j	Length of the jump
L	Length of the stilling basin
L_x	Distance along the centerline of channel from the leading edge of the jump to the section of velocity measurement
m	Slope of the curves of y_0 vs. F_1
n	Manning coefficient
p/γ	Pressure head on flow media
p_2/γ	Pressure head on the bed of entrance channel
$P_{s1,2}$	Hydrostatic pressure forces acting on the sides of a segment of circular jump
P_1	Hydrostatic pressure force acting on the upstream section of a segment of circular jump
P_2	Hydrostatic pressure force acting on the downstream section of a segment of circular jump
Q	Discharge
r	Radius of curvature of an element of streamline
r_f	Radial distance from the intersection of the flaring wingwalls to the beginning of radial flow stilling basin
r_o	Ratio of r_2 to r_1
r_1	Radial distance from the origin of coordinates to the leading edge of a circular jump

r_2	Radial distance from the origin of coordinates to the end of a circular jump
R	Radius at any point of the radial flow field also, the radius of the vertical curvature of entrance channel
R_c	Critical hydraulic radius of flow
S_c	Critical slope of flow
S_f	Slope of the total energy line
S_o	Slope of the channel bottom
T	Proportionality constant
V	Average flow velocity, also measured velocity in the downstream channel
V_f	Index mean velocity at the beginning of radial flow basin
V_m	Mean velocity in the downstream channel
V_s	Mean velocity on the end sill
V_t	Mean velocity at the top of the entrance channel
V_1	Mean flow velocity before the jump
V_2	Mean flow velocity after the jump
x	Distance along the centerline of channel from the beginning of the flared wingwalls to the leading edge of the jump
X	Distance from the reference section to the section of water surface profile measurements
y_c	Critical depth of flow
y_f	Depth of water standing behind a water fall also, index flow depth at the beginning of radial flow basin
y_n	Normal depth of flow
y_s	Mean flow depth on end sill
y_t	Mean depth of flow at the top of entrance channel
y_o	Ratio of y_2 to y_1
y_1	Depth of flow before hydraulic jump

y_2	Depth of flow after hydraulic jump
y_3	Depth of flow in the downstream channel or tailwater depth
Y	Average flow depth in a channel
z	Elevation of any point with respect to a reference section
Z	Height of drop of entrance channel
α	Vertical angle of intersection of entrance channel and the horizontal bottom of radial flow basin, also proportionality constant
γ	Specific weight of water
θ	Angle between the flaring wingwalls and the centerline of channel of radial flow basin
ρ	Density of water

CHAPTER 1

INTRODUCTION

Drainage culverts under highways are a major source of maintenance expense in some areas due to the frequent occurrence of scour and erosion in the vicinity of the culvert outlet. A culvert, because of its hydraulic characteristics, increases the velocity of flow over that in the natural channel. High velocities are most damaging just downstream from the culvert and the erosion potential at this point is a feature to be considered in culvert design. Improved methods for reducing this local scour and erosion will result in considerable reduction in the cost of building and maintaining highways. Conventional methods of attacking the erosion problem utilize sills, baffles, and impact walls for dissipating the high-velocity energy of the culvert flow. These methods are of limited effectiveness, however, because the flow leaving the energy dissipating structure is usually confined to a narrow stream of about the same width as the culvert.

The engineer working in a particular area should determine the need and the type of energy dissipators for use at culvert outlets. As an aid in evaluating this need, culvert outlet velocities should be computed. These computed velocities can be compared with outlet velocities of alternate culvert designs, existing culverts in the area, or the natural stream velocities. It should be noted that the increased kinetic energy in the culvert is not the only factor in causing damage in the vicinity of the culvert outlet, but also an additional cause of the damage is the

concentration of the flow into a deep and narrow stream of water within the culvert. The rapid drawdown in the water surface elevation of the concentrated flow at the culvert outlet is accompanied by an additional increase in the kinetic energy of flow. Therefore, the dissipation of excess energy should be associated with the lateral spreading of the flow to reduce the flow depth and diminish scour potential at the culvert outlet.

Objective

A new type energy dissipator based on the principle of the circular hydraulic jump could be designed which is very effective in dissipating energy and spreading the width of the flow before it is discharged into the downstream channel. The structure makes use of an abrupt vertical curvature to induce radial flow in a rapidly flared basin where an arc of a circular hydraulic jump is formed. High pressures are developed when the flow impinges on the beginning of the basin floor. These pressures force the flow to spread laterally and stay in contact with the flared wingwalls of the stilling basin.

The new energy dissipator is expected to be especially useful in regions of steep topography because of the following important advantages: (1) The flow entering the channel is spread to a width of several times that of the culvert, thus reducing the flow depth and the concentrated attack on the downstream channel, (2) the geometry of the basin produces greater stability of the hydraulic jump thus permitting it to function effectively as an energy dissipator over a considerable range of tailwater levels, (3) the hydraulic jump created in this structure has a shorter length than that of a comparable parallel flow jump, thus resulting in a reduced length of the basin, (4) there are no walls or blocks within the basin which

would catch drift and impair its operation, and (5) the structure is self-cleaning and there is no danger of debris accumulation within the stilling basin.

Model studies were undertaken in the present investigation to demonstrate the satisfactory performance of the radial flow dissipator in stabilizing the jump and reducing the high velocity of the flow for a wide range of geometrical variables. The sensitivity of the performance of the basin to such variables as the flaring angle of wingwalls in the basin, the ratio of the width of downstream channel to the width of the beginning of the basin, and the total height of the drop from the culvert outlet to the basin floor were explored. Also, the adaptability of a trapezoidal downstream channel with a transition section from the basin to downstream channel was studied by model simulation.

Another objective of the research reported herein was to develop a semi-analytical design procedure for the proper selection of the appropriate dimensions of such a structure under given set of field conditions. The field conditions included such features as design discharge, topography, natural channel dimensions, and highway embankment cross section. The design procedure was based on the application of the circular hydraulic jump equation.

Scope of Investigation

Since knowledge of the effectiveness and sensitivity of different dimensional variables in the performance of radial flow energy dissipator was a necessity in development of a design procedure, several geometric configurations of this structure were constructed and tested in the

hydraulic laboratory during the course of experimentation. Nine different configurations of the model were tested. The basic parameters varied in constructing these geometrical configurations included: the horizontal angles of wingwalls of 10° , 15° , 22.5° , and 30° ; the ratios of the width of the downstream channel to the width or diameter of the culvert of 1, 2, and 4; and the ratios of the height of drop, from the culvert outlet to basin floor, to the culvert width of 1 and 3. The experiments were performed in models with rectangular as well as trapezoidal downstream channels. Five models having a trapezoidal downstream channel incorporated a transition section and an end sill.

Experimental procedure included determination of the position of the jump for a wide range of tailwater levels, velocity measurements downstream from the hydraulic jump, and water surface profiles of the supercritical flow within the basin. Velocities were measured at three different transverse sections in the downstream channel. Water surface profile measurements were made along radial lines to demonstrate the efficiency of the spreading action of flow within the basin.

A systematic procedure was developed to enable the engineer to design an effective radial flow energy dissipator at the outlet of highway culverts. A simplified circular jump equation was derived and its application was the basis for the design procedure. Based on the proposed method, a prototype structure was designed for a set of known field conditions. A model having a scale ratio of $1/3$ of the suggested prototype structure was constructed and tested.

CHAPTER 2

ENERGY DISSIPATION

The excessive energy at the outlet of many hydraulic structures requires some type of energy dissipating device which can modify the energy of high-velocity flow and prevent or minimize scour, erosion, and undermining of the structure. This excessive energy could be dissipated by the internal friction and turbulence or the external energy dissipation by friction between the contact surface of structure and water.

The basic principle involved in different types of energy dissipators is the conversion of the kinetic energy of flow into turbulent energy, and ultimately into heat energy. One of the most efficient methods of dissipating energy is by creation of a hydraulic jump in the flow medium. Besides dissipating energy the hydraulic jump may increase piezometric head, extract air from a closed conduit, and increase uplift force.

Since the investigation reported in this research work deals specifically with the application of a particular type of hydraulic jump, a review of the various aspects of this energy dissipating method was made.

Height and Length of the Hydraulic Jump

The height of the jump is defined as the difference between the depth of water upstream and downstream from the jump. It is designated as:

$$h_j = y_2 - y_1 \quad (2.1)$$

where y_1 and y_2 are the depths of flow before and after the jump respectively.

There is not as yet any analytical method to determine the length of the hydraulic jump, however, some experimental work has been conducted for a small range of Froude number, using relations between, L_j/y_1 , L_j/y_2 , or $L_j/(y_2 - y_1)$, and F_1 , where L_j is the length of the jump and F_1 is the Froude number upstream from the jump. Comparison of the length of hydraulic jump in different shapes of channel cross section indicates that the shortest length occurs in the rectangular channel. The existence of a reverse flow in the sloped sides of channels causes longer jump lengths and more energy dissipation. The flatter the side slopes the higher the reverse flow, hence the longer is the jump length.

Silvester (1)* proposed a general equation expressing the jump length as follows:

$$\frac{L_j}{y_1} = K(F_1 - 1)^\alpha \quad (2.2)$$

where K and α are constants and should be determined experimentally by plotting graphs of L_j/y_1 versus $(F_1 - 1)$ on logarithmic paper.

USBR (2) developed the following equation for rectangular channel with $F_1 < 15$:

$$L_j = 6.9 (y_2 - y_1) \quad (2.3)$$

Argyropoulos (3) developed a graph for a triangular channel which yielded:

$$L_j = 3.65 (y_2 - y_1) \quad (2.4)$$

* Numbers in parenthesis refer to the similarly numbered items in the Bibliography.

Kindsvater (4) proposed the following equation for a circular section:

$$L_j = 12.5 (y_2 - y_1) \quad (2.5)$$

where $y_2 \leq$ pipe diameter.

Rajaratnam (5) stated that although the pressure distribution is not hydrostatic in the complete body of the jump, the pressure profile on the bed is essentially the same as the mean water surface profile, except in a small portion near the toe of the jump where the pressure profile is somewhat higher. On the basis of this statement and through utilization of existing data and some experimental work, Rajaratnam developed a generalized profile for the water surface of hydraulic jump in a smooth level rectangular channel with $F_1 > 4$.

Sadler and Higgins (6) proposed an experimental relationship expressing the length of the jump for the case of radial hydraulic jump in a horizontal bottom basin. They indicated that:

$$L_j = T (y_2 - y_1) \quad (2.6)$$

where T is a constant having an average value of 4.0.

Location of Hydraulic Jump

The hydraulic jump will form only when pressure plus momentum per unit time after the jump equals the pressure plus momentum per unit time before the jump at a distance approximately equal to the length of the jump between the sections. The pressure plus momentum term consists of two components. The first component is the momentum of the flow passing

through the channel section per unit time, and the second is the total pressure force acting at the channel section. It is an important design factor to know where the jump occurs. This can be predicted, within reasonable limits, depending upon the accuracy with which the friction losses can be estimated. One method of determining where the pressure plus momentum quantities are equal within a channel reach is by backwater-curve computations.

Conjugate Depths for Different Channel Shapes

Solution of conjugate depths for hydraulic jump in rectangular, triangular, trapezoidal, and parabolic channels may be given in terms of upstream Froude number. In the case of the radial hydraulic jump, however, the solution of conjugate depths is given in terms of upstream Froude number and the ratio of the radial distance from the toe of the jump to the radial distance from the end of the jump. The radial distance is measured from the origin of coordinates to the section of jump in question. Usually in the design of hydraulic jump type energy dissipators the following information is sought: The ratio of the conjugate depths, the energy losses, and the length of the jump.

A general solution begins with the application of the momentum principle to a horizontal channel bed, neglecting frictional losses, assuming uniform velocity distribution upstream and downstream of the jump, and considering hydrostatic pressure distribution. The general momentum equation in this case is as follows:

$$A_1 K_1' y_1 - A_2 K_2' y_2 = \frac{Q^2}{g} \left(\frac{1}{A_2} - \frac{1}{A_1} \right) \quad (2.7)$$

where

A_1 = Cross sectional area of flow before the jump.

A_2 = Cross sectional area of flow after the jump.

K_1' = Proportion of the depth of flow to the center of gravity before the jump.

K_2' = Proportion of the depth of flow to the center of gravity after the jump.

Q = Discharge.

g = Acceleration of gravity.

and

$$F_1 = \frac{Q}{A_1 \sqrt{gy_1}} \quad \text{Froude number before the jump} \quad (2.8)$$

Through the application of equations 2.7 and 2.8 the following jump equations are determined:

$$a) \frac{y_2}{y_1} = \frac{1}{2} (\sqrt{1 + 8F_1^2} - 1) \quad \text{in a rectangular channel} \quad (2.9)$$

$$b) \left(\frac{y_2}{y_1}\right)^3 - 1 = 2F_1^2 \left[1 - \left(\frac{y_1}{y_2}\right)^2\right] \quad \text{in a triangular channel} \quad (2.10)$$

$$c) \left(\frac{y_2}{y_1}\right)^{5/2} - 1 = 2.5F_1^2 \left[1 - \left(\frac{y_1}{y_2}\right)^{3/2}\right] \quad \text{in a first degree parabolic channel} \quad (2.11)$$

$$d) K_2' \left(\frac{y_2}{y_1}\right)^2 \left(\frac{b_2'}{b_1'}\right) - K_1' = F_1^2 \left(1 - \frac{b_1' y_1}{b_2' y_2}\right) \quad \text{in a trapezoidal channel} \quad (2.12)$$

where

b' = average width

K' = $\frac{1}{3} + \frac{1}{6} \cdot \frac{b}{b'}$

b = bottom width.

e) A theoretical radial hydraulic jump equation is proposed by Koloseus and Ahmad (7) as follows:

$$y_o^3 - \frac{r_o - 1}{2r_o + 1} y_o^2 - \frac{r_o + 6F_1^2 + 2}{2r_o + 1} y_o + \frac{6F_1^2}{r_o(2r_o + 1)} = 0 \quad (2.13)$$

$$\text{where } y_o = y_2/y_1, \quad r_o = r_2/r_1, \quad F_1 = \frac{V_1}{\sqrt{gy_1}}$$

The variables shown in equation 2.13 are represented in Figure 2-1.

Koloseus and Ahmad made the following assumptions in deriving the equation for a sector of an entire radial jump on a horizontal surface: (1) The liquid is incompressible; (2) the flow is radial and steady; (3) the frictional shear along all solid boundaries in the region of the jump is negligible in comparison with other forces involved; (4) the energy coefficient and momentum coefficient are equal to one; (5) the pressure distribution is hydrostatic before and after the jump; (6) there is no air entrainment within the jump and the vertical acceleration of fluid is negligible; and (7) the profile of the jump is straight line. It is noteworthy that as r_1 and r_2 approach infinity, $r_o = 1.0$ which corresponds to a segment of the circular jump with parallel sides. Equation 2.13 then reduces to the classical jump equation for a rectangular channel:

$$y_o = \frac{1}{2} \left(\sqrt{1 + 8F_1^2} - 1 \right) \quad (2.14)$$

It should be recalled that all of the conjugate depth equations were derived on the basis of assumptions that the floor is horizontal, and frictional losses are negligible. However, in dealing with the hydraulic jump in steep sloping channels, consideration should be given to the weight of water when the momentum principle is applied. In channels with mild

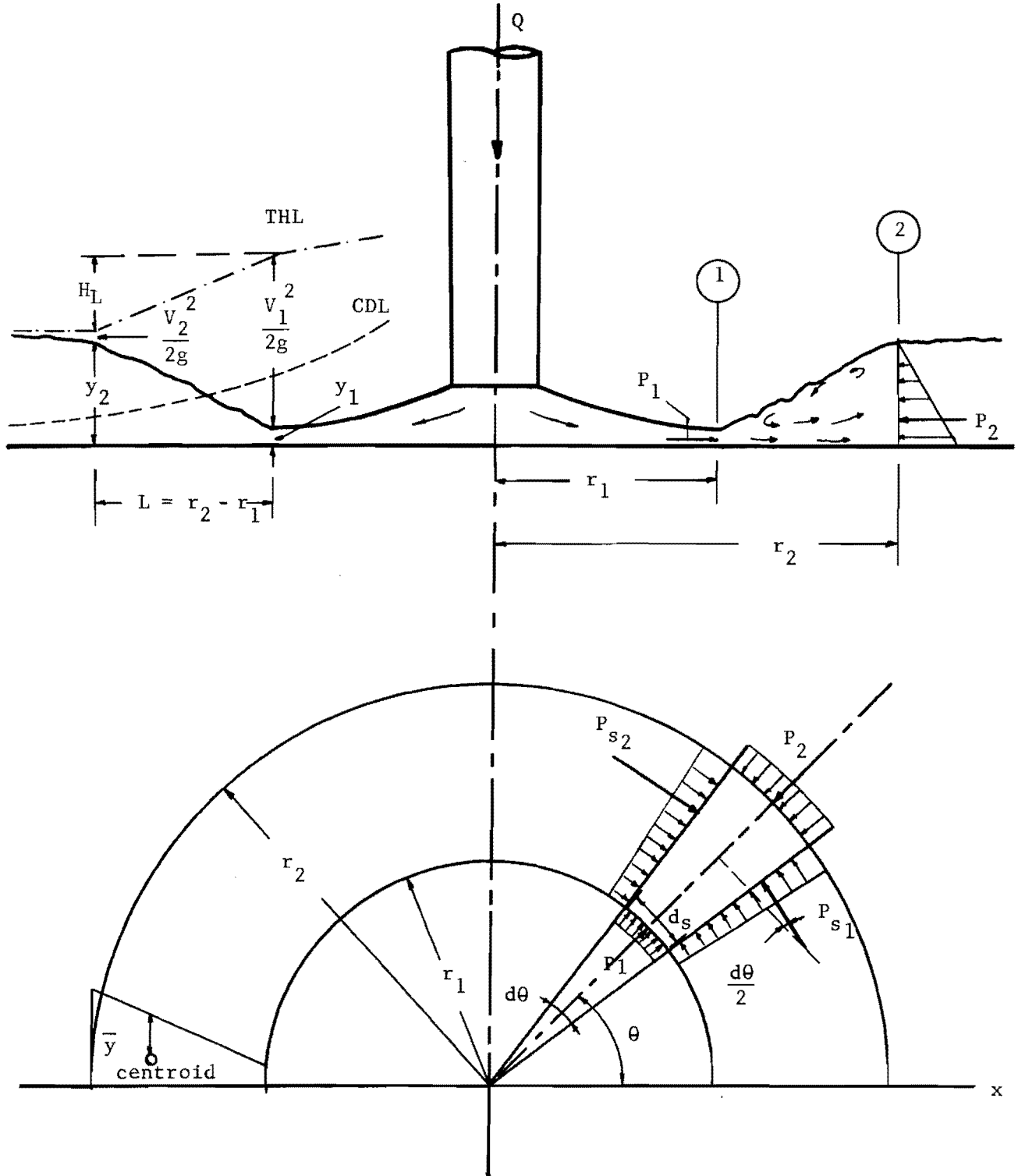


Figure 2-1 DEFINITION SKETCH FOR THE CIRCULAR JUMP

slope, the effect of the weight of water in momentum equation is not appreciable and hence it could be neglected.

Several methods have been attempted to include the frictional losses in conjugate depth computations, but their effect is usually unimportant, and they could safely be neglected.

Energy Losses in Hydraulic Jump

The general expression for determining the relative energy losses for all shapes of horizontal channel is:

$$\frac{E_L}{E_1} = \frac{y_1 + \frac{V_1^2}{2g} - y_2 - \frac{V_2^2}{2g}}{y_1 + \frac{V_1^2}{2g}} \quad (2.15)$$

where

- V = average flow velocity,
- E_L = specific energy loss,
- E_1 = specific energy upstream of the jump, and
- g = acceleration of gravity.

Silvester (1) plotted the energy losses from the above equation for various channel shapes against F_1 , resulting in graphs of E_L/E_1 versus F_1 . It is observed, from these graphs, that all channel shapes (except circular with $y_2 > \text{diameter}$) give a greater percentage of energy loss than the rectangular channel for any given Froude number. This difference is due to the type of velocity distribution pattern and the recirculation of flow on the sloping sides of the channel.

Existing Energy Dissipators

Many types of energy dissipators have been used throughout the world, and usually the design of each has varied quite radically to meet the problem at hand. Normally, the dissipation of energy is initiated within a stilling basin defined as a structure in which all or part of the hydraulic jump, or any other energy-reducing action, is confined. Several of these energy dissipating basins are briefly explained as follows:

Drop Structure Stilling Basins: A drop structure is sometimes used to change the slope of a canal from steep to mild. The drop could be vertical or inclined, rectangular or trapezoidal and is especially applicable to steep topography. Figure 2-2 shows a typical drop structure stilling basin. Experimental investigation by Rand (8) indicated that for vertical drop basins:

$$\frac{y_2}{y_1} = \frac{3.07}{(y_c/H)^{0.465}} \quad (2.16)$$

and

$$y_f = y_c \left[\left(\frac{y_1}{y_2}\right)^2 + 2 \left(\frac{y_c}{y_f}\right) - 3 \right]^{\frac{1}{2}} \quad (2.17)$$

where

y_c = critical depth,

y_f = depth of water standing behind the fall, and

H = height of drop in the structure.

UngROUTED Rock-Lined Depression: This type of basin is provided at the outlet of culverts. The basin consists of a depression with an ungrouted rock-lined bottom having a positive gradual slope at the upstream portion of the basin and an adverse slope at the downstream portion of the

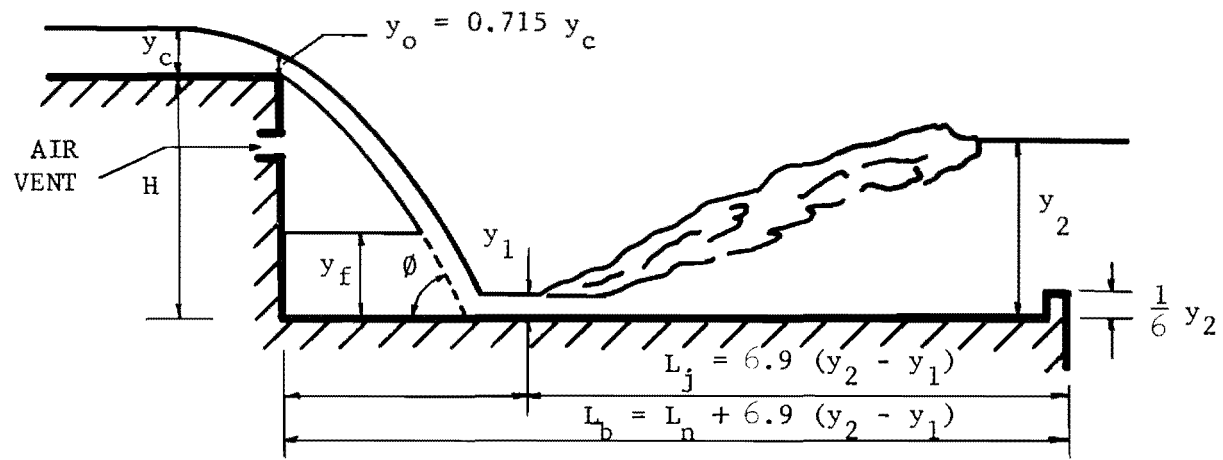


FIG. 2-2 VERTICAL DROP BASIN

basin terminating to the outlet channel bottom elevation. The ungrouted bottom permits the complete drainage of the left-over pool after a flood. The dissipation of energy is accomplished when the culvert flow is discharged at a downward angle into the basin.

Bucket Type Dissipators: The bucket type energy dissipator is used when the streambed is composed of rock. Because of a relatively short length of structure, marked economy is observed in its construction over many other kinds of comparable structures. The bucket type dissipators are mostly used at the outlet of large hydraulic structures such as dams with the primary purpose of either dissipating the energy of flow in the bucket or to deflect the flow as far away from the outlet of the structure as possible. Some of the more commonly used bucket type energy dissipators are:

- (a) Solid Roller Buckets - The basin consists of a bucketlike apron with a concave, circular profile of large radius, and a lip which deflect the high-velocity flow away from the streambed as shown in Figure 2-3. Energy dissipation results from the intersection of a ground roller in the bucket and a surface roller on the water surface created through the deflecting property of the lip of the bucket. The basin has the disadvantage that at high-velocity flow the material is moved backward to the bucket and may be trapped and become erosive. It is mostly used in flood control structures where the bucket is not in constant contact with water.

- (b) Slotted Roller Bucket Basin - The slotted roller bucket was designed to reduce the intensity of violent ground and surface rollers mentioned in solid roller buckets hence diminishing the deposition potential of loose material within the bucket. Figure 2-4 shows a sketch of a typical slotted roller bucket. The part of the flow which is discharged through the slots is spread laterally and is lifted away from the channel bottom downward from the slots. Consequently, the flow is expanded and distributed over a greater area after passing through the slots, providing less flow concentration than occurs with a solid roller bucket.
- (c) Trajectory Bucket Basin - When the tailwater conditions are such that it is difficult to form a satisfactory hydraulic jump for protection against scouring at the outlet structure then the flow could be deflected as far as possible from the end of the structure by the so called trajectory bucket. The trajectory bucket basin forces the jet of water to leave the stream-bed by deflecting its direction upward, creating a trajectory impacting with the stream-bed at some distance downstream from the end of the basin. In this type of basin the elevation of the bottom of the bucket is usually higher than the stream-bed elevation.
- (d) Tunnel Deflectors - Tunnel deflectors are utilized to deflect the high-velocity flow as far as possible away from the tunnel outlet. They are constructed in areas where the stream-bed

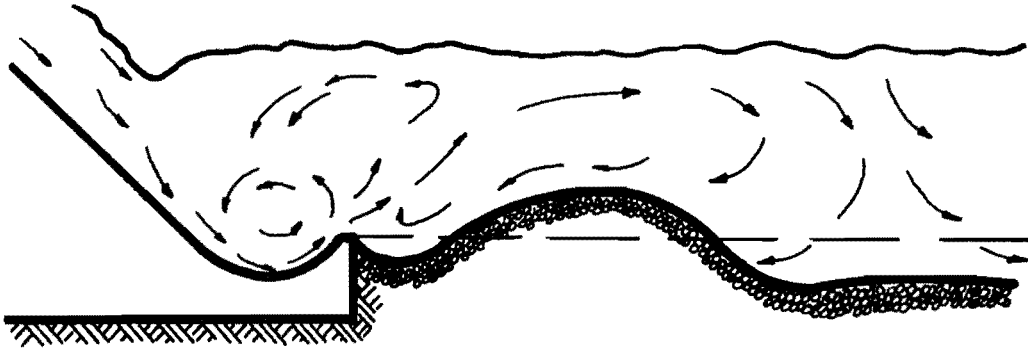


FIG. 2-3 SOLID ROLLER BUCKET TYPE BASIN

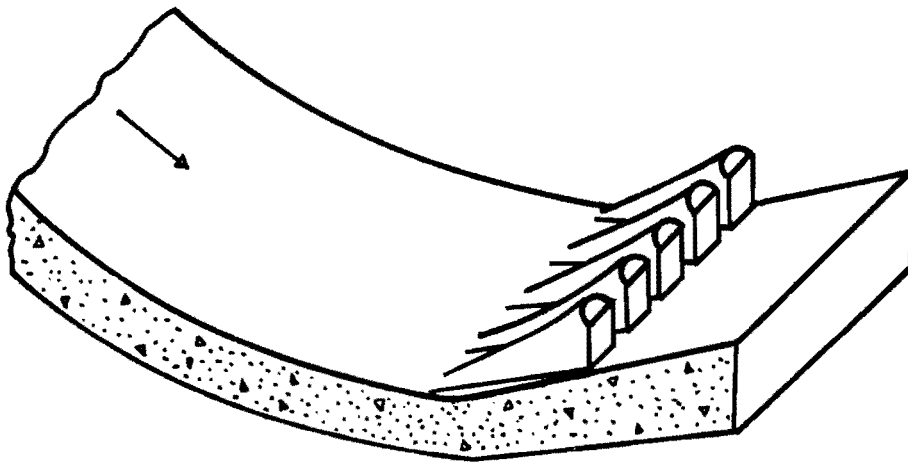


FIG. 2-4 SLOTTED ROLLER BUCKET

below the tunnel is composed of firm rock which can resist scour damage. Generally, the operation of tunnel deflectors should be confined to emergency or infrequent use.

Impact Type Energy Dissipators: This type of dissipator is used for a flow with specific energy in excess of $2D$ (where D is the outlet pipe diameter at basin's entrance). The dissipator is constructed in such a manner that all or most of the flow is forced to change direction locally, and then discharged in the original direction into a concrete basin. Two well known impact type energy dissipators are Bradly-Peterka (9) and Contra-Costa (10) basins.

- (a) Bradly-Peterka Basin - This basin is only effective when F_1 is greater than three in which the entire flow impacts with a hanging baffle installed in the basin. Energy dissipation is initiated when the flow strikes the vertical hanging baffle and changes its direction. A sketch of Bradly-Peterka basin is shown in Figure 2-5. This structure requires no tailwater for its effective operation in dissipating the energy although sufficient tailwater depth may improve the performance of the basin by reducing the outlet velocities.
- (b) Contra-Costa Energy Dissipator - This dissipator consists of a trapezoidal basin with two impact walls across it as shown in Figure 2-6. The upstream impact wall has a height which is half as much as the height of the downstream wall. The least desirable feature of this stilling basin occurs when the entering flow into the basin is completely submerged by the

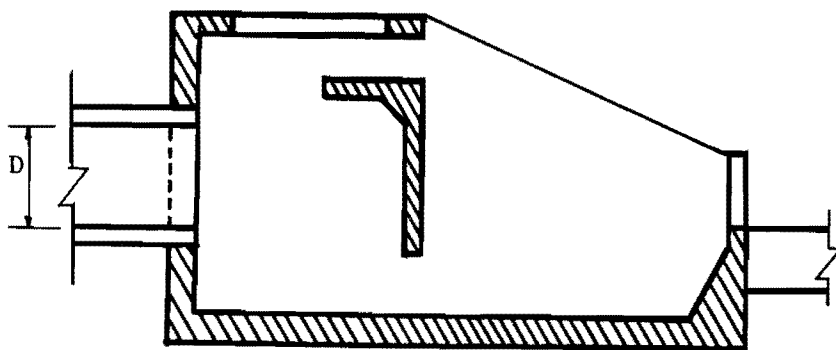


FIG. 2-5 BRADLY - PETERKA BASIN

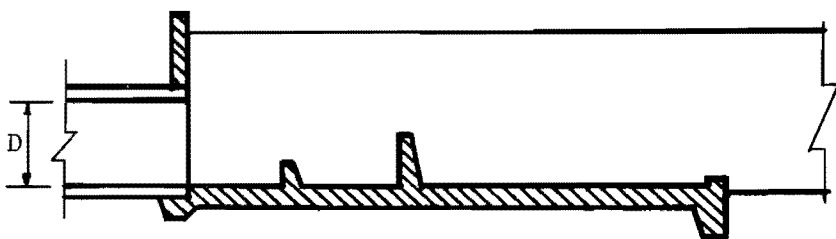


FIG. 2-6 CONTRA-COSTA ENERGY DISSIPATOR

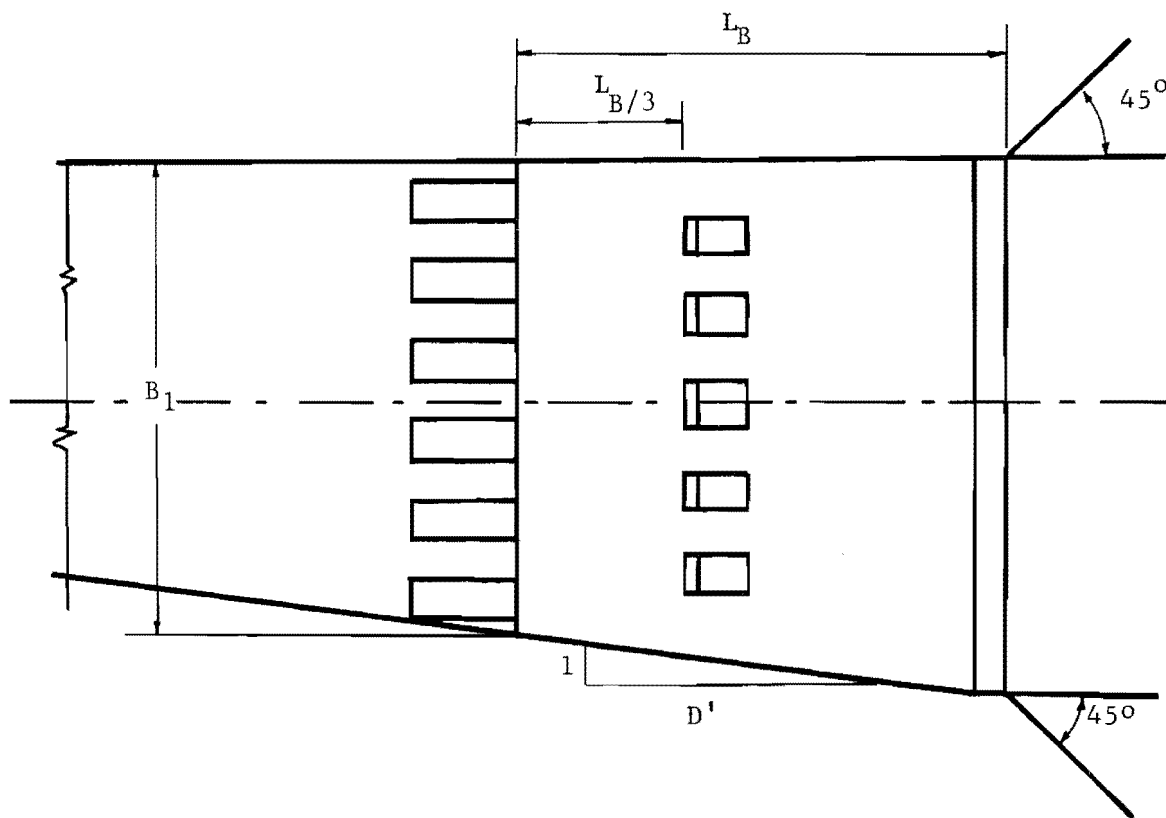
tailwater. Debris accumulation within the basin may be anticipated for certain discharge conditions.

Saint Anthony Fall Basin: Principally, the SAF basin has been used for drainage structures where relatively small quantities of flow are expected. The dissipation of energy is accomplished through the formation of a hydraulic jump within the basin. Through the addition of stilling basin appurtenances the SAF basin can considerably reduce the length of the conventional hydraulic jump type stilling basins. Figure 2-7 shows the general configuration of the SAF basin. The component parts of this basin are:

1. a steep chute, with chute blocks at its downstream end,
2. a trapezoidal apron with baffle blocks,
3. an end sill which extends for the full width of the basin, and
4. the basin training walls which may be parallel or divergent.

It should be noted that in most of the basins discussed so far, the undesirable characteristic is debris accumulation, especially in impact type energy dissipators.

Several other special stilling basins are in use throughout the world which have performed very satisfactory for their intended purpose. Elevatorski (11) compiled the description of some of the more commonly known of these basins such as: sluiceway stilling basin, jet-diffusion basin; free-jet basin; and Bahavani stilling basin. Modified shapes and dimensions of stilling basin appurtenances such as chute blocks, baffle blocks, and end sills have been used to improve the performance and to reduce the length of the basin. An example of this type of modification



Centerline Section

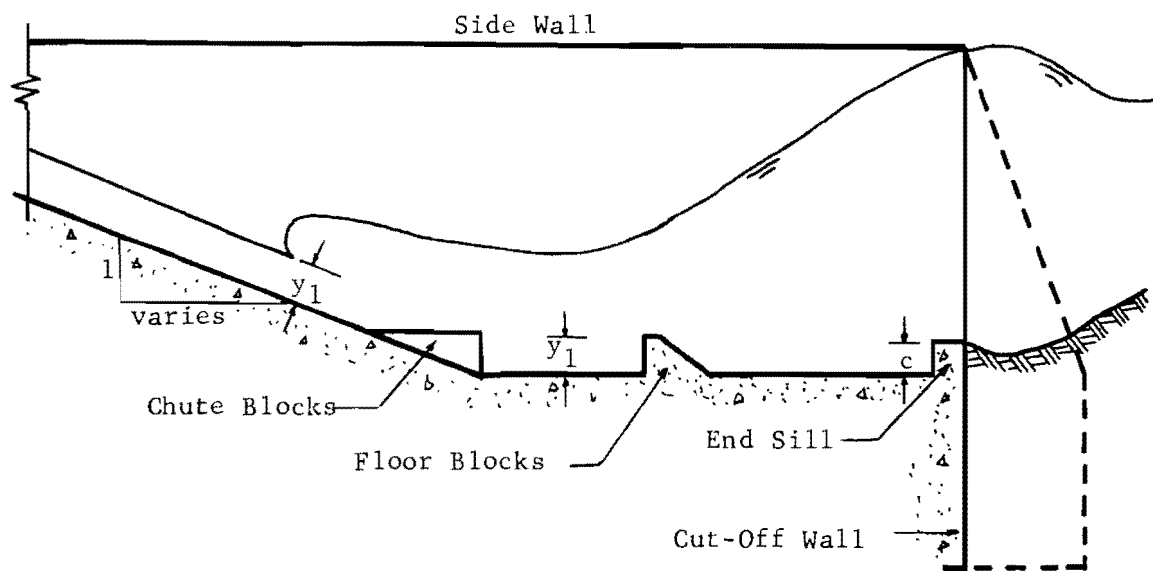


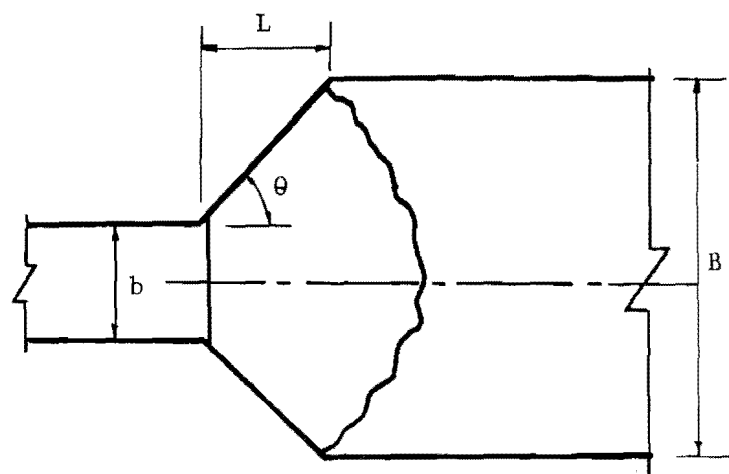
FIG. 2-7 SAF STILLING BASIN

is the Bahavani stilling basin in India which utilized T-shaped floor blocks.

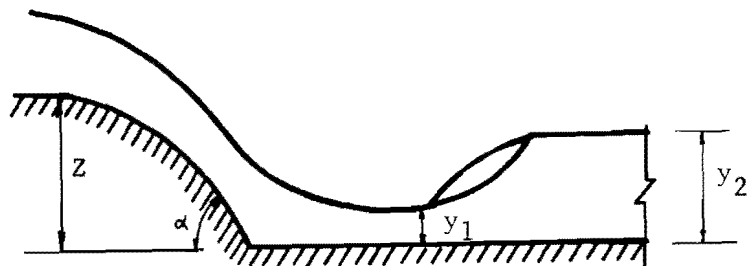
Radial Flow Dissipator: The original laboratory experimental investigations of a radial flow energy dissipator was conducted by Aguirre (12). In this dissipator the culvert flow dropped along a steep chute, which ended at its intersection with the horizontal bottom of the stilling basin. As the flow impinged on the horizontal bottom, it was forced to spread rapidly, thus avoiding separation from the flared wingwalls. In this process the flow was changed from parallel to radial flow, and again to parallel flow in the downstream channel.

The combination of this supercritical radial flow and the required tailwater depth resulted in the formation of a hydraulic jump whose leading edge was approximately a circular arc. The required tailwater for such a hydraulic jump could be substantially varied while the location of the jump itself varied over a relatively short distance. Figure 2-8 shows a general sketch of a Radial Flow Dissipator. The geometric parameters used in the design of this dissipator were:

- b = width of entrance channel,
- B = width of downstream channel,
- L = projected length of flared wingwalls on a plane parallel to the centerline of the channel,
- Z = height of drop of curved channel section,
- α = deflection angle between the tangent to the downstream end of the curved channel section and the horizontal bottom basin,
and
- θ = angle between the flaring wingwalls and the centerline of the channel.



Plan



Elevation

FIG. 2-8 RADIAL FLOW ENERGY DISSIPATOR

Aguirre conducted experiments on eight different geometric arrangements of this energy dissipator which included B/b ratios of 4 and 6 and θ values of 30 and 45 degrees.

Wear (13) investigated by model simulation, the effect of a partial transverse sill or an abrupt rise, located near the downstream end of the apron of a radial flow basin, on the performance of this type of dissipator. He reported on the hydraulic performance of radial flow basins independently incorporating four different rise heights, two sill locations, and sills with or without 45° beveled face. Wear concluded that an abrupt rise as part of a radial flow energy dissipator permitted efficient operation of the basin with low values of downstream tailwater depth. Furthermore, significantly lower values of tailwater depth were required to stabilize the jump within the basin as the rise height was increased.

The adaptability of radial flow energy dissipator for use with circular or box culvert was further explored by Moore and Meshgin (14), who investigated the performance of the basin with some modifications of the shape of the curved-drop channel such as a "V" shaped cross section and sloping of the flaring wingwalls backward in order that they were continuation of the two planes forming the "V" section at the bottom end of the drop. The possibility of eliminating the curved drop and replacing it with a simple vertical wall was also studied. Although this arrangement performed well when the falling jet impinged on the apron in the proper place, an increase in Froude number caused the impingement point to shift downstream resulting in very unsatisfactory performance. It was concluded from this investigation that the relative simplicity of construction was a strong argument in favor of the structural arrangements with the simple

curved drop and straight horizontal elements incorporating a box or a circular culvert.

Aguirre, Wear, and Moore all concluded that the radial flow energy dissipator stabilized the jump, reduced the outlet velocity, and permitted efficient operation of the basin over a high range of tailwater variations.

Development of the Radial Flow Surface Curve Equation

An equation for free surface radial flow was originally developed by Davis (15) and later it was slightly revised by Sadler and Higgins (6). The basic approach to the development of this equation was through the application of the specific energy relationship in open channels and the use of classical Chezy equation to evaluate the average channel velocity. The derivation of the radial flow surface curve by Sadler and Higgins (6) is as follows:

$$E = Y + V^2/2g \quad (2.18)$$

Assuming that the hydraulic radius is equal to the depth of radial flow and the head loss at a section is the same as for uniform flow, the Chezy equation becomes:

$$S_f = \frac{V^2}{C^2 Y} \quad (2.19)$$

where

E = specific energy of the flow,

V = mean velocity of the flow,

C = Chezy coefficient,

Y = depth of flow at distance R , and

S_f = slope of the total energy line.

Differentiating equation (2.18) with respect to R yields:

$$\frac{dE}{dR} = \frac{dY}{dR} + \frac{V}{g} \cdot \frac{dV}{dR} \quad (2.20)$$

The total specific energy at any subsequent cross section is:

$$E = E_1 + \int_{R_1}^R S_o dR - \int_{R_1}^R S_f dR \quad (2.21)$$

where

R = radius at any point of the radial flow field, and

S_o = slope of the channel bottom.

Differentiation of equation (2.21) results in:

$$\frac{dE}{dR} = S_o - S_f \quad (2.22)$$

Equating equation (2.20) and (2.22):

$$\frac{dE}{dR} = \frac{dY}{dR} + \frac{V}{g} \frac{dV}{dR} = S_o - S_f \quad (2.23)$$

From continuity principle:

$$V = \frac{Q}{2\pi RY} \quad (2.24)$$

hence,

$$\frac{dV}{dR} = \frac{Q}{2\pi RY} \left(\frac{1}{R} + \frac{1}{Y} \frac{dY}{dR} \right) \quad (2.25)$$

Direct substitution of equations (2.19), (2.24), and (2.25) in equation (2.23) results in:

$$\frac{dE}{dR} = S_o - \frac{Q^2}{4c \pi^2 R^2 Y^3} = \frac{dY}{dR} - \frac{Q^2}{4\pi^2 R^2 Y g} \cdot \left(\frac{1}{R} + \frac{1}{Y} \frac{dY}{dR} \right) \quad (2.26)$$

Introducing the Froude number as:

$$F^2 = \frac{V^2}{gY} = \frac{Q^2}{4\pi^2 gR^2 Y^3} \quad (2.27)$$

into equation (2.26) and solving for dY/dR ,

$$\frac{dY}{dR} = \frac{S_o + F^2 \left(-\frac{g}{c^2} + \frac{Y}{R} \right)}{1 - F^2} \quad (2.28)$$

or

$$\frac{dY}{dR} = S_o + \frac{F^2}{F^2 - 1} \left(\frac{g}{c^2} - S_o - \frac{Y}{R} \right) \quad (2.29)$$

For horizontal channel bottom ($S_o = 0$) and frictionless flow condition ($g/c^2 = 0$) equation (2.29) becomes:

$$\frac{dY}{dR} = \frac{F^2}{F^2 - 1} \left(-\frac{Y}{R} \right) \quad (2.30)$$

When $F \gg 1.0$ then $F^2/(F^2 - 1)$ approaches unity and hence,

$$\frac{dY}{dR} = -\frac{Y}{R} \quad (2.31)$$

or

$$\frac{dY}{Y} = -\frac{dR}{R} \quad (2.32)$$

integrating:

$$\int_{Y_1}^Y \frac{dY}{Y} = - \int_{R_1}^R \frac{dR}{R} \quad (2.33)$$

After introducing boundary conditions the solution of equation (2.33)

yields:

$$Y_1 R_1 = YR \quad (2.34)$$

where Y_1 and R_1 are known flow depth and radius respectively.

Equation (2.34) indicates that constant velocity prevails everywhere within the radial flow field if the assumptions made in its derivation hold true.

In the case of flow with boundary friction, high Froude number ($F_1 \gg 1.0$), and constant C , Davis (15) derived the following radial flow surface curve:

$$\frac{Y}{Y_1} = \frac{R_1}{R} \left[\frac{R_1}{Y_1} \cdot \frac{g}{2C^2} \left(\frac{R^2}{R_1^2} - 1 \right) + 1 \right] \quad (2.35)$$

CHAPTER 3

MODEL CONSTRUCTION AND EXPERIMENTAL RESULTS

Model Construction

The experimental work was conducted in the Hydraulic Laboratory of the Civil Engineering Department of The University of Texas using an apparatus similar to the one used by Aguirre (12) and Wear (13). The schematic layout of this apparatus with trapezoidal downstream channel is shown in Figure 3-1. Certain improvements were made in the previous structural arrangement for better performance of the model such as utilization of a large head tank open at the top and containing several transverse screens and baffles to damp out the flow disturbances from the supply pipe. A horizontal circular culvert, six inches in diameter and three feet long, conveyed the water from the stilling tank to a six inch wide rectangular channel. The six inch rectangular section is referred to as an entrance channel throughout this report. The circular culvert was formed from a piece of aluminum sheet metal rolled to a 0.5 foot diameter. The sheet metal was rolled in such a manner that it formed a butt joint held in place with tape and placed at the top of the pipe thus preventing any possible leakage. An adjustable sluice gate installed at the upstream end of the pipe controlled the depth of flow in the model culvert.

The connection from the circular conduit to the entrance channel was a sudden expansion. The entrance channel had a vertically curved bottom with a tangent section intersecting at a 60° angle with the horizontal bottom of the stilling basin. The radius of curvature of the curved

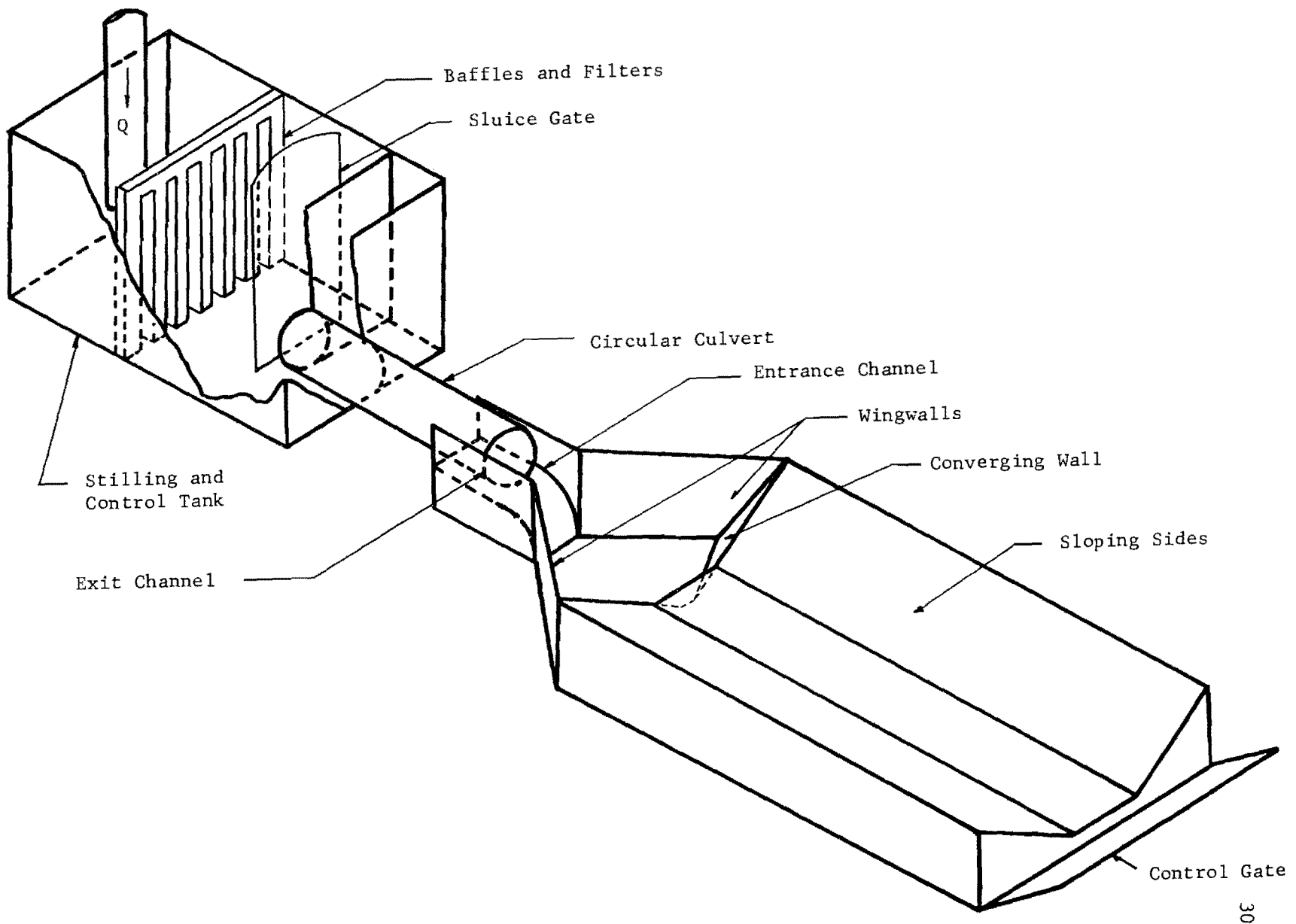


FIG. 3-1 SCHEMATIC LAYOUT OF MODEL WITH TRAPEZOIDAL DOWNSTREAM CHANNEL

section of entrance channel was nine inches. The stilling basin was a diverging structure with six inch upstream width and flaring vertical wingwalls set at various horizontal angles which terminated to either a rectangular or a trapezoidal downstream channel.

The downstream channel was 8.5 feet long as measured from the beginning of the flared wingwalls along the channel centerline. This was 3.0 feet longer than the downstream channel used by Aguirre and Wear which helped to minimize any possible influence of the downstream control gate on the flow conditions in the model. A six inch flap gate at the end of the downstream channel controlled the tailwater depth.

The required flow for the experiments was supplied through a low head pump from the laboratory sump directly into the laboratory distribution system. Flow was regulated by a three inch gate valve and measured by a calibrated-in-place three inch elbow meter. A precision differential water manometer with a vernier reading to the nearest 0.001 foot was used to determine the piezometric head difference from the elbow meter.

Several geometric configurations of the model were constructed and tested during the course of experimentation. Three basic parameters were altered in constructing different configurations of the model. These parameters were the horizontal angle of the flaring wingwalls, the bottom width of the downstream channel, and the drop height of the entrance channel. The experiments were performed in models with rectangular as well as trapezoidal downstream channels. The schematic representation of the rectangular and trapezoidal channel models are shown in Figures 3-2 and 3-3 respectively.

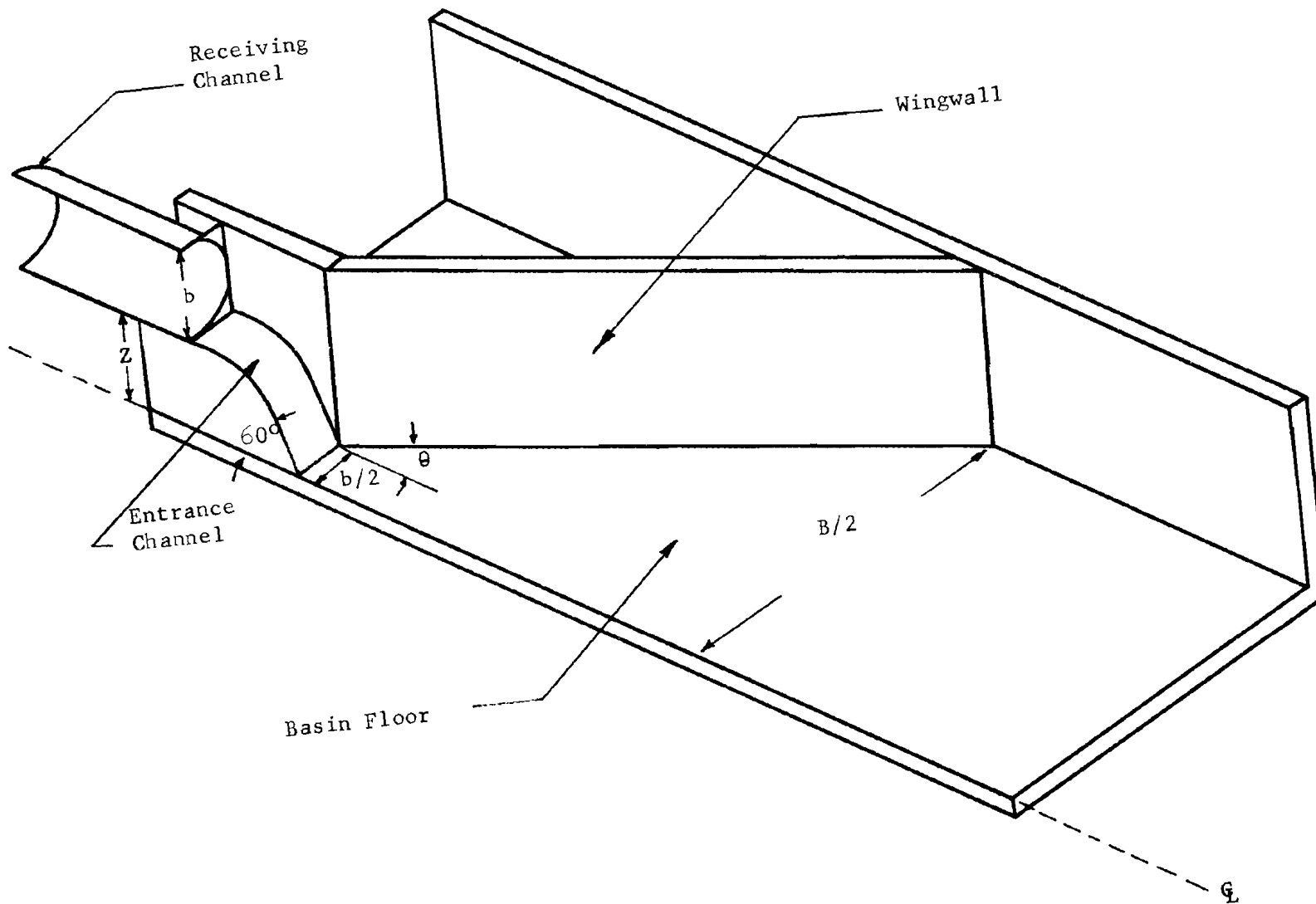


FIG. 3-2 SECTIONAL VIEW OF RECTANGULAR CHANNEL BASIN

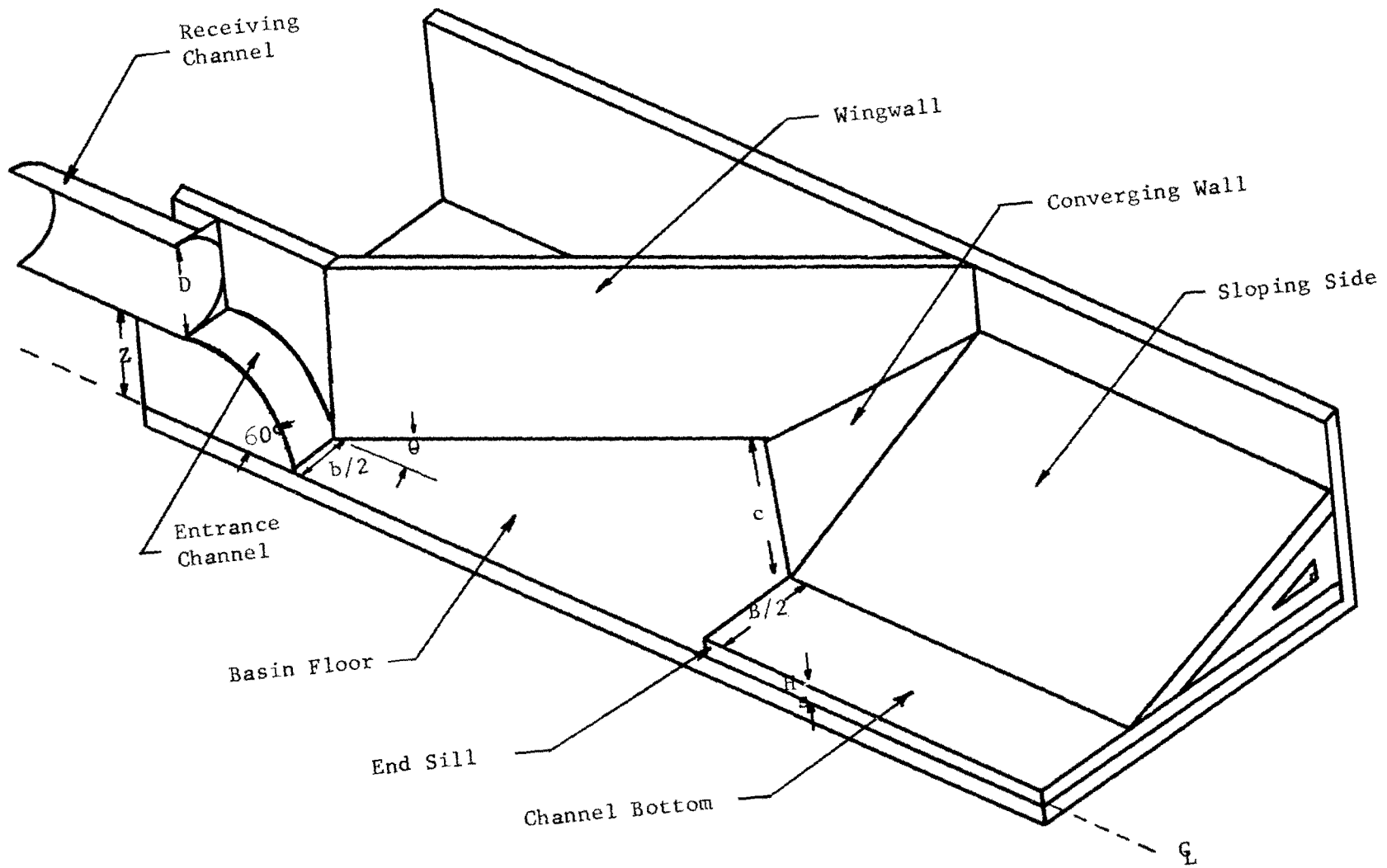


FIG. 3-3 SECTIONAL VIEW OF TRAPEZOIDAL CHANNEL BASIN

The model with rectangular downstream channel incorporated the following dimensional variations: The ratios of the width of entrance channel to the width of the downstream channel were two and four; the flaring wingwalls were set at horizontal angles of 10° , 15° , 22.5° , and 30° measured with respect to the channel centerline. The height of the drop of entrance channel was six inches in all geometric arrangements.

In the case of the trapezoidal downstream channel the following modifications were made to observe the performance characteristics of different structures: The ratios of the bottom width of downstream channel to the width of entrance channel were one and two. The flaring wingwalls had 30° horizontal angles measured from the channel centerline. The length of the stilling basin along the channel centerline was twenty-six inches. The downstream channel side slopes were 2:1 in all structures. Two abrupt rises, 0.75 inch and 1.50 inches in height, were constructed at the end of the stilling basin. Two different drop heights of the entrance channel were used for this model, six inches, and eighteen inches.

The transition from the stilling basin to the trapezoidal downstream channel consisted of a pair of converging triangular walls. The base of each converging wall was located on the stilling basin bottom and its apex was fixed at the point of intersection of the flared wingwalls and the side slopes of the trapezoidal channel. The surface area of each wall was changed by either decreasing or increasing the wall's base length.

Experimental Procedure

Nine different geometric configurations of the model were tested to demonstrate the efficiency and performance of the energy dissipating structure. As stated previously, the geometric parameters varied consisted of θ , B/b , ss , H_s , c/b , and Z , where θ , B/b , and Z were defined previously, and

ss = side slopes of the downstream channel,

H_s = sill height of the end of the stilling basin in inches, and

c/b = ratio of the base length of converging walls to the width of the entrance channel.

The combination of different geometric parameters used in the model and the designation given to each one are indicated in Table 3-1. A photographic view of the entrance channel and the stilling basin layout for a trapezoidal downstream channel is shown in Figure 3-4.

Jump stability, velocity distribution, and water surface profile measurements were made to determine the nature and degree of the spreading action, energy dissipation, and performance of the basin. Radial water surface profile measurements were obtained within the stilling basin in the case of the rectangular downstream channel. For the trapezoidal channel model the profile measurements were only recorded along the centerline of the channel.

The stability of the hydraulic jump was determined in terms of the longitudinal movement in jump position as the result of variation in the tailwater depth. The position of the jump was defined by the distance along the basin centerline from a section at the beginning of the flared wingwalls to the leading edge of the jump.

TABLE 3-1 DESIGNATION AND CHARACTERISTICS OF VARIOUS GEOMETRIC ARRANGEMENTS

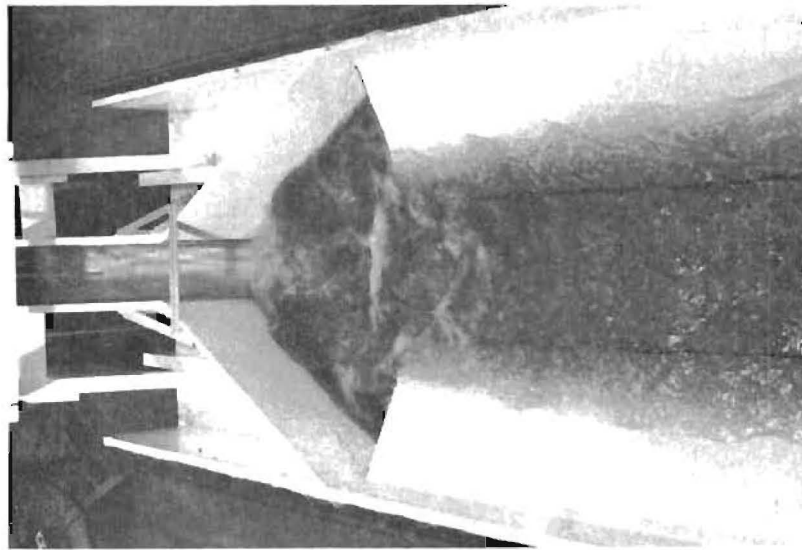
	θ , deg.	$\frac{B}{b}$	Side Slope	H_s , in.	c/b	Z, in.	F_t	y_t	y_1	y_2	r_1	r_2
*REC 1	10	2	vert.	0.0		6	2.56	0.225		0.490 0.510 0.480 0.619 0.528 0.510	1.82 2.42 2.92 1.82 2.42 2.92	2.62 3.42 3.92 3.22 3.42 4.42
REC 2	15	4	vert.	0.0		6	1.12 2.56	0.306 0.225		0.519 0.461 0.414 0.489 0.414 0.368	1.33 1.93 2.43 1.33 1.93 2.43	
REC 3	22.5	4	vert.	0.0		6	2.01 1.91 2.56 1.86	0.257 0.278 0.225 0.302		0.453 0.416 0.363 0.460 0.403 0.367 0.441 0.412 0.356 0.486 0.460 0.402	1.01 1.61 2.11 1.01 1.61 2.11 1.01 1.61 2.11 1.01 1.61 2.11	2.11 2.51 3.01 2.11 2.56 3.01
REC 4	30	4	vert.	0.0		6	1.11 3.125 2.56	0.314 0.211 0.225		0.532 0.458 0.377 0.724 0.523 0.414 0.407 0.360 0.325 0.424 0.414	0.83 1.43 1.93 0.83 1.43 1.93 0.83 1.43 1.93 0.83	
**TRAP 1	30	1	2:1	2.25	2.25	6	2.56	0.225				
TRAP 2	30	1	2:1	0.75	2.50	6	2.56 1.86	0.225 0.302	0.115 0.170	0.395# 0.405#	0.83 0.83	2.43 2.43
TRAP 3	30	2	2:1	0.75	2.50	6	2.56	0.225			1.13	2.13
TRAP 4	30	2	2:1	0.75	1.80	6	2.56 1.86	0.225 0.300	0.109 0.083	0.293# 0.313#	1.73 0.83 1.23 1.58	2.63 1.83 2.23 2.58
TRAP 5	30	2	2:1	1.50	2.25	18	1.86	0.260	0.235	0.353#	1.73	2.63

* "REC" indicates rectangular downstream channel.

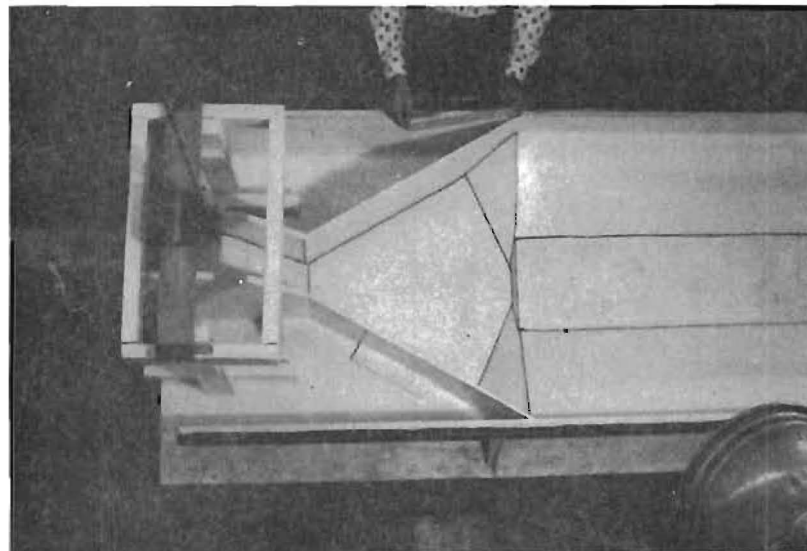
** "TRAP" indicates trapezoidal downstream channel.

NOTE: (1) Values marked # are influenced by the sill, and therefore may not agree with a calculated value.

(2) y_1 can be obtained by applying the continuity and energy equations based on known values of F_t and y_t .



(a) With Flow



(b) Without Flow

FIG. 3-4 PHOTOGRAPHIC VIEW OF ENTRANCE CHANNEL AND STILLING BASIN
LAYOUT FOR TRAPEZOIDAL DOWNSTREAM SECTION

The position of the jump was determined through the application of a Lory type point gage mounted on a rigid carriage instrument which could be easily moved back and forth in the longitudinal as well as transverse directions. The point gage was placed along the basin centerline over the leading edge of the jump. A calibrated tape, placed on a longitudinal track, facilitated the determination of the position of the leading edge of the jump with respect to the reference section. Since constant fluctuations of the leading edge of the jump could not be prevented, a visual temporal average for each reading was recorded as the jump position in each test run.

A piezometer was placed at the beginning of the stilling basin bottom along the centerline of the channel. This piezometer could determine the pressure variations of the flow at the entrance of the stilling basin. A flexible plastic tube connected the piezometer to an open manometer. The pressure readings obtained at this section were especially helpful in determining the limiting Froude number at which the flow would spring free from the bottom of the entrance channel.

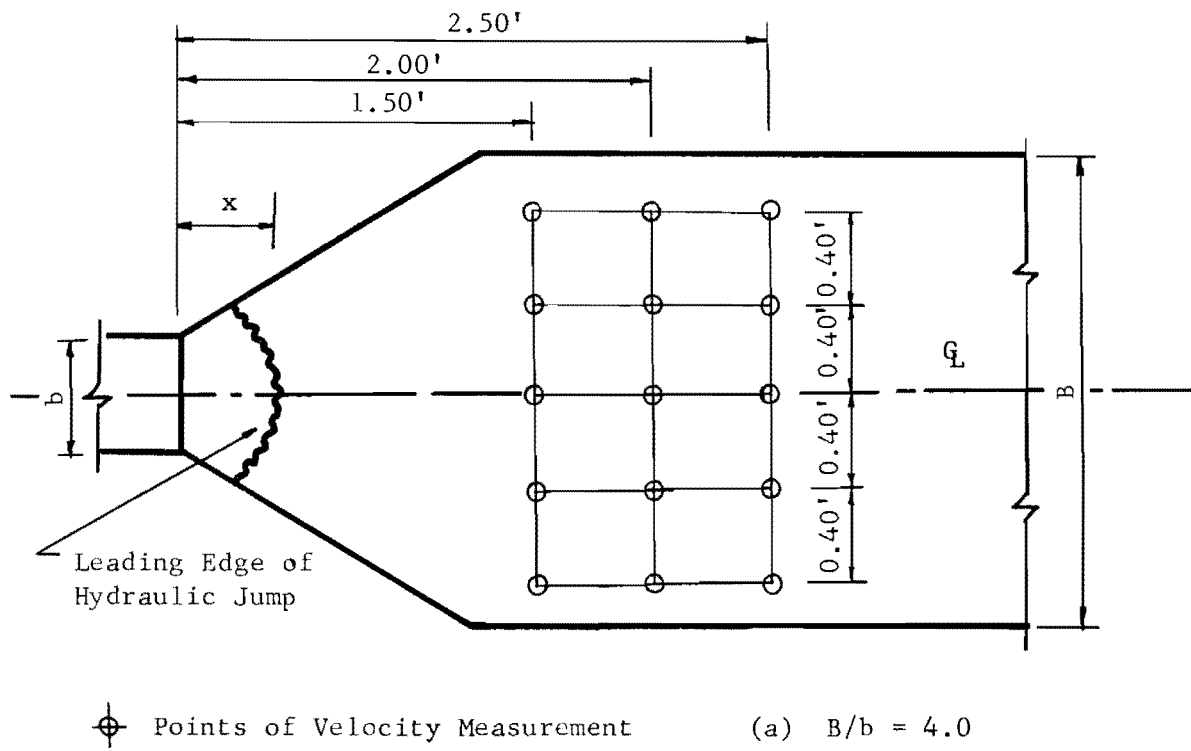
The control of the jump position at various sections was accomplished by means of a six inch flap gate placed at the end of the downstream channel. The flap gate was used to increase or decrease the tailwater depth thus changing the position of the jump. Tailwater depth measurements were made by means of the previously mentioned point gage which was used to locate the jump position.

Velocity measurements were obtained for the purpose of indicating the efficiency, the spreading action, and the degree of velocity reduction

in the jump. A Pitot tube mounted on a sliding carriage was used for velocity measurements. The Pitot tube was placed parallel to the channel centerline and measured the velocity head at 0.03 foot and $0.4y_2$ from the bottom of the channel. The flow velocity on the sloping face of the trapezoidal downstream channel was measured as close to the bottom as possible. Prior to making the velocity measurements, a discharge with a suitable Froude number was selected and provided for the test run under consideration. The hydraulic jump was then stabilized at three different positions for rectangular downstream channel set up, located at $x = 0.4$ ft., $x = 1.0$ ft., and $x = 1.5$ ft., where, x was the distance along the centerline of channel from the beginning of the flared wingwalls to the leading edge of the jump. In trapezoidal downstream channel model, the converging walls and the abrupt rise acted as a contraction which forced the jump to form within the stilling basin independent of the tailwater depth.

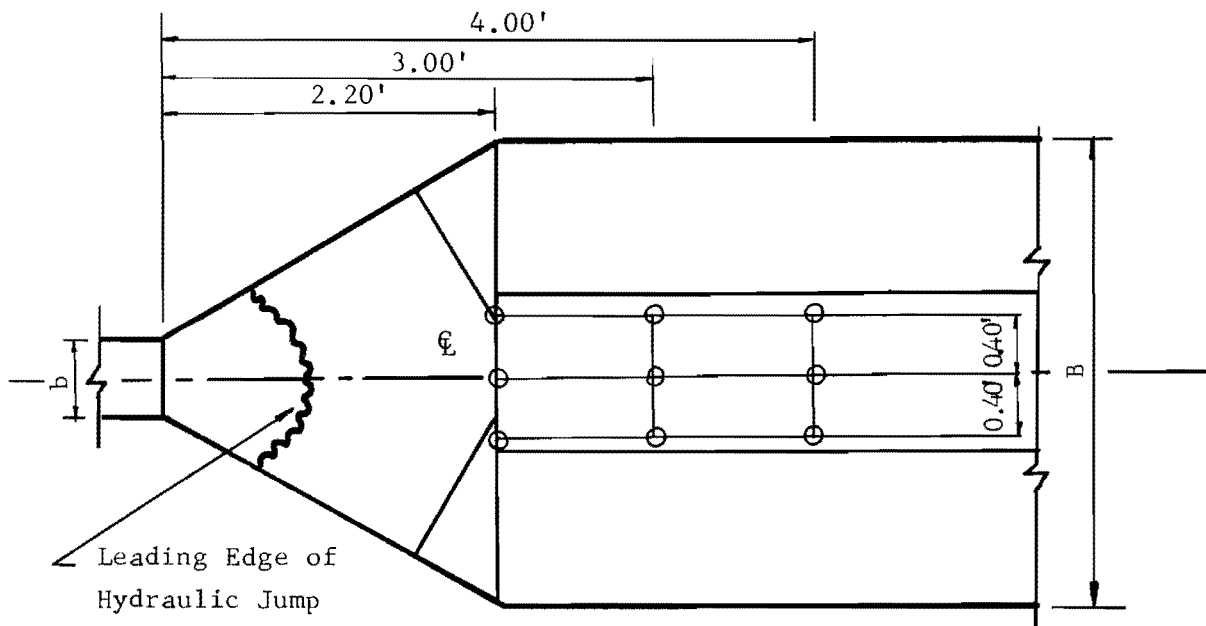
The Pitot tube used during the course of this investigation was connected to a differential water manometer, the accuracy of which was to the nearest ± 0.001 ft. Figure 3-5 shows the typical location of velocity measurements for the rectangular as well as the trapezoidal models.

In order to study the degree of angular uniformity and the effect of the flaring wingwalls on the spreading action of the supercritical flow in the basin, water surface profiles were determined along radial lines by direct measurement of water depth within the basin. Typical location of these radial lines are shown in Figure 3-6. A Lory type "A" point gage resulting in readings to the nearest ± 0.002 ft. was used to measure the depth of water. The radial lines used as reference were the



(a) $B/b = 4.0$

Rectangular Section



(b) $B/b = 2.0$

Trapezoidal Section

FIG. 3-5 LOCATION OF VELOCITY MEASUREMENTS FOR RECTANGULAR AND TRAPEZOIDAL CHANNELS

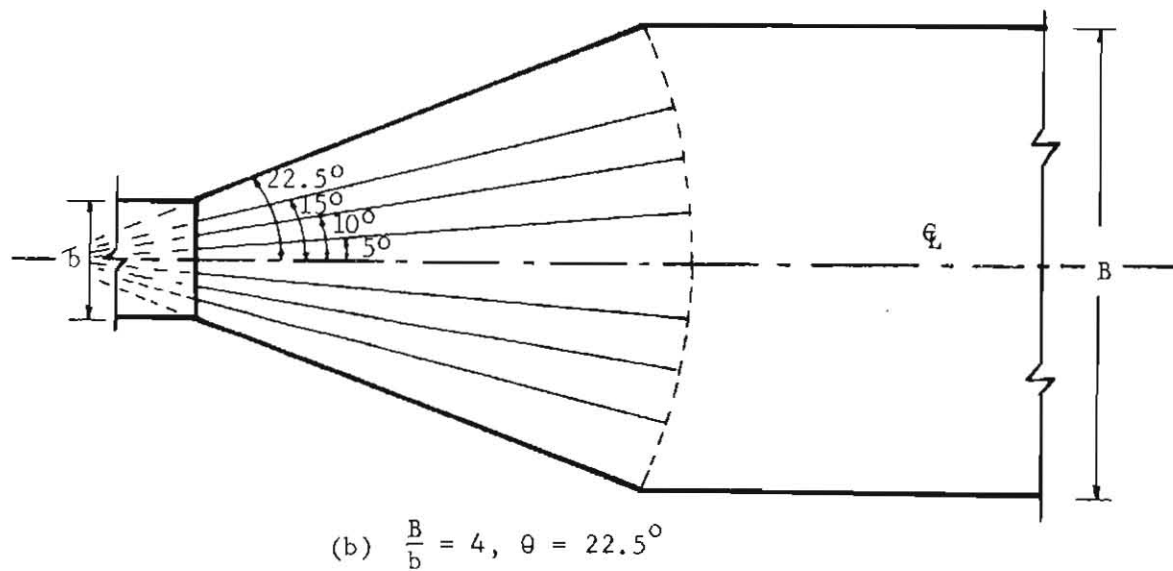
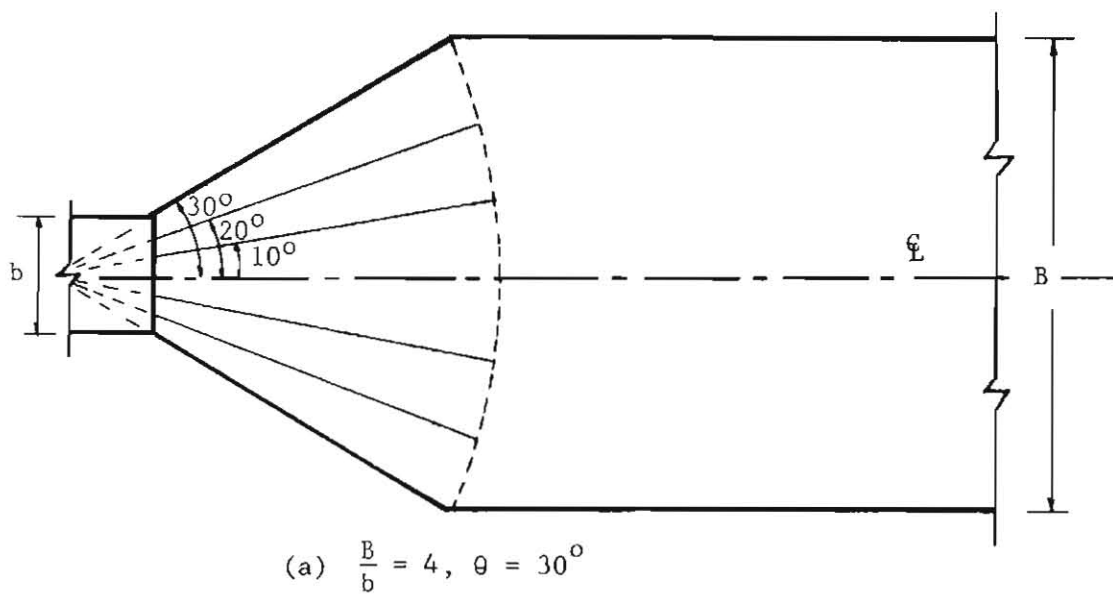


FIG. 3-6 LOCATION OF WATER SURFACE MEASUREMENTS IN RECTANGULAR CHANNEL FOR $\theta = 30^\circ$ and $\theta = 22.5^\circ$

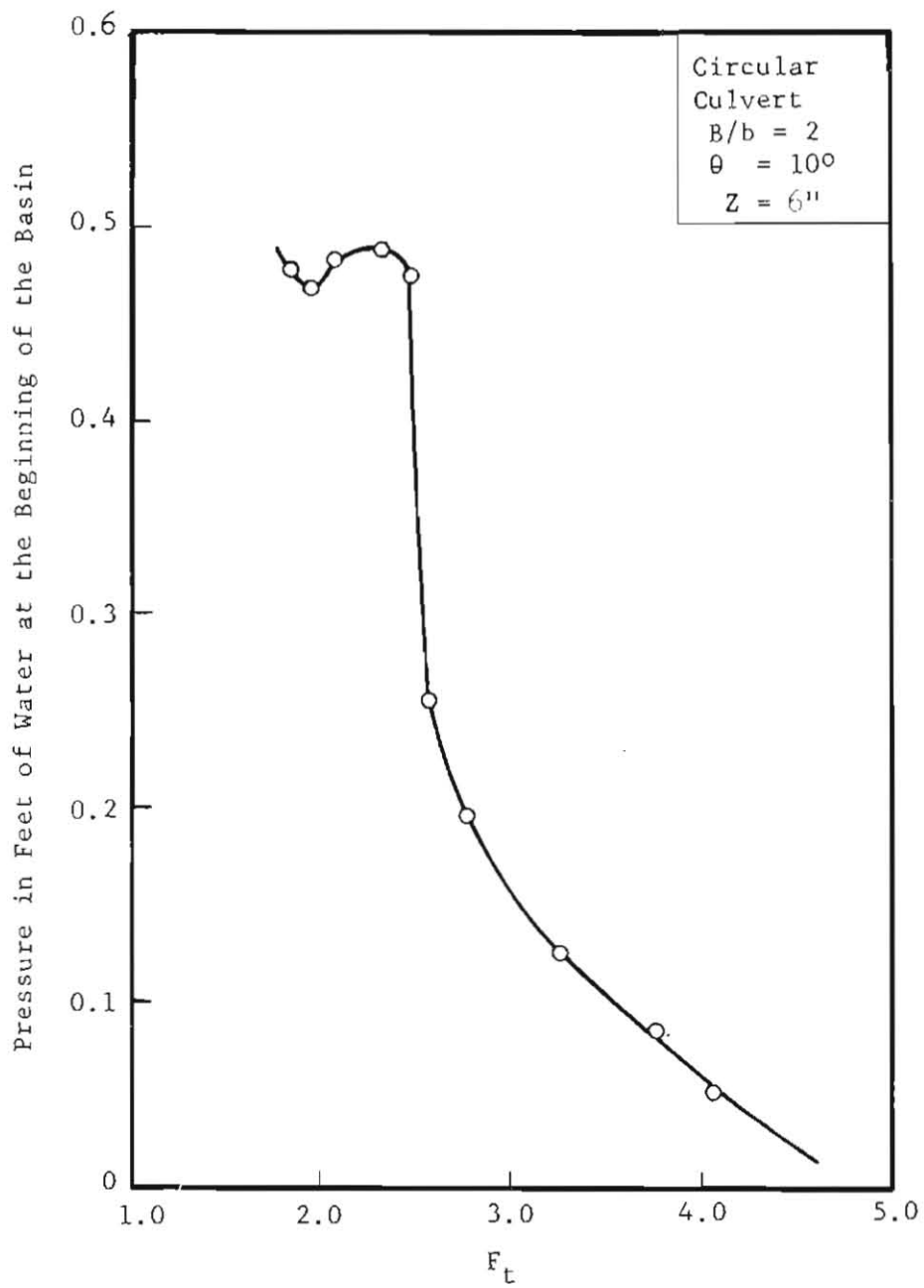
centerline and several symmetrical lines. The symmetrical lines for $\theta = 30^\circ$ were set at 10° , 20° , and 30° from the channel centerline; for $\theta = 22.5^\circ$ they were set at 5° , 10° , 15° , and 22.5° ; for $\theta = 15^\circ$ at 5° , 10° , and 15° ; and for $\theta = 10^\circ$ at 5° and 10° .

Along the wingwalls an oscillating high wave was formed which caused a decrease in the accuracy of the depth reading to ± 0.003 ft. As the supercritical flow advanced downstream into the rectangular channel, some shock waves were formed which reduced the accuracy of depth reading to ± 0.01 ft. The shock waves are usually found in supercritical flow in channels of nonlinear alignment or nonprismatic section.

Since the general configuration of the trapezoidal section was such that the jump was formed primarily due to the contraction in the stilling basin with hardly any tailwater requirements, the radial profile of the supercritical flow was not determined for this configuration. The hydraulic jump in this case was normally formed close to the beginning section of the flared wingwalls within the basin. A noticeable increase in the tailwater depth forced the jump to move upstream and eventually submerged it.

Limiting Froude Number F_t for Valid Experimentation

Several undesirable characteristics were observed when the Froude number (F_t) exceeded a certain limit. One of the most important of these characteristics is indicated in the graph of pressure at the beginning of the stilling basin vs. Froude number at the entrance channel in Figure 3-7. Study of this graph indicated that when F_t was increased to 2.56 for the geometrical arrangement which was tested, there was a sudden decrease in

FIG. 3-7 FROUDE NUMBER F_t vs. PRESSURE

pressure quickly approaching atmospheric or zero gage pressure. This was attributed to the fact that above this limiting F_t , separation between the flow and channel bottom at the downstream portion of the entrance channel took place. This separation of flow defeated the purpose of proper design of the curvature of entrance channel. It was expected to have a negative pressure beneath the nappe when separation of flow occurred. In this case, however, when the separation occurred the overfalling jet was completely aerated; that is, the upper and lower nappe surfaces were subject to full atmospheric pressures. The negative pressure would be only due to the removal of the air from underneath the nappe by the overfalling jet. For other design values of F_t proper dimensions of the structure could be determined to avoid any serious problem. Another undesirable feature of high F_t in this experiment was an extremely rough surface which occurred on the flow because of sudden expansion from the circular conduit to the rectangular entrance channel. This factor affected the degree of uniformity of the supercritical flow in the stilling basin.

Because of the above mentioned features, the range of valid experimentation was limited to F_t of less than or equal to 2.56 when value of Z was six inches. A graph similar to Figure 3-7 for a Z value of eighteen inches showed a limiting F_t of 2.25. It should be noted, however, that higher Froude numbers (F_t) could be used if the design of the curvature of the entrance channel is changed to suit the particular range of F_y in mind. The design of the curvature of entrance channel is dependent upon the magnitude of the allowable negative pressure on the bed of entrance channel and its detailed procedure is outlined in the next chapter. Previous experimental work showed that higher limits of F_t could be tolerated if a

box culvert was used instead of the circular pipe when the dimensions of the entrance channel were unchanged.

Discussion of the performance characteristics and factors influencing basin design is treated separately for rectangular and trapezoidal downstream channel models to prevent complications in the analyses of the results. An overall comparison of the two models would be made with special emphasis on advantages or disadvantages of each model after they are discussed separately.

I - Rectangular Downstream Channel

Three basic performance characteristics are of interest in the study of rectangular downstream channel basins. These characteristics are the degree of stability of the hydraulic jump, the degree of velocity reduction when flow passes over the basin, and the general appearance of water surface profile. A detailed study of each one of these factors is followed:

Stability of the Hydraulic Jump: The criterion chosen for determination of the stability of the jump was the change in the position of the jump when flow condition was subject to a change in tailwater depth keeping all other parameters constant. The position of the jump was indicated by distance x , where x was the distance along the centerline from beginning of the basin to the leading edge of the jump. An increase in tailwater depth corresponded to a decrease in the magnitude of x , and a decrease in tailwater depth corresponded to an increase in the magnitude of x .

When the tailwater continued to increase, the hydraulic jump moved upstream until the jump was completely submerged. After the jump was submerged, a further increase in the tailwater depth did not affect the position of the jump. On the other hand, if the tailwater depth continued to decrease, it reached a value in which the jump was completely eliminated. When the jump was eliminated a series of shock waves appeared on the downstream channel. Therefore, the effectiveness of this type of geometric arrangement was dependent upon an upper and lower limits of the tailwater depth.

Experimental as well as analytical investigations of this type of basin configuration revealed that the required depth of tailwater to stabilize the hydraulic jump at a certain position (x) depended on V_t , y_t , and g . Where, V_t and y_t were the mean velocity and the depth of flow at the upstream end of the entrance channel respectively, and g was the acceleration of gravity.

These variables were combined to obtain the dimensionless parameters y_2/y_t , x/y_t , and F_t . F_t is the Froude number at the upstream end of the entrance channel, and y_2 is the sequent depth of the hydraulic jump. The computation of F_t was based on the mean velocity of flow at the end of the circular conduit. The mean velocity was determined by using y_t as the depth of flow inside the circular conduit. The dimensionless parameters y_2/y_t , x/y_t , and F_t are especially advantageous in the analysis of results and the graphical representation of the variables.

Experimental procedures established for the study of the stability of the hydraulic jump required determination of the functional relationships between y_2/y_t and x/y_t for constant values of F_t and y_t/b . These

functional relationships are presented graphically on plots of y_2/y_t vs. x/y_t for a given F_t in Figures 3-8 through 3-11. Different values of F_t were selected by either changing the discharge and keeping y_t unchanged, or by keeping the discharge unchanged and varying y_t .

The degree of the stability of hydraulic jump at any given section of the basin is indicated by the slope of the curve of y_2/y_t vs. x/y_t at that section. The slope of the curve could be determined from a tangent to the curves at the intended section. Study of the general pattern of these curves indicated that as x/y_t increased the slope of the curve decreased until it became nearly horizontal. It should be noted that the stability of the jump was directly related to the absolute value of the slope of the curves of y_2/y_t vs. x/y_t . The higher the absolute value of the slope the more stable was the jump position. Furthermore, it was interesting to note that, within the stilling basin the absolute value of the slope was quite high. As soon as the jump moved downstream outside the region of wingwalls, the magnitude of slope decreased rapidly approaching zero. This pattern of variation in the absolute value of slope was an indication of the effectiveness of the basin and flaring wingwalls in stabilizing the jump. The position of the end of the wingwalls was marked in every curve for the purpose of comparing jump stability within the basin and downstream from the basin. Analyses of these curves also indicated that when the jump moved downstream, leaving the stilling basin, the slope of the curve did not immediately reach its limiting low value. This was an indication of the radial flow effectiveness in stabilizing the jump even when it was moved outside the basin. Of course, this stabilizing effect did not continue to exist if the jump continued moving downstream.

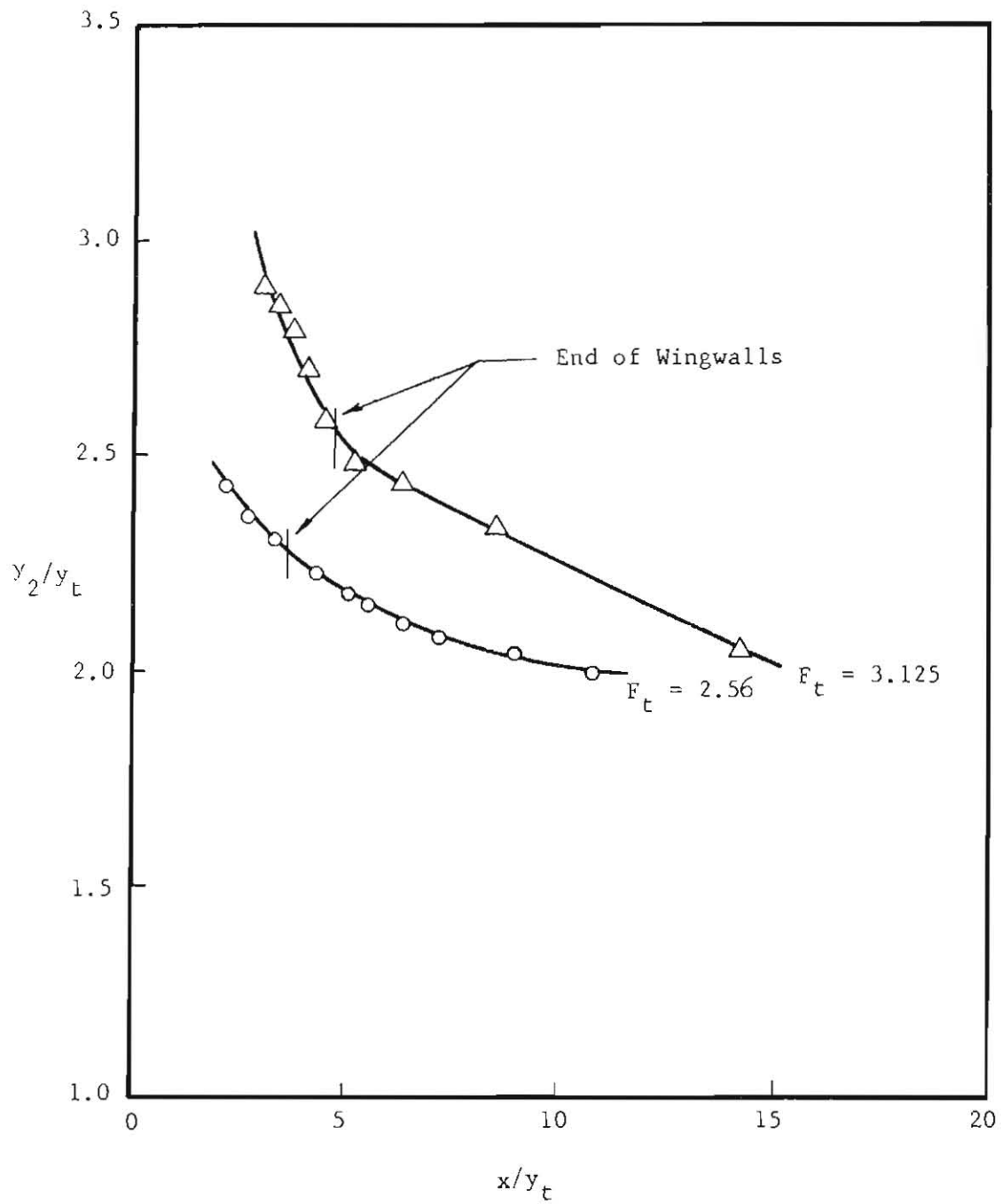


FIG. 3-8 PLOT OF y_2/y_t vs. x/y_t FOR ARRANGEMENT REC1

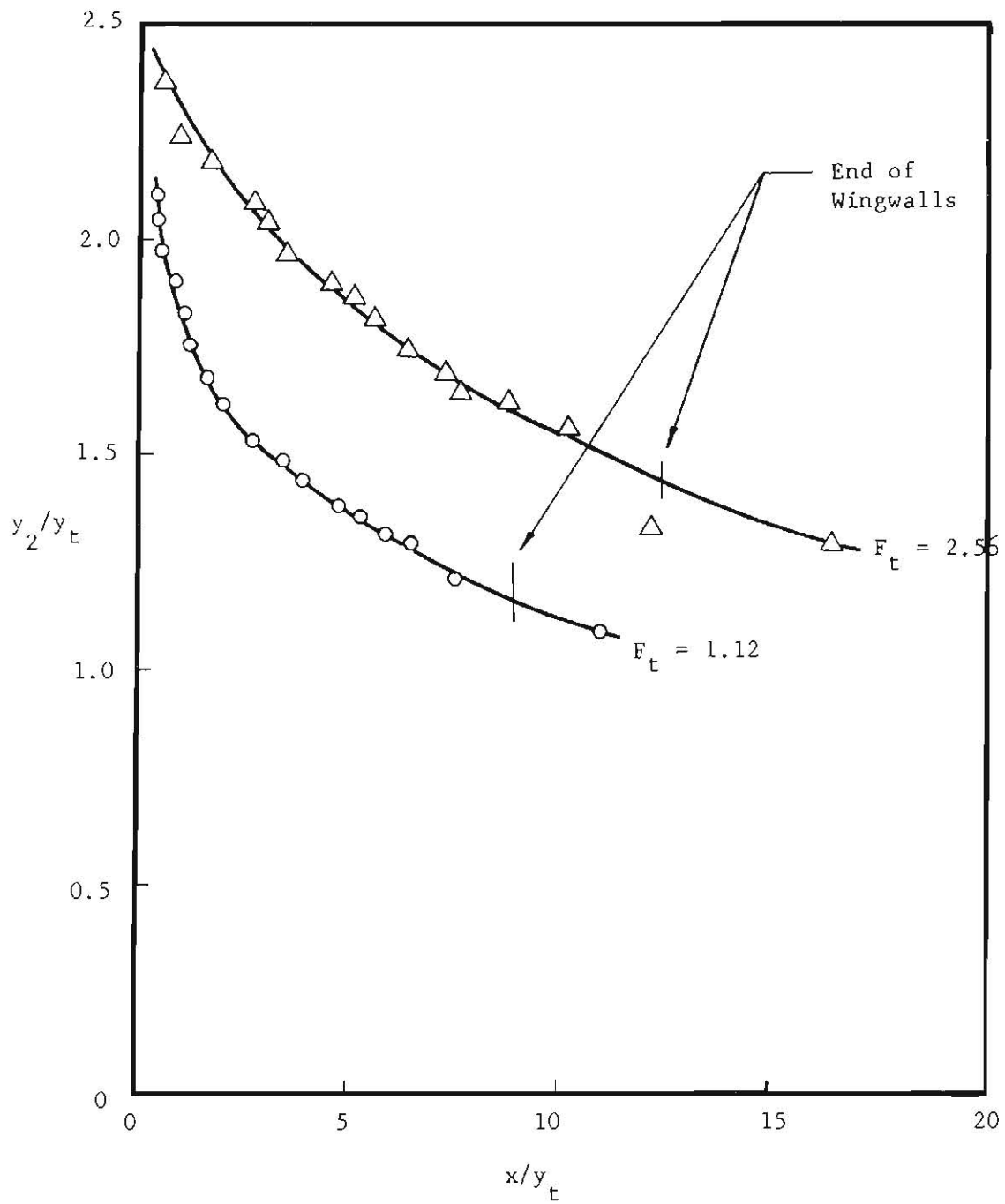


FIG. 3-9 PLOT OF y_2/y_t vs. x/y_t FOR ARRANGEMENT REC2

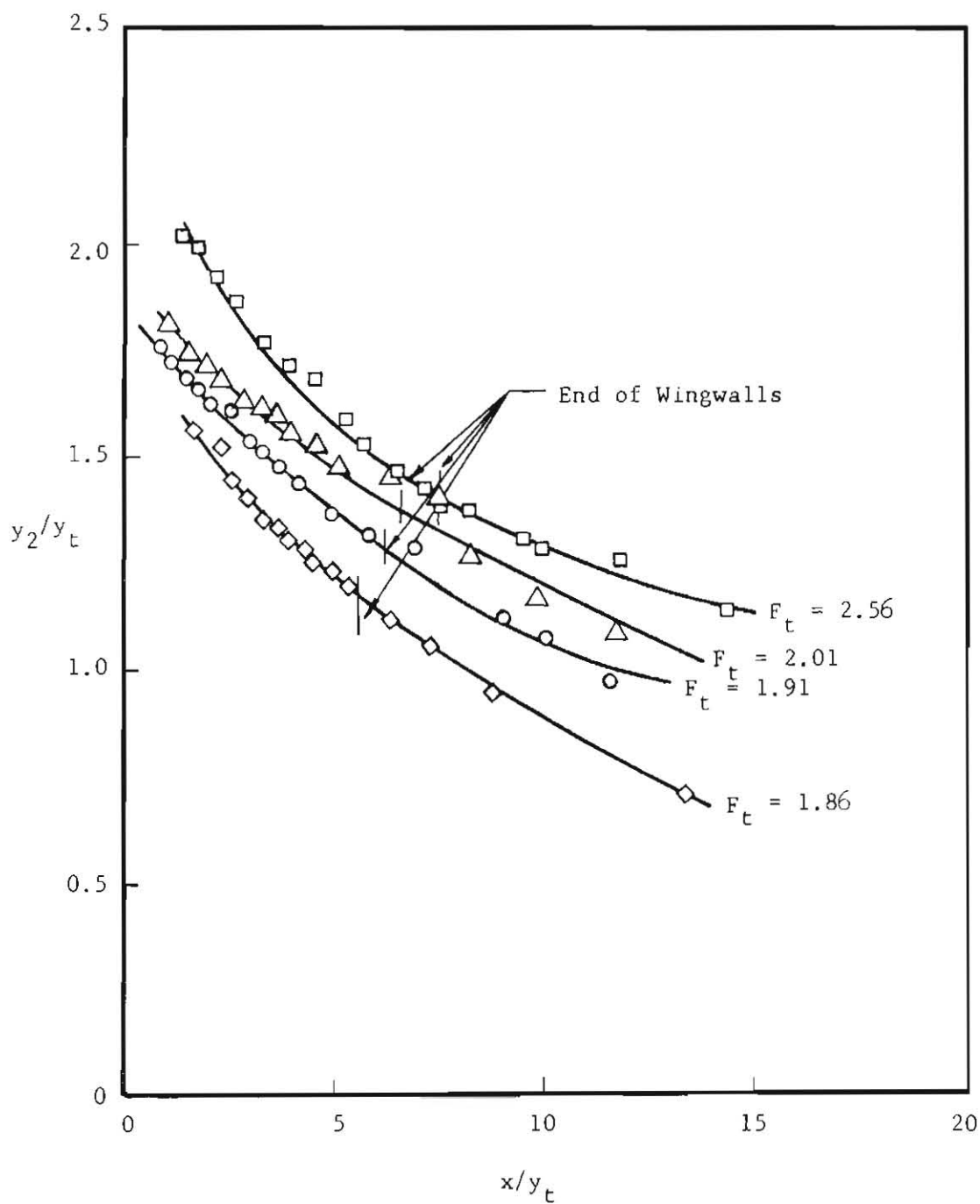


FIG. 3-10 PLOT OF y_2/y_t vs. x/y_t FOR ARRANGEMENT REC3

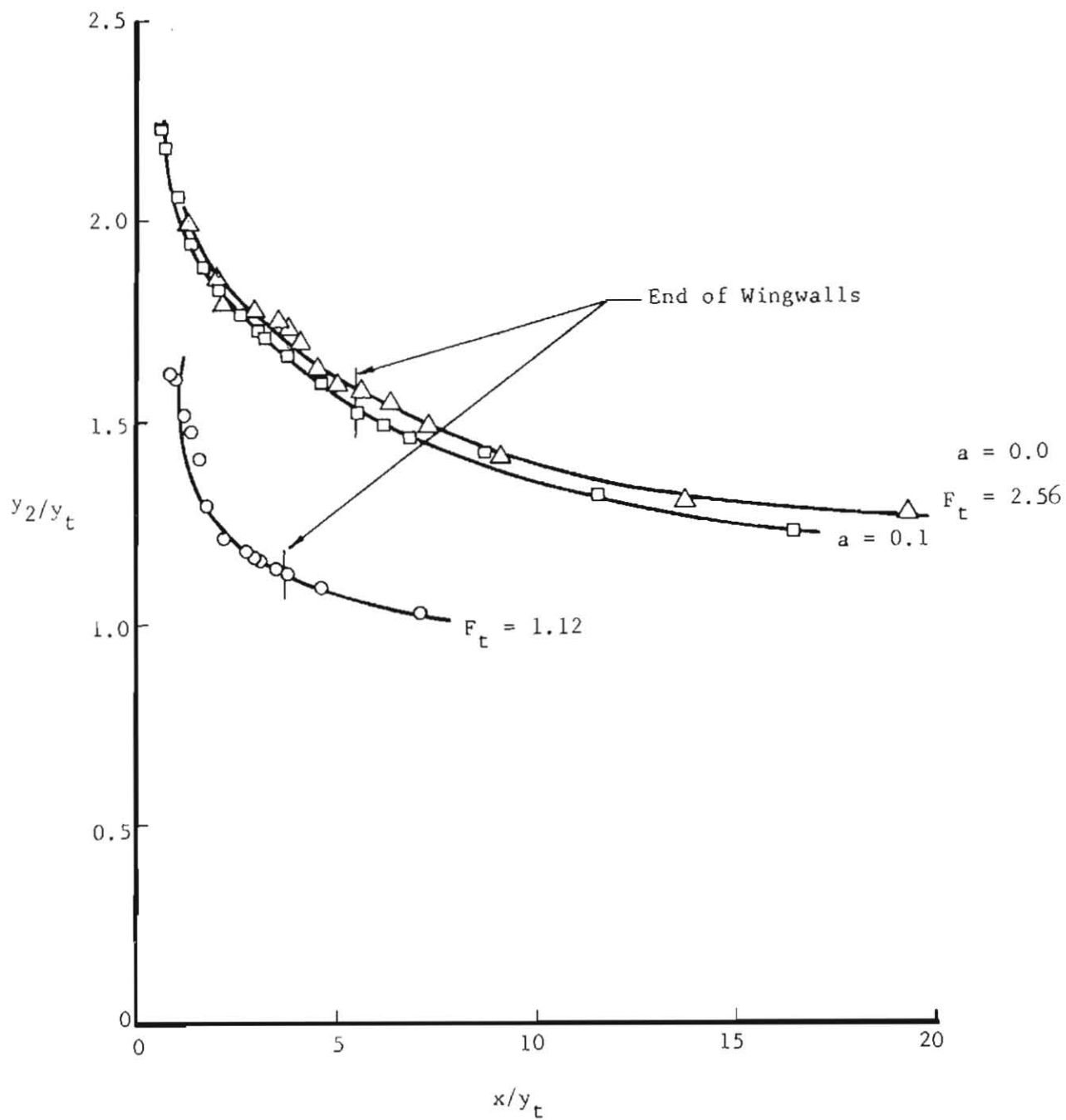


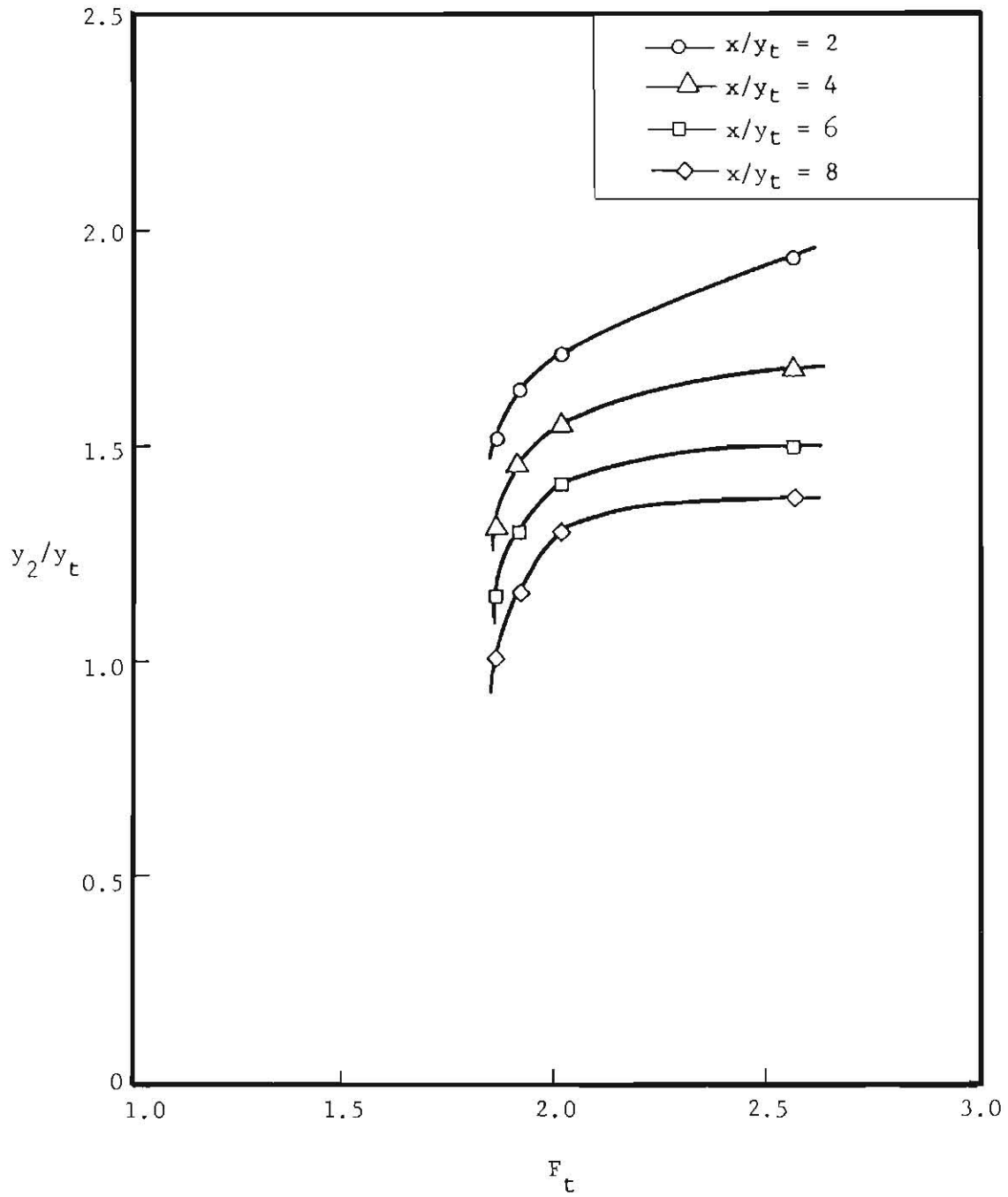
FIG. 3-11 PLOT OF y_2/y_t vs. x/y_t FOR ARRANGEMENT REC4

Eventually, at some point in the downstream channel the jump was completely eliminated.

In order to investigate the effect of Froude number (F_t) on the stability of hydraulic jump a graph of y_2/y_t vs. F_t was prepared as shown in Figure 3-12. The values used in plotting the curves of this figure were interpolated from the curves of Figure 3-10 and should not be interpreted as original data. The most effective range of F_t , resulting in a large variation of y_2/y_t for constant values of x/y_t , occurred when F_t was smaller than 2.0. Since this effective range of F_t was only investigated in arrangement REC 3 a general statement with regard to its importance cannot be made at this time. On the other hand, examination of Figures 3-8 to 3-11 indicated the effectiveness of F_t on jump stability. As shown in these figures, the absolute slope of the curves within the basin increased as F_t decreased for a given position of the jump.

The comparison of the relative jump stability characteristic of each geometric arrangement tested in this experimental study could be made from the curves of y_2/y_t vs. x/y_t . So far as the stability criterion was concerned, arrangement REC 3 appeared to be the most effective basin followed by arrangement REC 4. Arrangement REC 1 was not particularly suitable for radial jump energy dissipation as it did not provide sufficient expansion of flaring wingwalls which in turn limited the opportunity for full radial flow development.

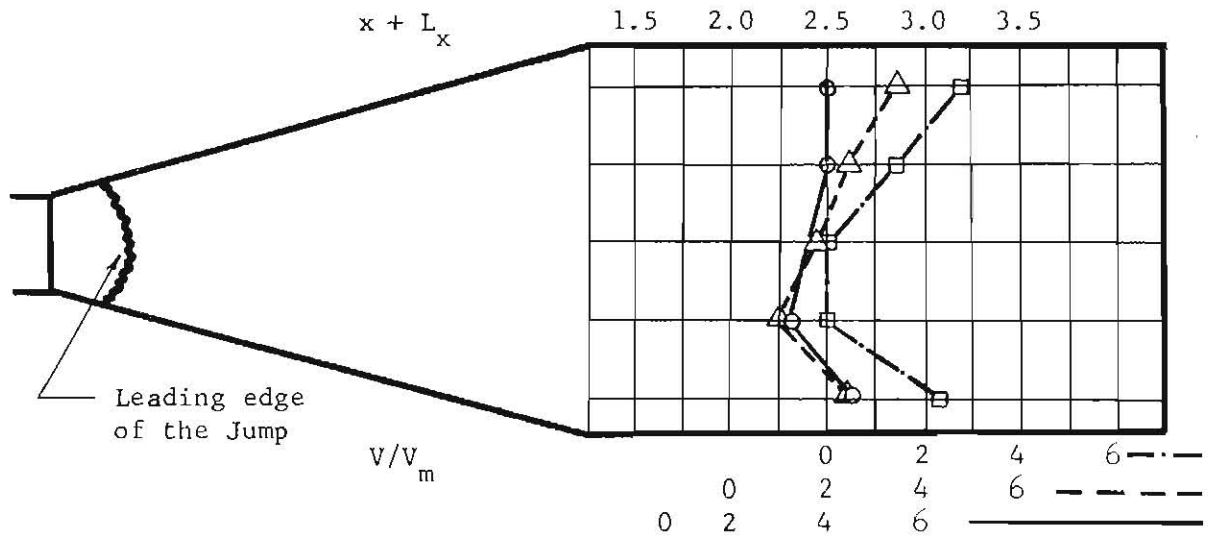
Velocity Distribution and Reduction: Velocity measurement were obtained at 0.03 foot and $0.4 y_2$ from the channel bottom at the downstream channel to determine the transverse velocity distribution and gain some

FIG. 3-12 PLOT OF y_2/y_t vs. F_t FOR ARRANGEMENT REC3

knowledge of the degree of velocity reduction within the basin. The procedure followed in making the velocity measurements was to set the flow at a particular Froude number (F_t) and stabilize the position of the jump by adjusting the tailwater depth. Three different jump positions were tested in each experiment. The leading edge of the jump for these positions was set at 0.4, 1.0, and 1.5 ft. from the beginning of the flaring wingwalls. The transverse sections downstream from the jump at which the velocity measurements were made are indicated by the distance $x + L_x$. Parameter x was defined previously and L_x was the distance along the centerline of channel from the leading edge of the jump to the section at which velocities were measured. Distance $x + L_x$ is shown in Figures 3-13 through 3-24. The relative importance of velocity at each section in these figures is indicated by a dimensionless parameter, V/V_m . The plotted velocities were measured at three different transverse sections. These figures facilitated the comparison of general pattern and magnitude of velocities for a given F_t and a fixed jump position. The measurements of velocity were obtained for F_t equal to 1.12, 1.86, and 2.56.

It should be noted that in all velocity measurements the Pitot tube was placed in a longitudinal direction parallel to the channel centerline. Therefore, the measured velocities at some points could have been slightly lower than the actual velocities. Within the center section of the channel the velocity direction was nearly parallel to the Pitot tube and the measured velocities in this region coincided with actual velocities. In regions close to the channel walls, however, some discrepancy from the true velocity was expected. This discrepancy was not appreciable for the purpose of this experimental work and could be safely neglected.

Pitot Tube at 0.03'



Pitot Tube at 0.4 y_2

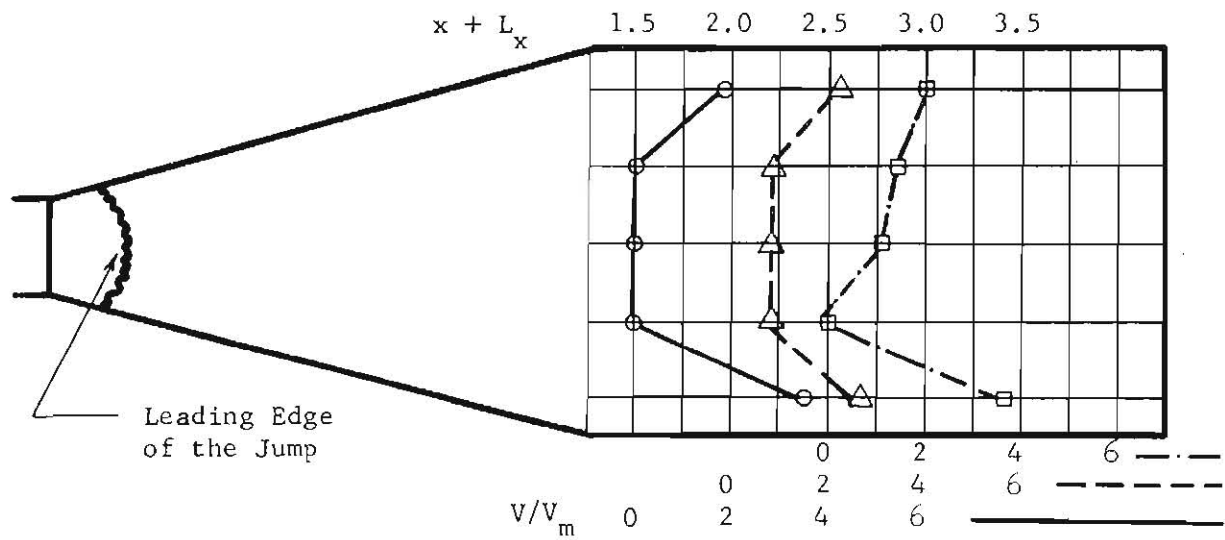


FIG. 3-13 VELOCITIES IN DOWNSTREAM CHANNEL FOR ARRANGEMENT REC2

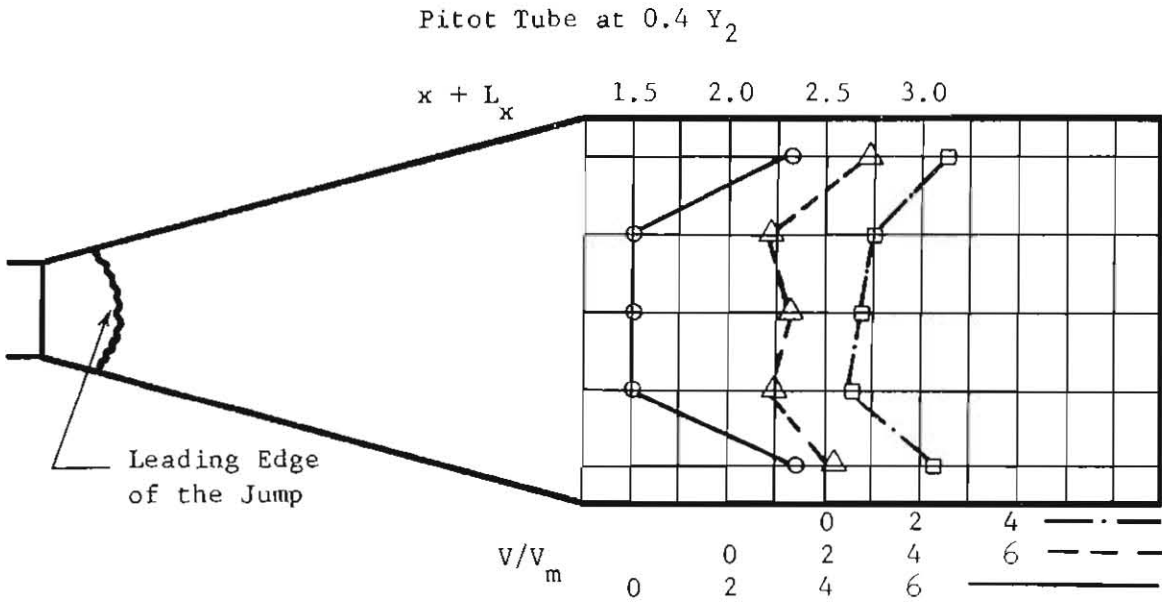
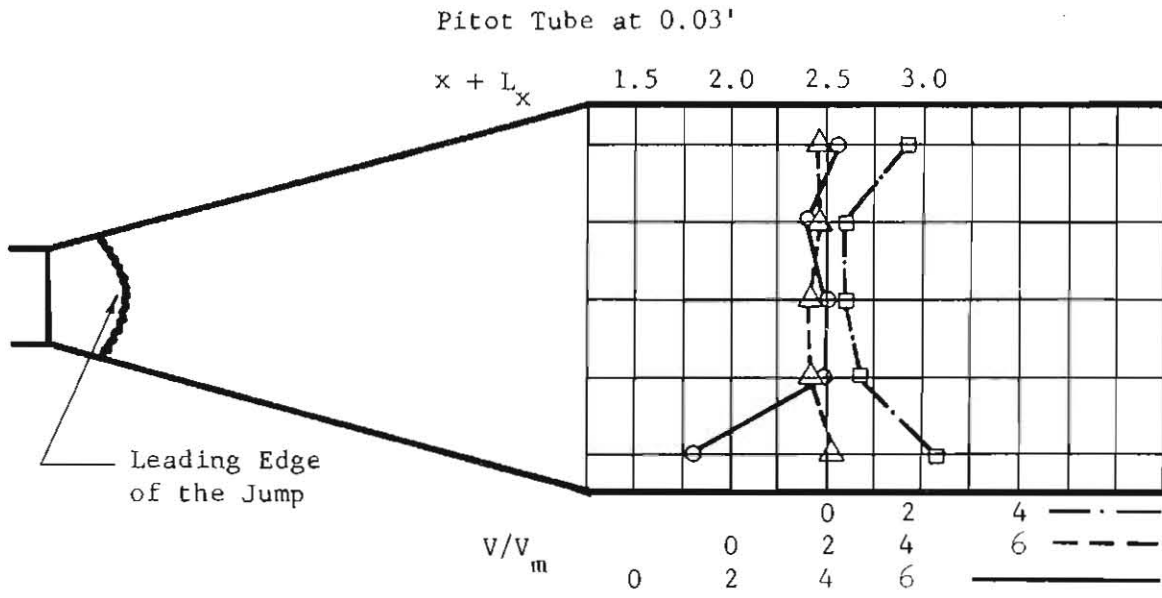


FIG. 3-14 VELOCITIES IN DOWNSTREAM CHANNEL FOR ARRANGEMENT REC2

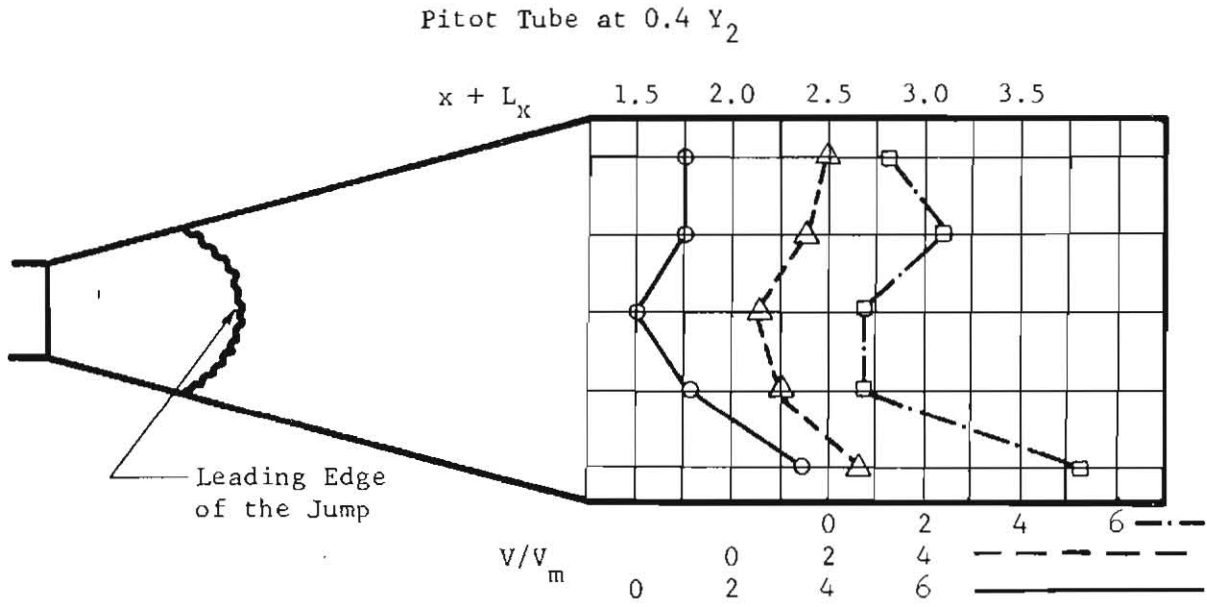
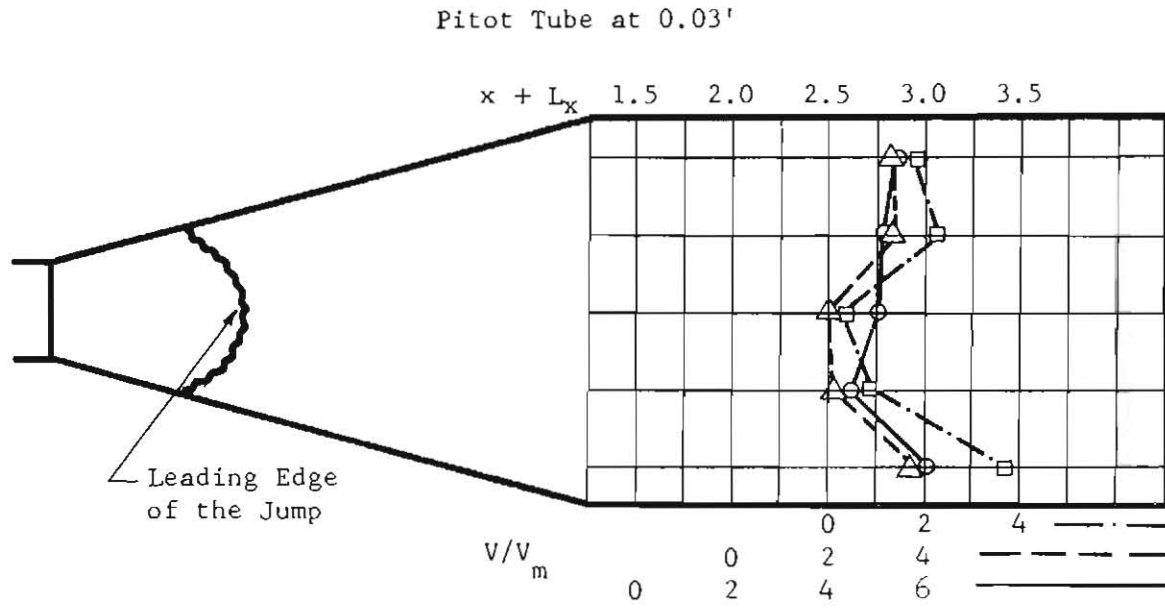


FIG. 3-15 VELOCITIES IN DOWNSTREAM CHANNEL FOR ARRANGEMENT REC2

$$F_t = 2.56$$

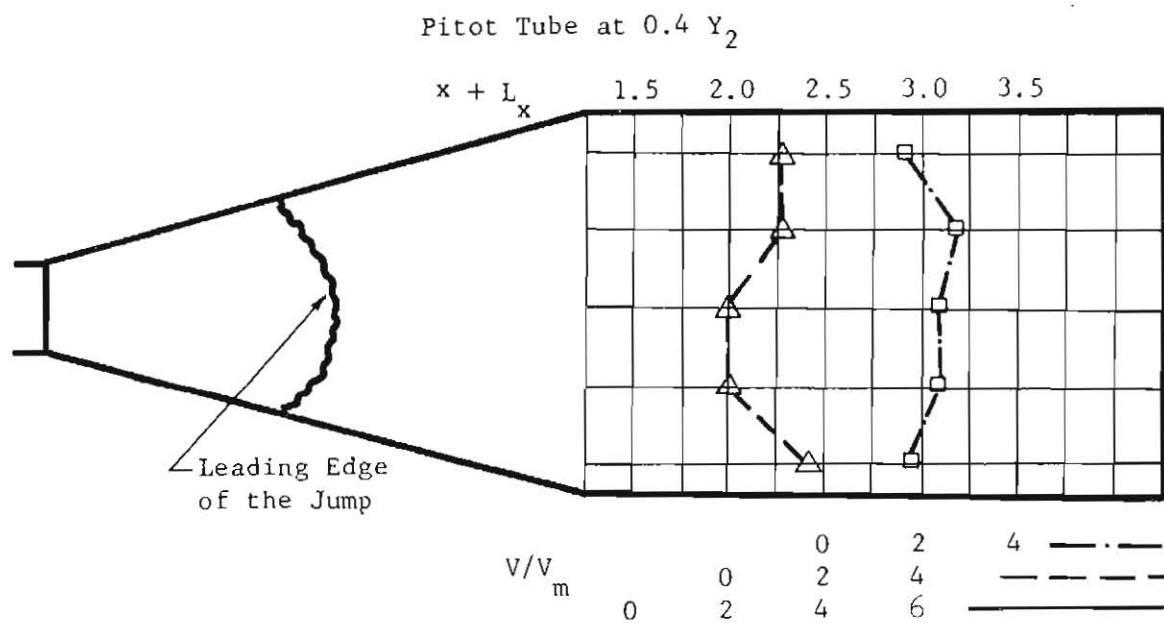
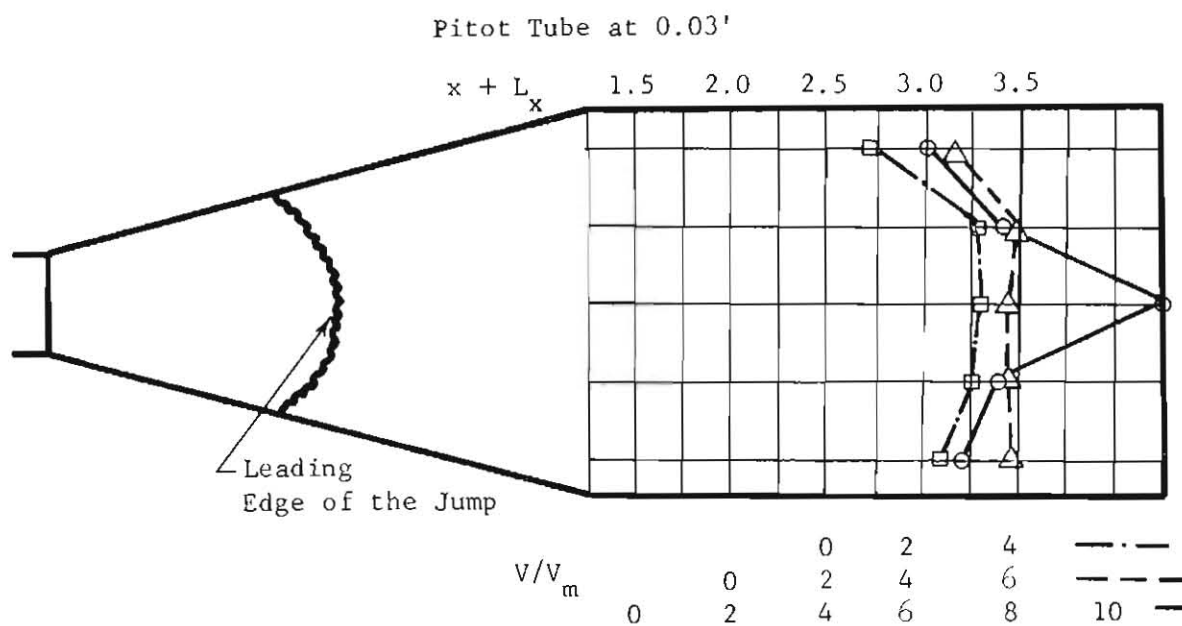


FIG. 3-16 VELOCITIES IN DOWNSTREAM CHANNEL FOR ARRANGEMENT REC2

$$F_t = 1.86$$

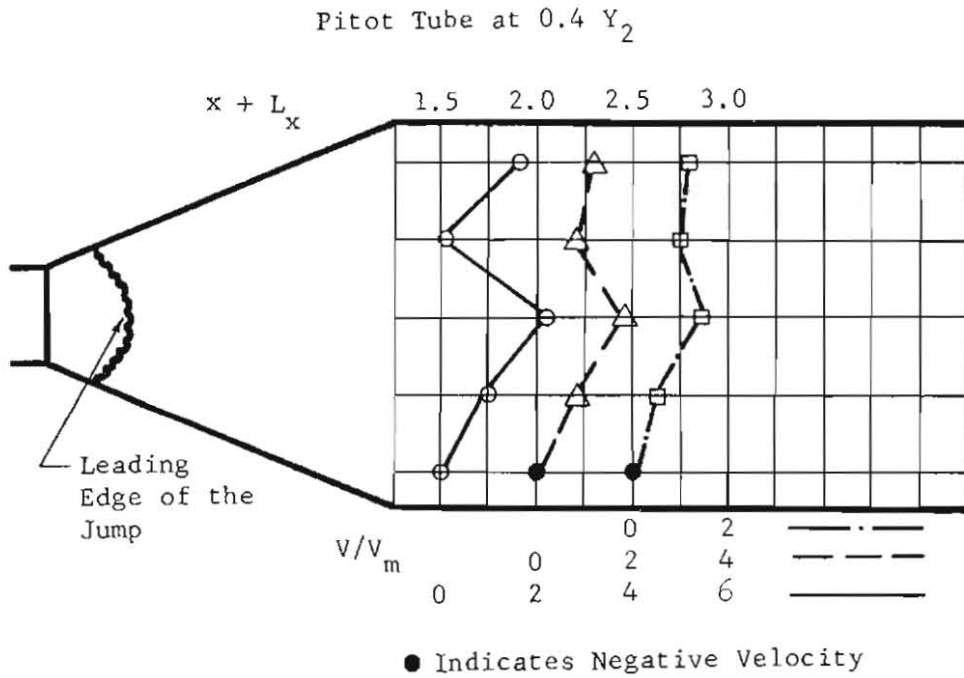
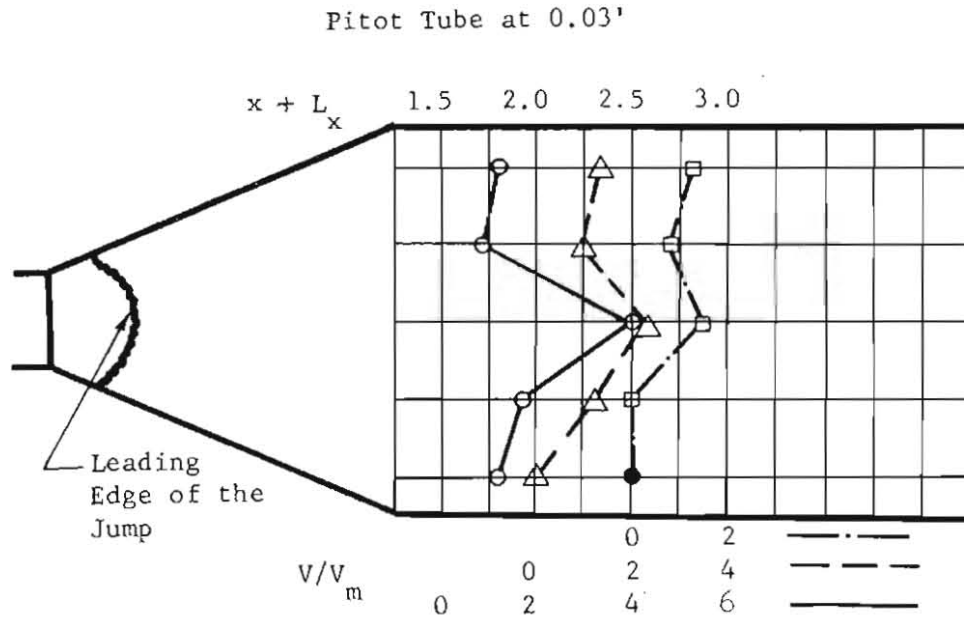
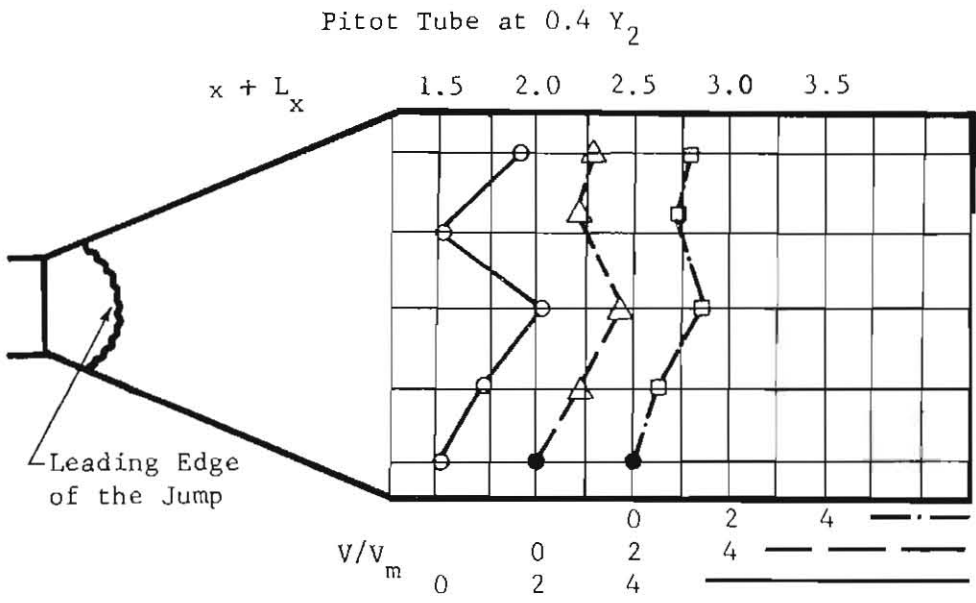
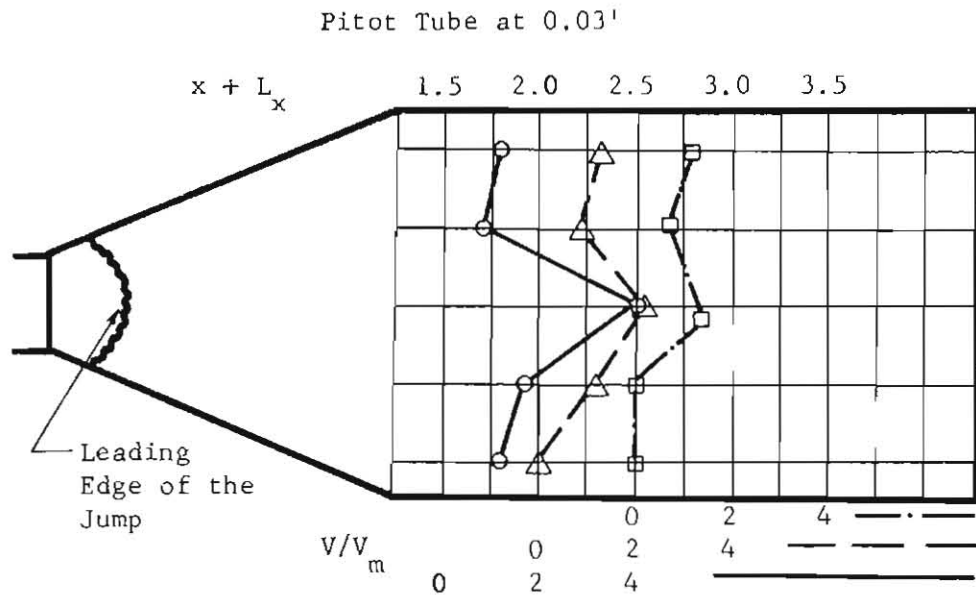
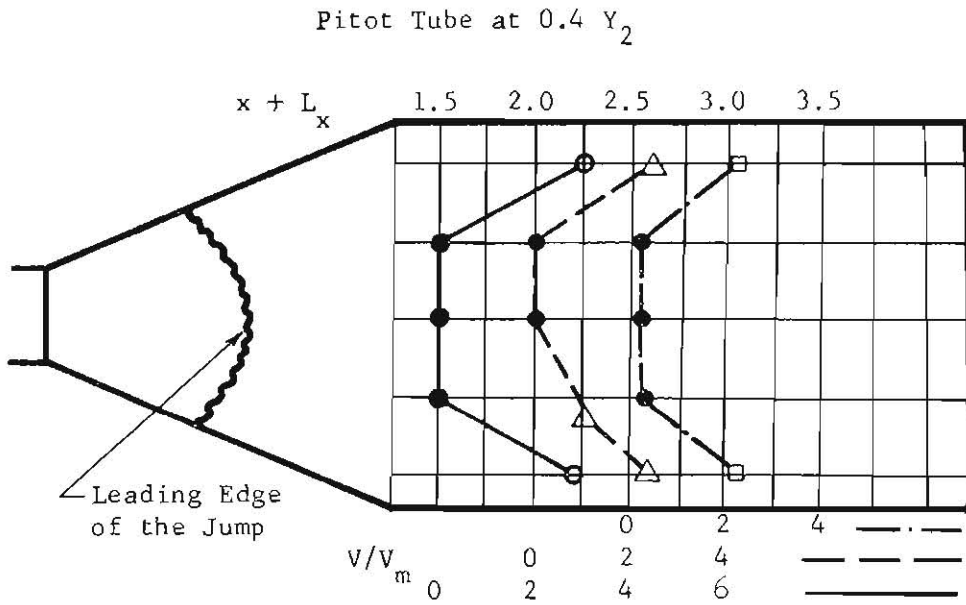
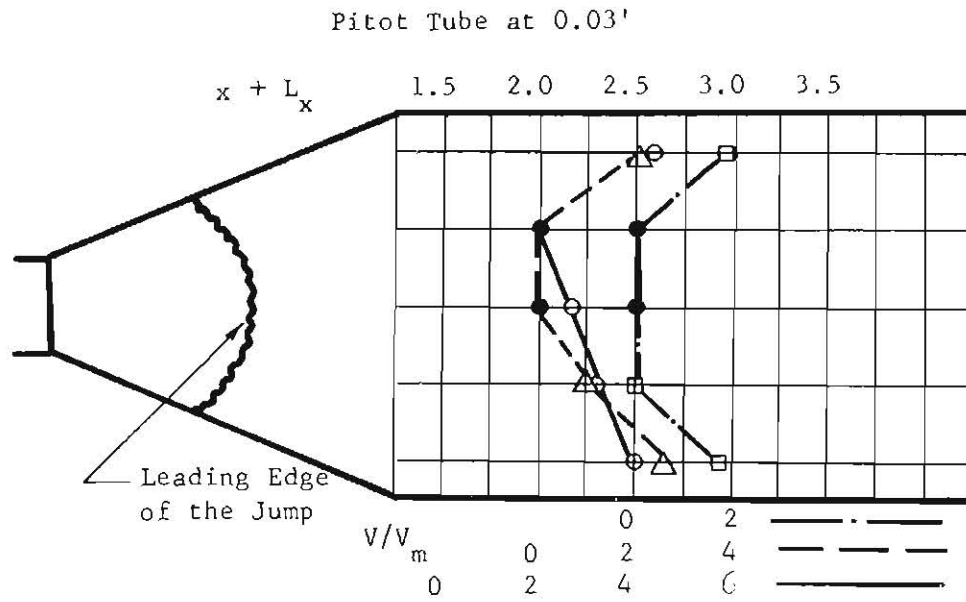


FIG. 3-17 VELOCITIES IN DOWNSTREAM CHANNEL FOR ARRANGEMENT REC3



● Indicates Negative Velocity

FIG. 3-18 VELOCITIES IN DOWNSTREAM CHANNEL FOR ARRANGEMENT REC3



● Indicates Negative Velocity

FIG. 3-19 VELOCITIES IN DOWNSTREAM CHANNEL FOR ARRANGEMENT REC3

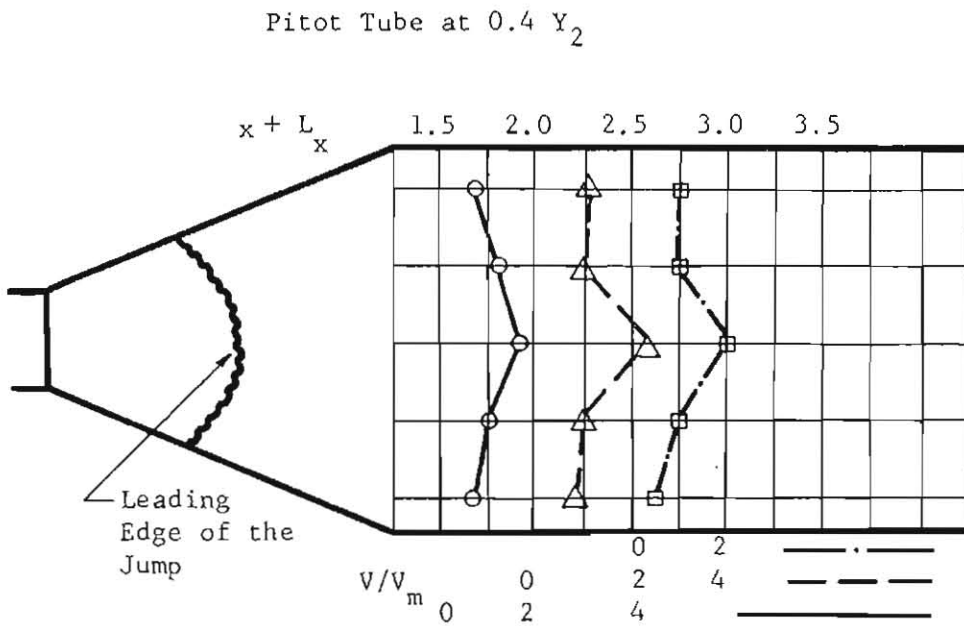
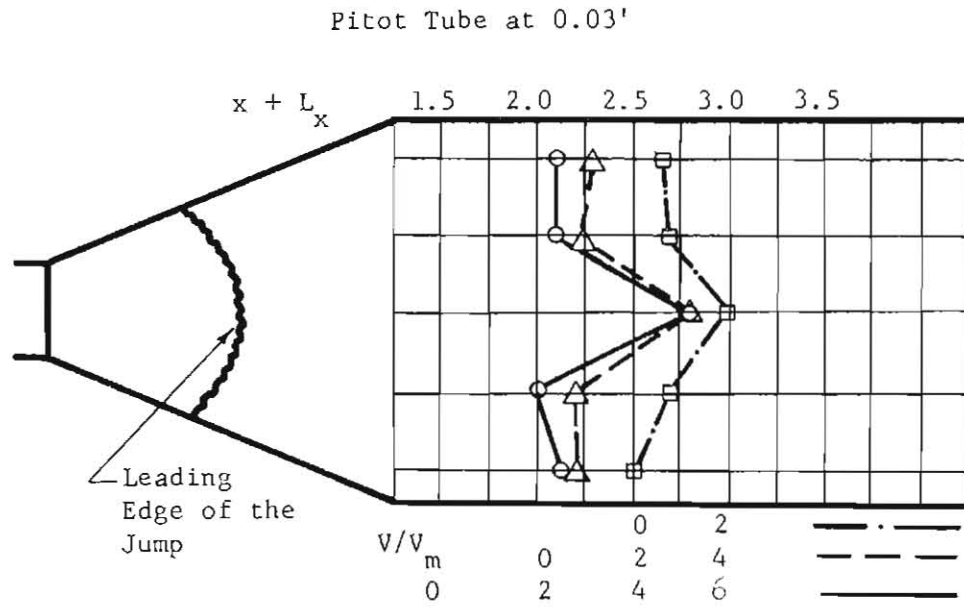


FIG. 3-20 VELOCITIES IN DOWNSTREAM CHANNEL FOR ARRANGEMENT REC3

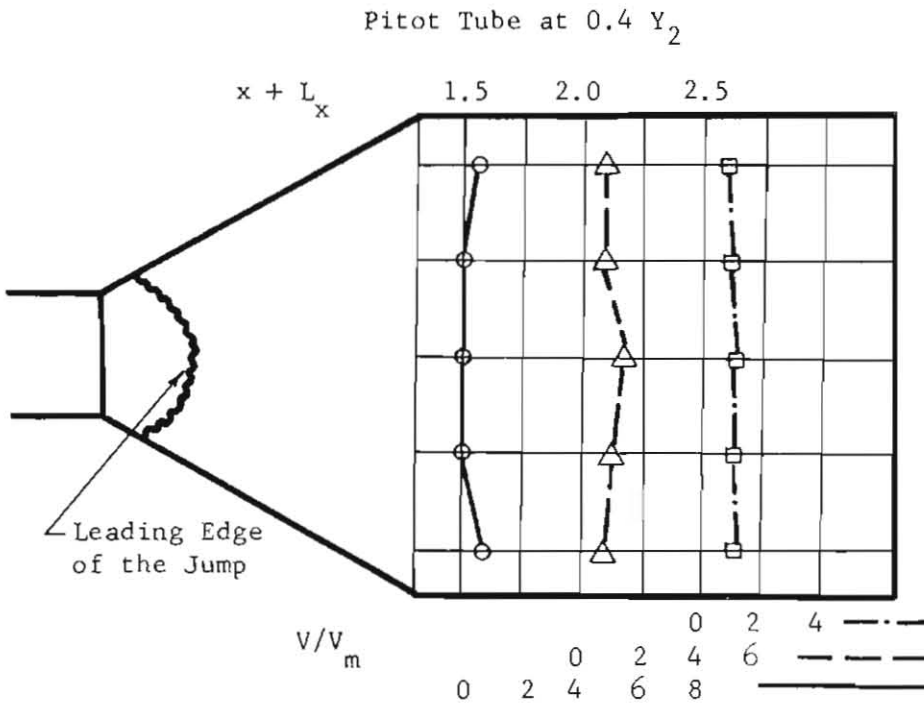
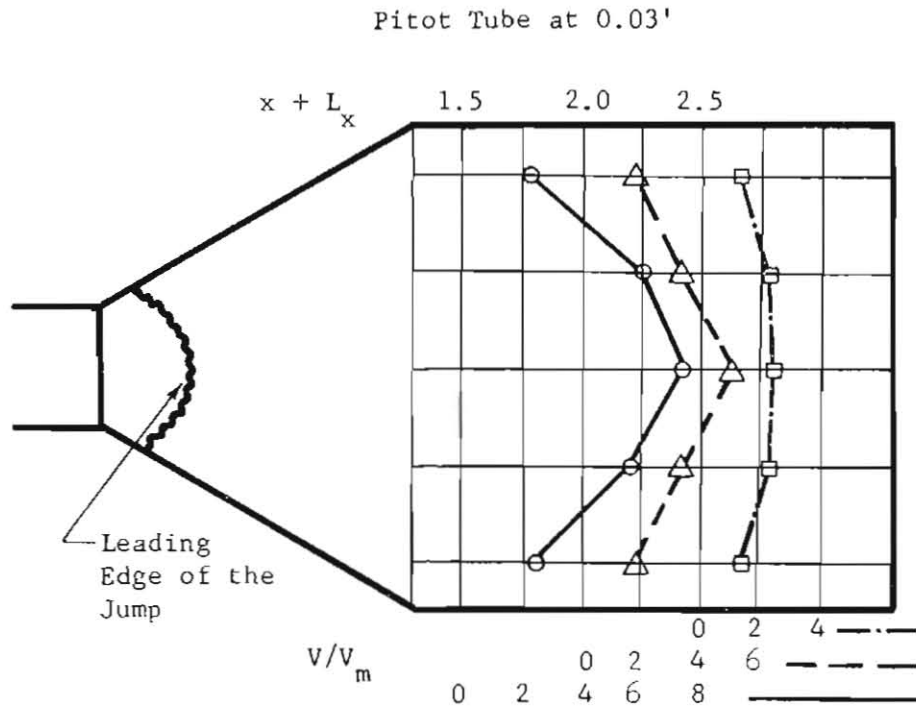


FIG. 3-21 VELOCITIES IN DOWNSTREAM CHANNEL FOR ARRANGEMENT REC4

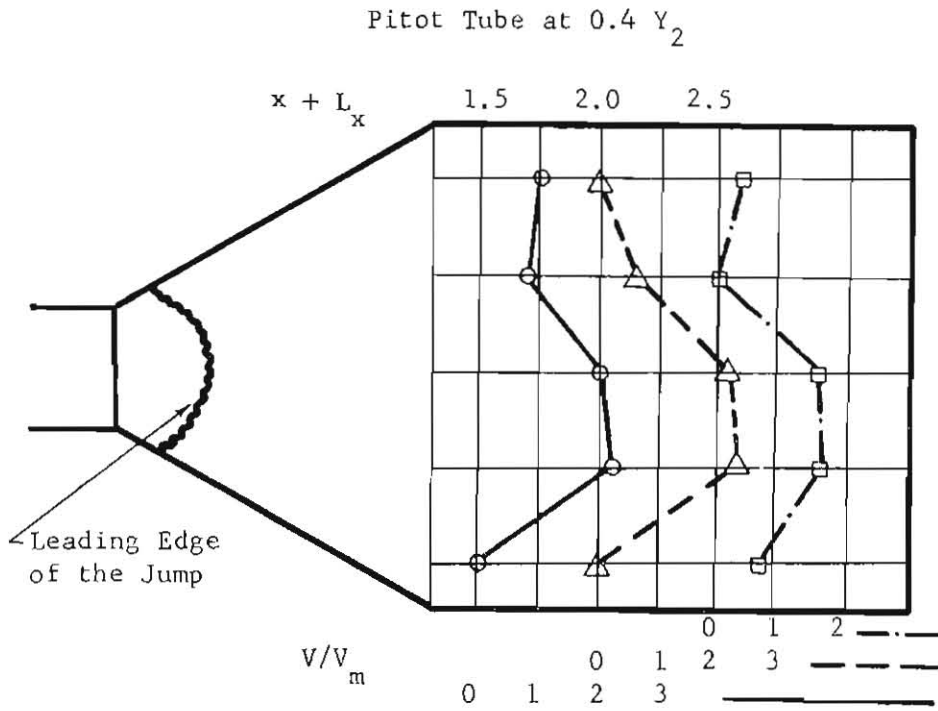
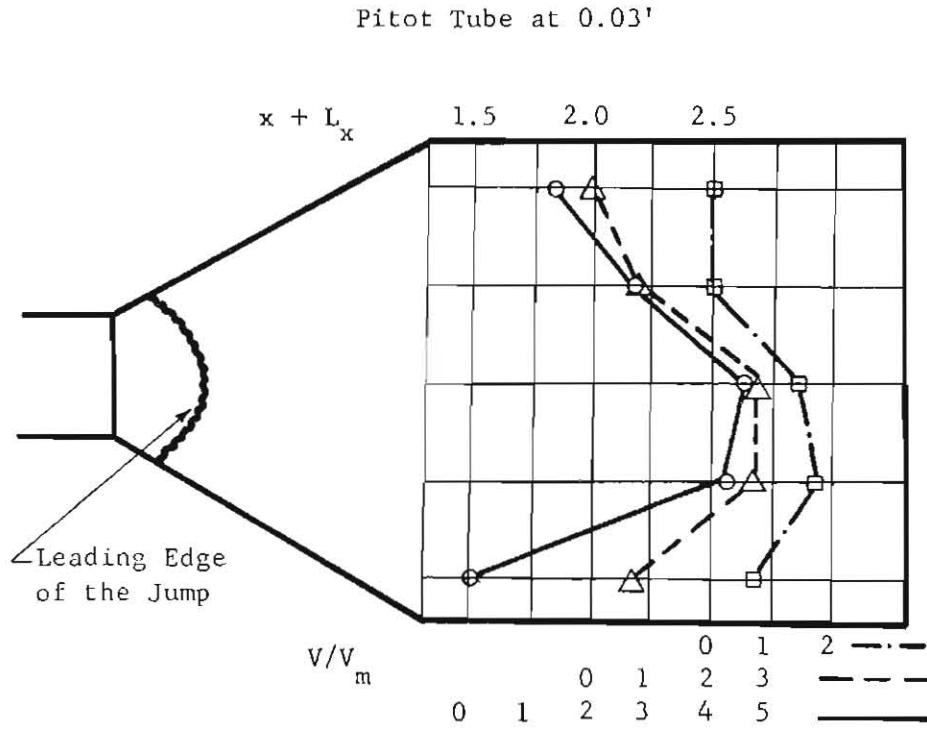
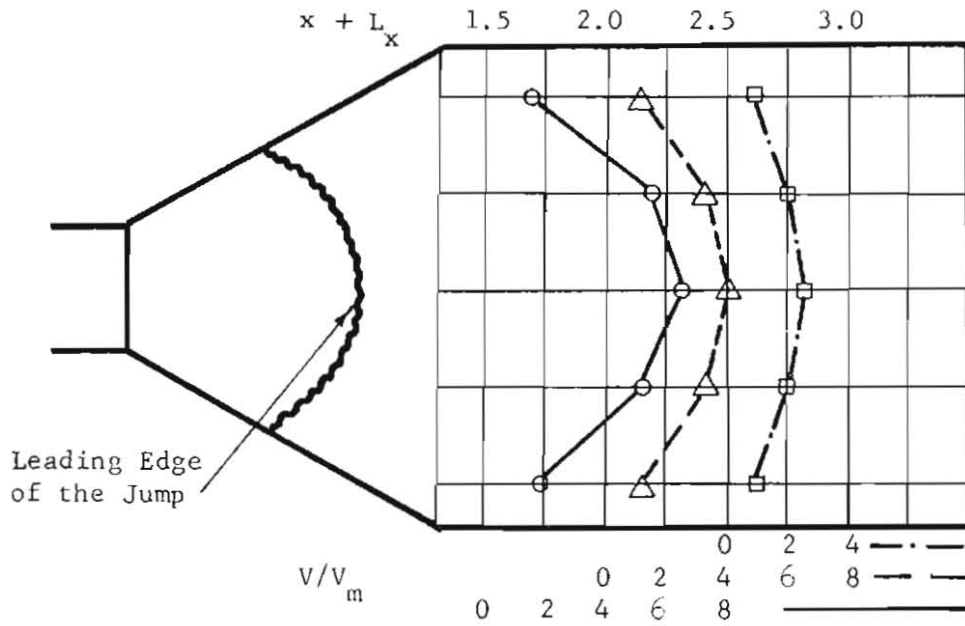
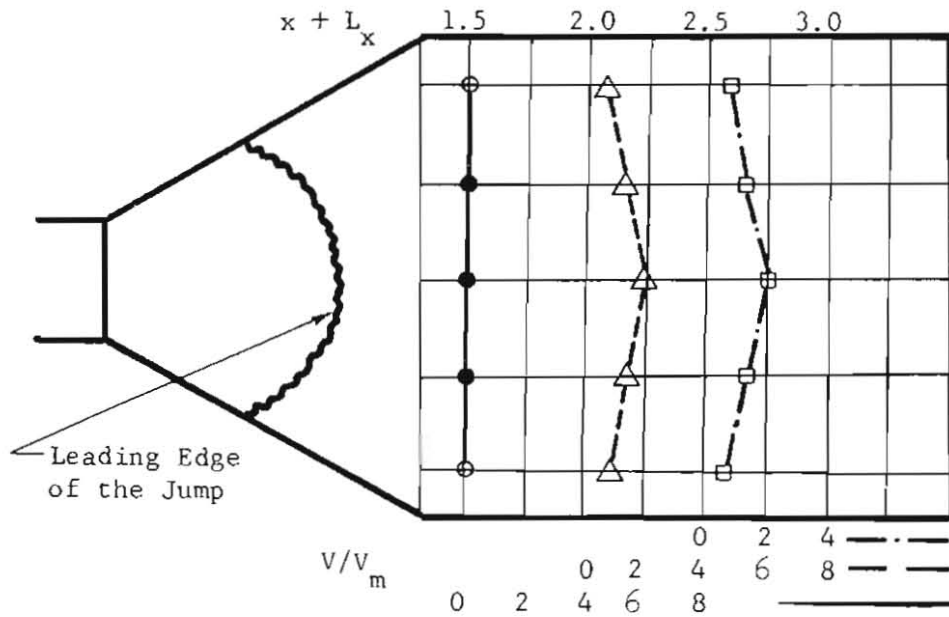


FIG. 3-22 VELOCITIES IN DOWNSTREAM CHANNEL FOR ARRANGEMENT REC4

Pitot Tube at 0.03'



Pitot Tube at 0.4 Y_2

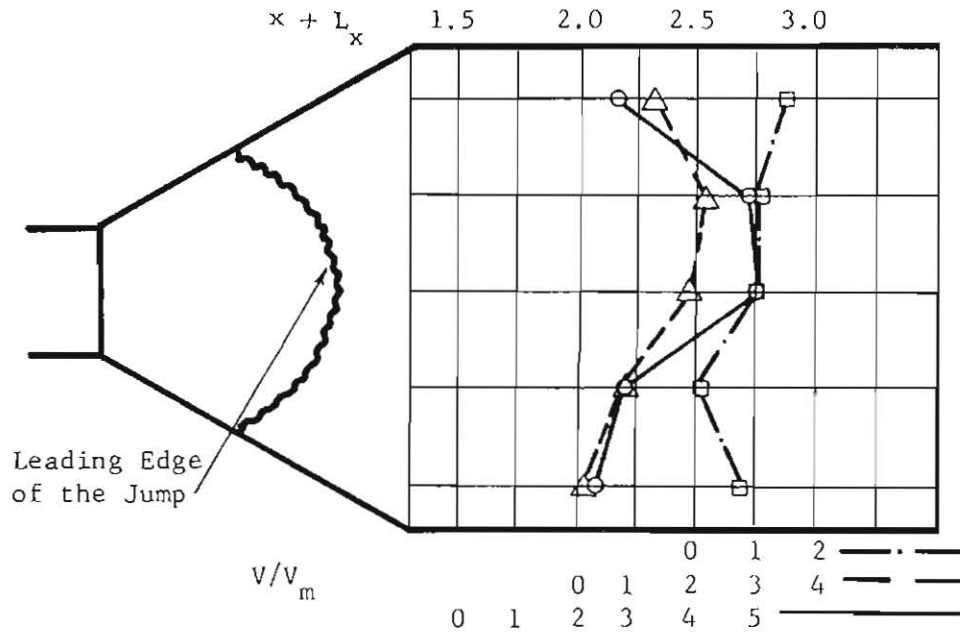


● Indicates Negative Velocity

FIG. 3-23 VELOCITIES IN DOWNSTREAM CHANNEL FOR ARRANGEMENT REC4

$$F_t = 2.56$$

Pitot Tube at 0.03'



Pitot Tube at 0.4 Y_2

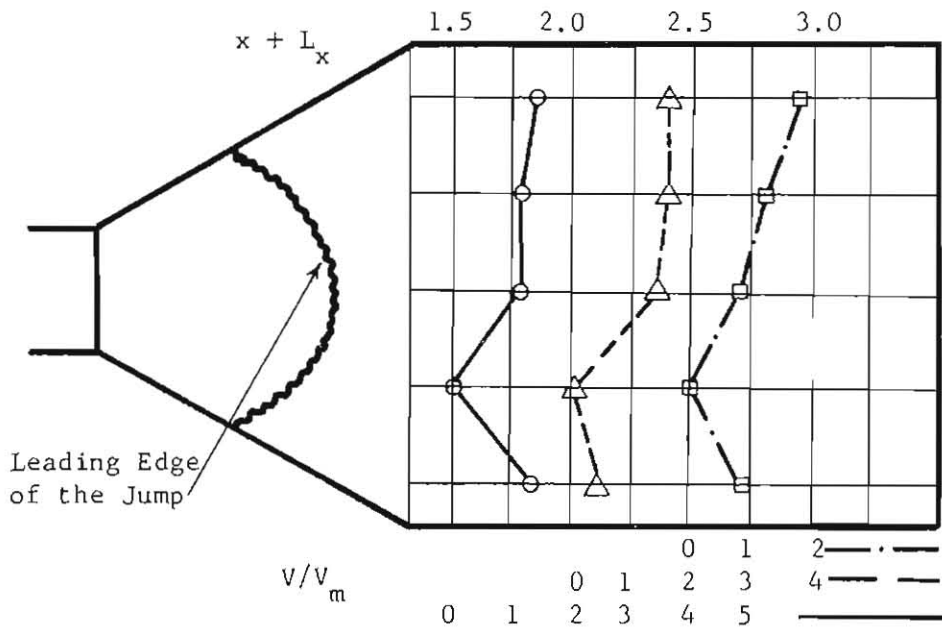


FIG. 3-24 VELOCITIES IN DOWNSTREAM CHANNEL FOR ARRANGEMENT REC4

It was expected that the centerline velocities would be considerably higher than the velocities measured near the sides of the channel. However, this general expected pattern was violated in arrangement REC 2 as shown in Figures 3-13 to 3-16. These figures indicated that the velocity ratios, V/V_m , along the centerline were lower than those near the sides of the channel. The general velocity pattern for arrangement REC 1 was similar to REC 2. This type of velocity variation indicated that when the flaring angle in the stilling basin was reduced to small magnitudes the velocity ratios (V/V_m) increased from the centerline of the channel toward the sides at any transverse section. The deviation from the expected velocity pattern in arrangements REC 1, and REC 2 could be attributed to the insufficient divergence of the flared wingwalls which did not allow full development of radial flow. It was, furthermore, possible that the velocities in the vicinity of centerline of the channel where the measurements were taken had still been under the influence of jump turbulence and radial flow characteristics, while near the sides velocities were resulted from purely parallel flows.

In view of the above discussion, arrangements REC 1, and REC 2 were not suitable basins as far as velocity reduction was concerned. The best structures were arrangements REC 4 followed by REC 3 for reducing the velocity and yet maintaining a fairly uniform velocity distribution in the downstream channel.

The magnitude of V/V_m was generally decreased as the position of the jump was moved downstream. However, the decrease in V/V_m was not an indication of lower velocity (V) for more downstream position of the jump.

The velocities for the downstream jump positions were significantly higher than velocities for the upstream jump positions. This variation in velocity was not indicated by V/V_m because the value of V_m increased at a faster rate than the value of V as the jump position moved downstream. The statement that the velocity increased as the jump moved downstream was confirmed by the magnitudes of the evaluated velocities compiled in test data.

The symmetry of the velocity distribution about the centerline was substantially disturbed in some test runs. The distribution of velocity was skewed to one side of the channel. This skewness could be due to small deviations in the symmetry of channel geometry, or the nonprismatic nature of channel cross section. Arrangement REC 4 performed with very little skewness of velocity distribution profile. Small values of flaring angle could also contribute to the shifting of velocity distribution profile.

The effect of F_t on the downstream velocity was such that, within the range of experimentation, an increase in F_t caused an increase in the ratio of V/V_m provided that the channel geometry and the position of the jump were unchanged.

Water Surface Profile: The degree of angular uniformity of flow was estimated from the water surface profile within the basin when tail-water conditions were such that no hydraulic jump was formed in the basin. In order to determine the degree of the angular uniformity, the flow profile measurements were made along radial distances in each arrangement. The radial lines, along which the flow depth measurements were obtained, were set at 5° , and 10° for arrangement REC 1; 5° , 10° , and 15° for REC 2; 5° , 10° , 15° , and 22.5° for REC 3; 10° , 20° , and 30° for REC 4. The

channel centerline was used as the reference for setting off the radial lines. Flow profile measurements were also taken along the centerline for all arrangements.

Several representative water surface profiles are shown in Figures 3-25 through 3-28. These figures indicate the surface profiles for all arrangements operating at F_t of 2.56. The study of these figures revealed that normally, at any given section, the flow depth on the centerline was slightly higher than the intermediate lines. Furthermore, the depth of flow decreased as the flow advanced downstream which was the characteristic of radial flow basin. A relatively high flow depth was observed adjacent to the flaring wingwalls, especially in the beginning portion of the basin. The existence of this high flow depth could be attributed to an intense pressure build-up in radial direction and the wall effect when the flow entered the basin from the entrance channel. This high pressure diminished as the flow advanced downstream and a rapid decrease in the depth of flow at the sides of the basin subsequently resulted.

Minor deviations in the uniformity of flow depth was observed in all transverse sections within the stilling basin. The nonuniformity of flow depth was mainly due to the upstream disturbance and the sudden expansion of the circular conduit to rectangular channel. Other factors such as boundary effects and the pressure distribution of flow within the basin also contributed to the slight nonuniformity of water depth within the basin.

Generally speaking, the radial flow basin maintained a fairly uniform spreading of the flow except for a high wave formation near the upstream portion of the flaring wingwalls. Comparison of Figures 3-25 to

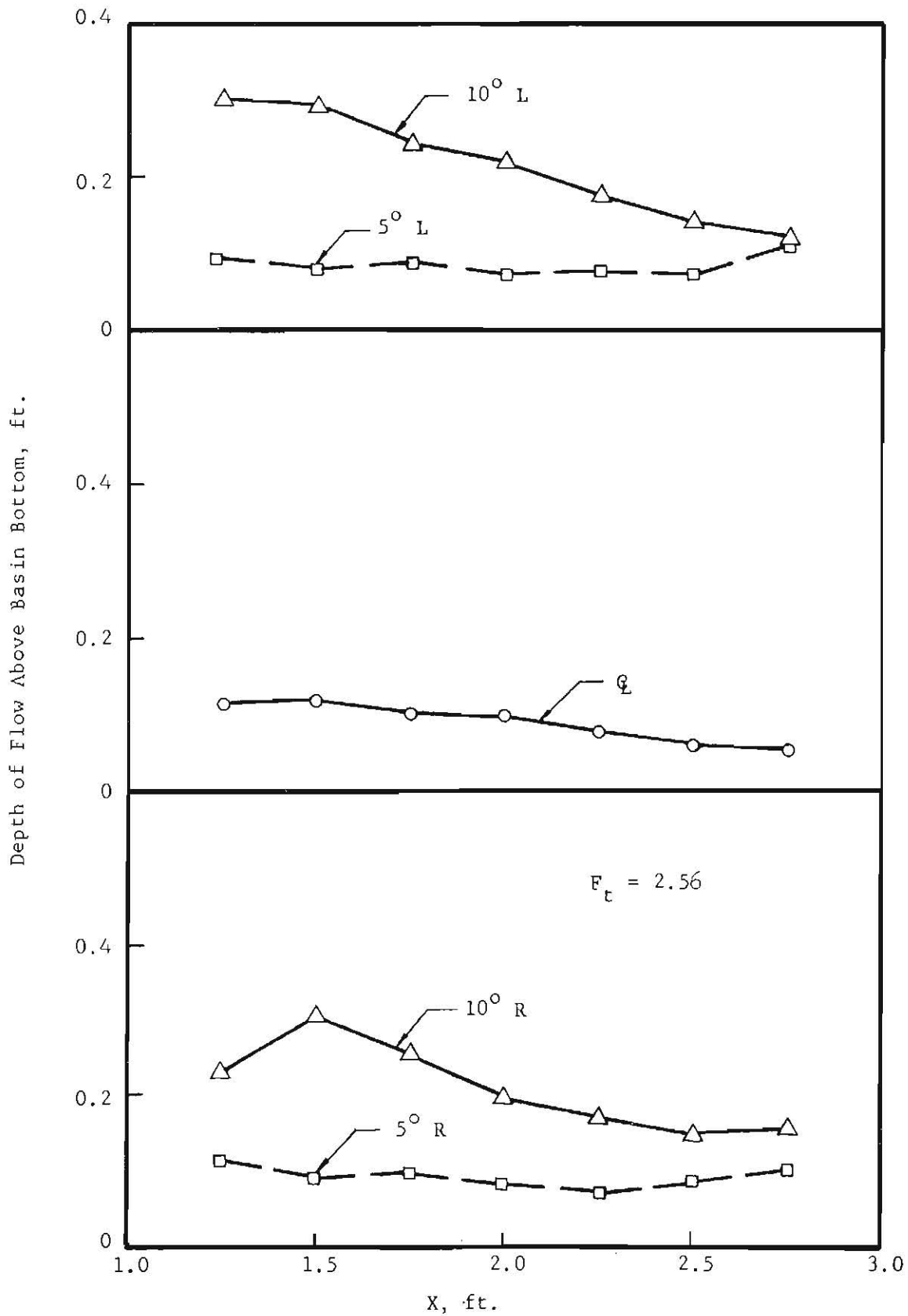


FIG. 3-25 WATER SURFACE PROFILES OF FLOW FOR
ARRANGEMENT RECI

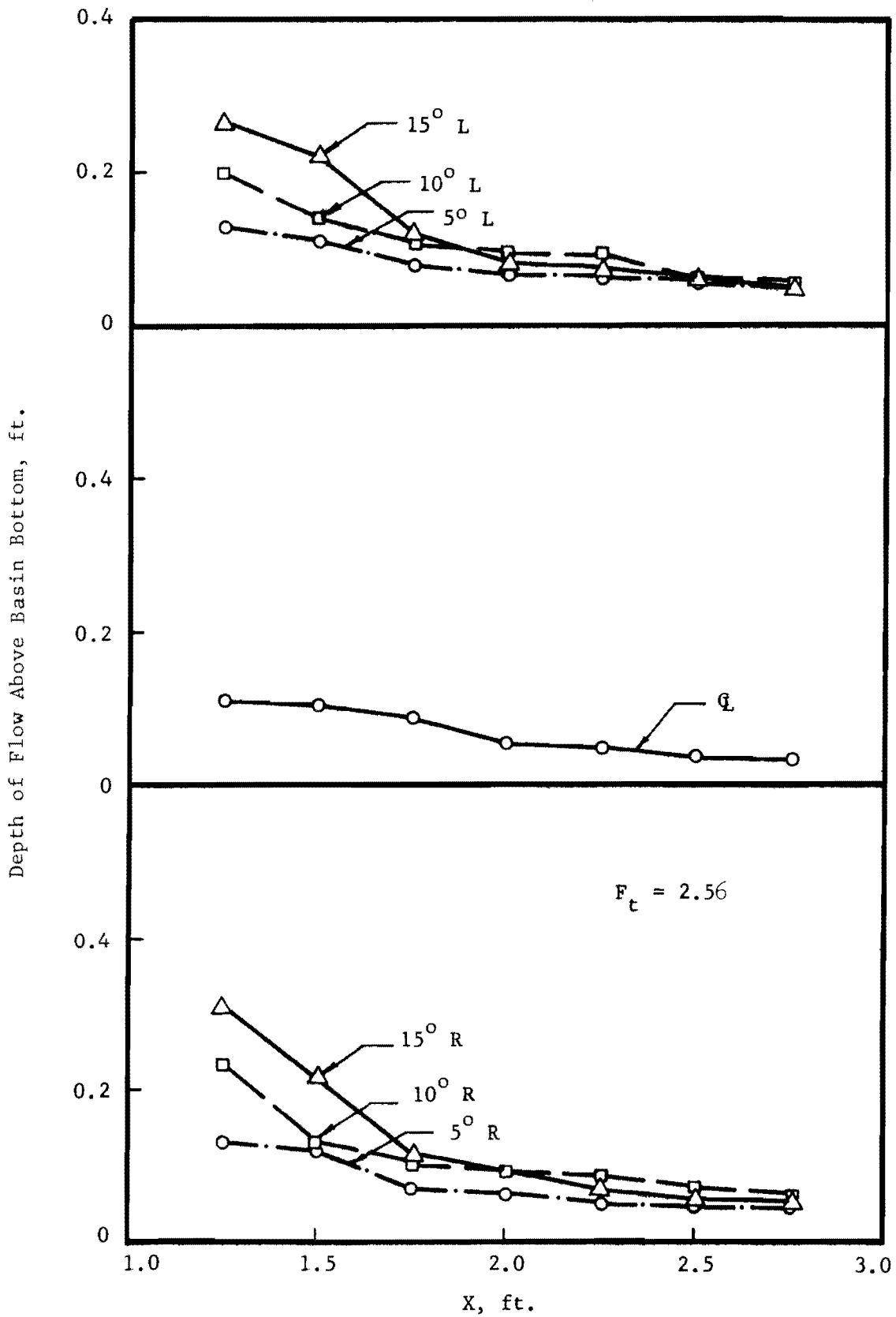


FIG. 3-26 WATER SURFACE PROFILES OF FLOW FOR ARRANGEMENT REC2

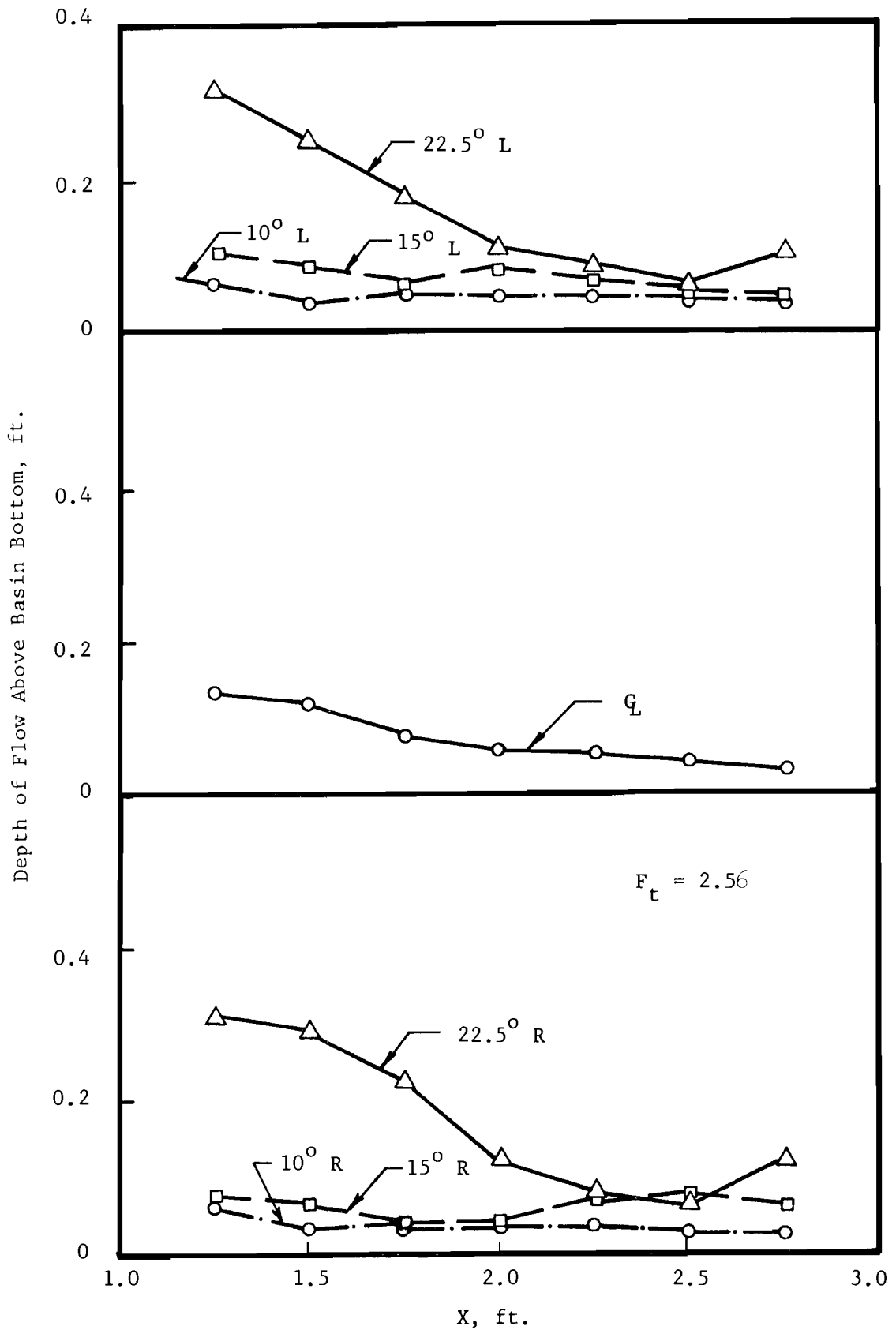


FIG. 3-27 WATER SURFACE PROFILE OF FLOW FOR
ARRANGEMENT REC3

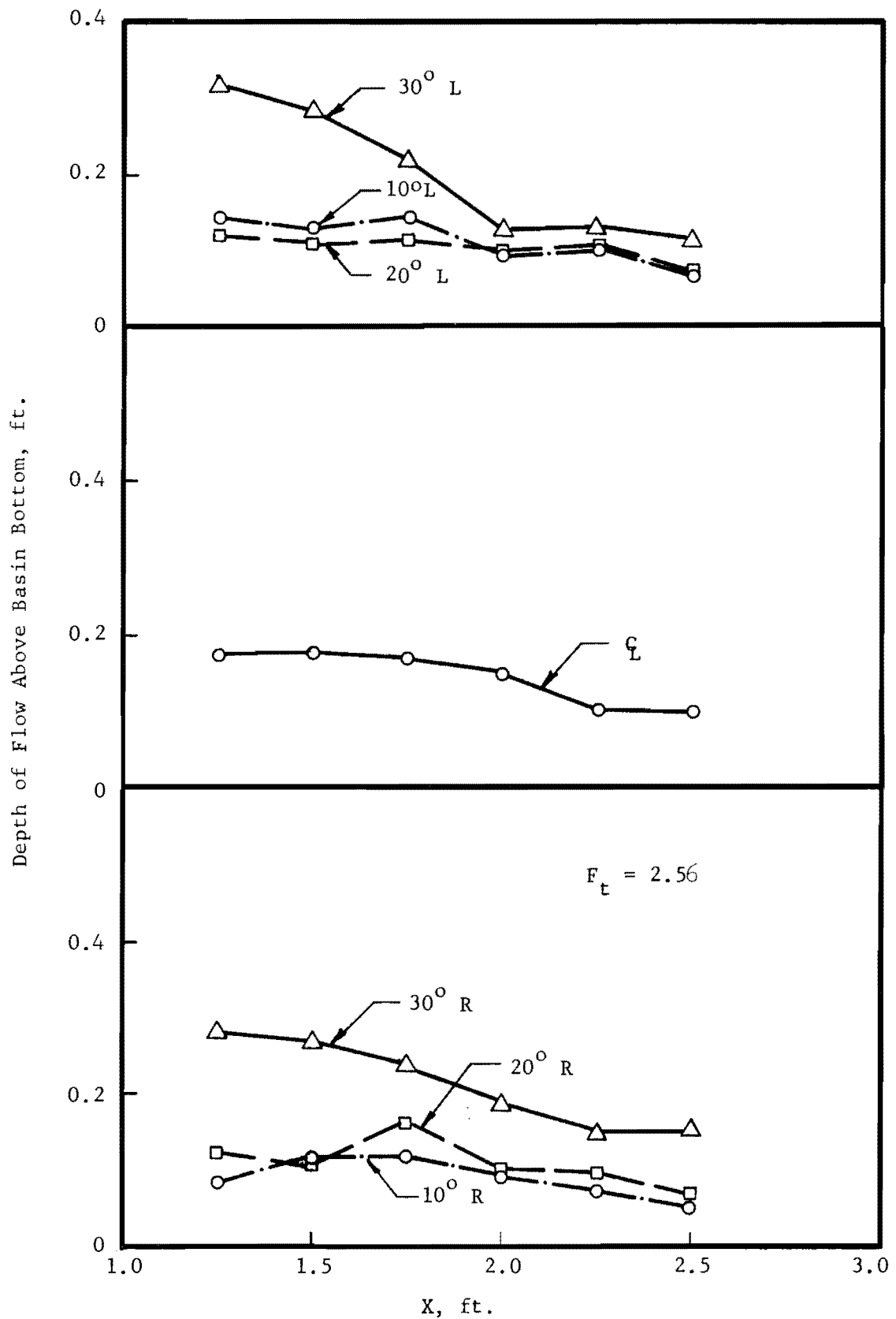


FIG. 3-28 WATER SURFACE PROFILES OF FLOW FOR
ARRANGEMENT REC4

3-28 indicated that the best spreading action with continuous decrease in the flow depth along the radial lines, the best symmetry of flow profile about the centerline, and the smallest depth of waves adjacent to the flaring side walls were provided by arrangement REC 2.

II - Trapezoidal Downstream Channel

Since many natural as well as artificial channels, in the interest of economy and bank stability, are trapezoidal, a study of flow performance of this type of downstream channel with a connection to a radial flow basin was needed. For this reason five different geometric arrangements were tested during this experimental study. The most difficulty in the selection of proper geometric dimensions was encountered in the design of a workable transition from the stilling basin to the trapezoidal downstream channel. A systematic method for estimating the general performance of any transition design in this case was not available prior to this experimental work. Therefore, several design configurations were considered and analyzed. The analysis was primarily based on construction possibilities and economical considerations. The principal interest in this study was centered around the trapezoidal downstream channel having 2:1 side slopes. The length of the basin along the centerline as well as the flaring angles of the wingwalls were fixed at 26 inches and 30° respectively in all arrangements.

Hydraulic performance of three structural configurations were of interest. These three structures had B/b ratios of 1, 2, and 2 corresponding to Z values of 6, 6, and 18 inches respectively. After choosing B/b and Z values, the variable dimensions such as the base length of the

triangular converging walls and the height of the abrupt rise at the end of the stilling basin were adjusted for the best basin performance.

The first visual observation was made on the hydraulic performance of an arrangement without any abrupt rise. The performance of this basin was extremely unsatisfactory. The flow of water with high kinetic energy entered the basin and advanced downstream until it came into contact with the converging walls. A considerable turbulence accompanied by shooting of water in the air was created as the result of the contraction of the converging walls in the direction of flow. This undesirable feature could only be eliminated by a tailwater control. The tailwater depth had to be high enough to ensure the formation of a hydraulic jump within the stilling basin. However, in actual field situations the required tailwater depth could not always be maintained. Since this type of arrangement exhibited a high scour potential with relatively low energy dissipation its practicality for the purpose of this investigation was ruled out.

In order to eliminate the aforementioned undesirable characteristic, it was decided to incorporate an abrupt rise at the end of the basin. Several different sill heights were experimentally investigated. On the basis of satisfactory performance, sill heights of 0.75 inch and 1.5 inches were selected for arrangements with Z values of 6 and 18 inches respectively. The abrupt rise at the end of the basin along with the contraction effects of the converging walls forced the formation of the hydraulic jump within the basin independent of the tailwater depth. This was especially advantageous since the tailwater could not be controlled always to a desirable depth under field conditions.

The effect of the magnitude of c/b in water surface profiles of the two structures showed that the hydraulic performance of the basin was not too sensitive to changes in c/b within the range of experimentation. c was the base length of the triangular converging walls. Based on the low sensitivity to c/b and construction advantages, specific values of c/b were selected for each arrangement.

Three arrangements were considered practical for actual construction purposes and satisfactory hydraulic performance. TRAP 1 was undesirable because the end sill was too high and would require unnecessary excavation for the apron. TRAP 3 was undesirable because c was too large giving a flatter slope to the triangular transition surface and causing the flow to climb higher on the outside walls. The satisfactory arrangements were TRAP 2, 4, and 5 shown in Table 1. The c/b ratios for these arrangements were 2.5, 1.80, and 2.25 respectively. A detailed study of the performance of these three arrangements follows. In the study of the performance of the trapezoidal downstream basin, the jump stability, the degree of velocity reduction of flow passing through the basin, and the shape of the water surface profile were of interest.

Stability of the Hydraulic Jump: So far as the jump stability was concerned, arrangements TRAP 2, 4, and 5 performed with satisfactory results. The hydraulic jump was formed in each arrangement independent of tailwater requirements within the allowable range of F_t . Figures 3-29, 30, and 31 show the locations of the jump when y_2 was larger than or equal to the tailwater depth. It should be noted that for different values of F_t in all arrangements the leading edge of the jump was positioned within the upper section of the stilling basin. Any tailwater depth lower than

$B/b = 1.0$	ARR. TRAP1	$c/b = 2.25$
$\theta = 30^\circ$	ARR. TRAP2	$c/b = 2.50$
$ss = 2:1$		
$F_t = 2.56$		
$H_s = 3/4''$		

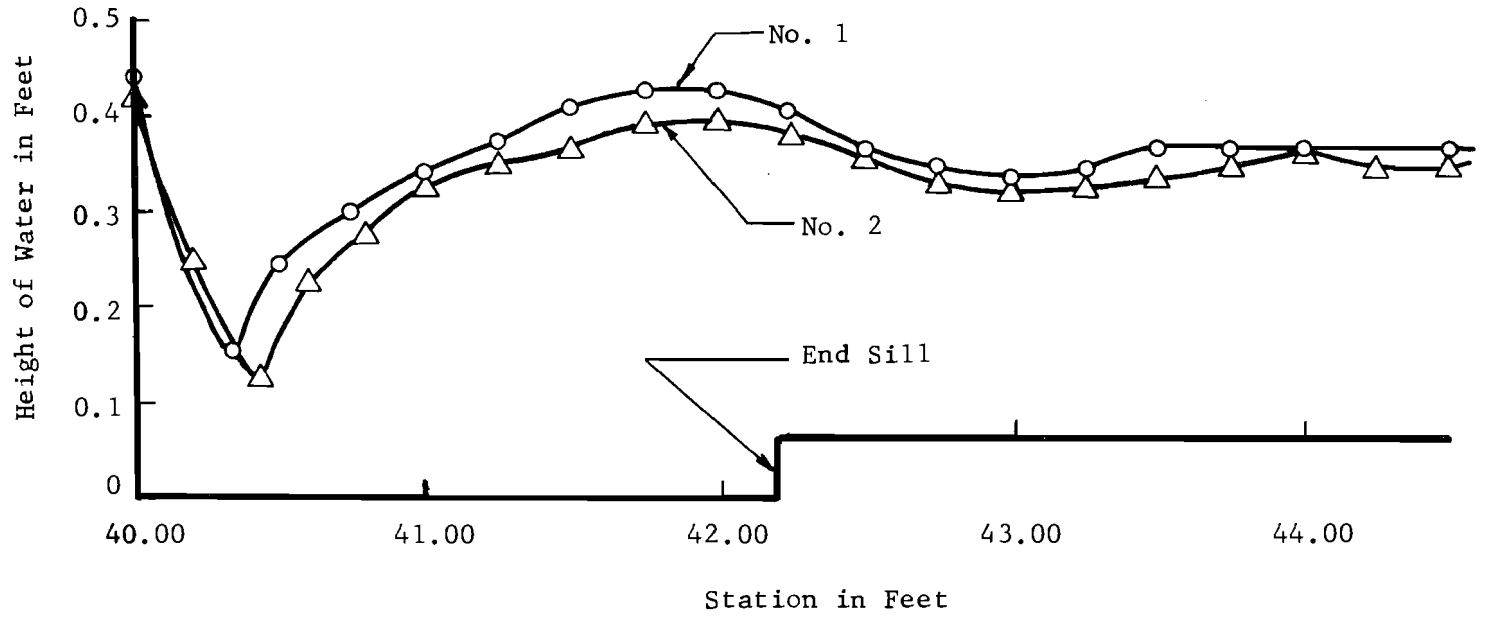


FIG. 3-29 WATER SURFACE PROFILES OF FLOW ALONG THE Q_c OF TRAPEZOIDAL DOWNSTREAM CHANNEL

$B/b = 2$ $c/b = 1.8$
 $\theta = 30^\circ$ $H_s = 3/4''$
 $ss = 2:1$ $Z = 6''$
 ARRANGEMENT TRAP 4

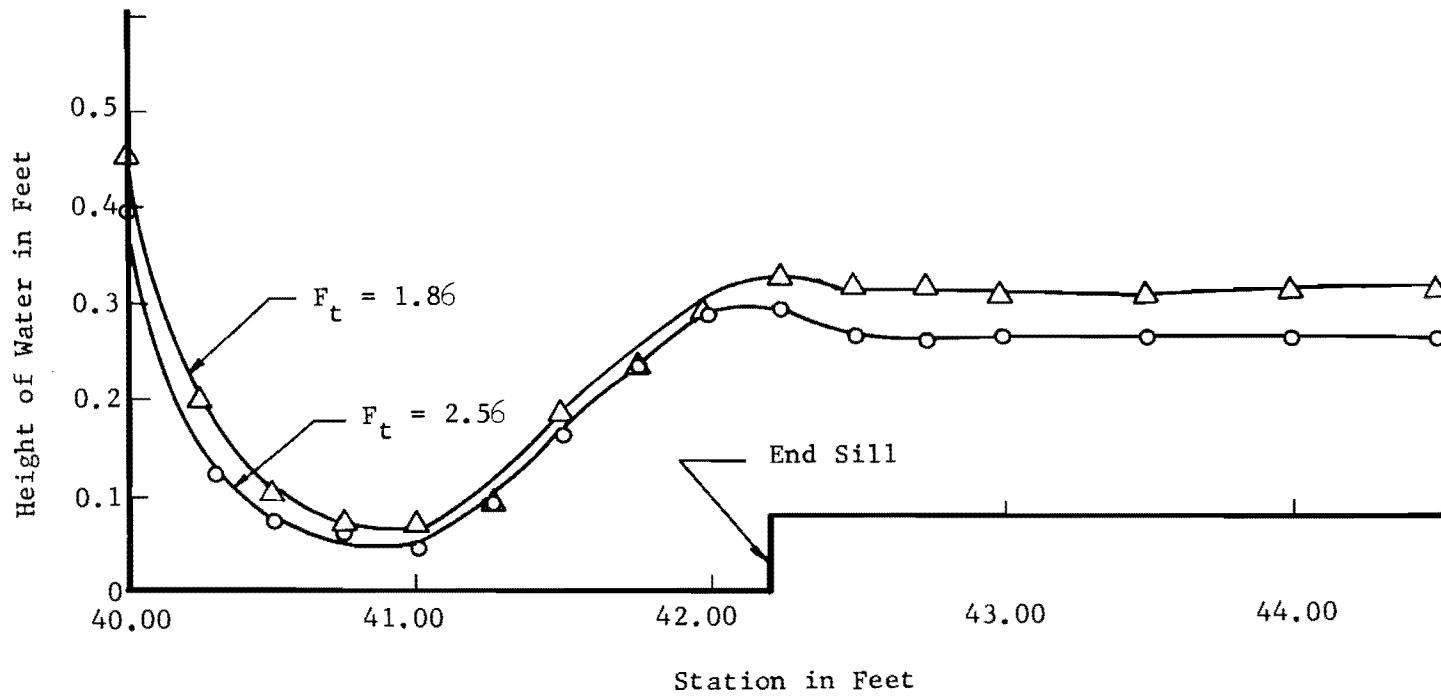


FIG. 3-30 WATER SURFACE PROFILES OF FLOW ALONG THE Q_c OF TRAPEZOIDAL DOWNSTREAM CHANNEL

$\frac{B}{b} = 2$ $H_s = 1\frac{1}{2}''$
 $\theta = 30^\circ$ $Z = 18''$
 $ss = 2:1$ $F_t = 1.86$
 ARRANGEMENT TRAP 5

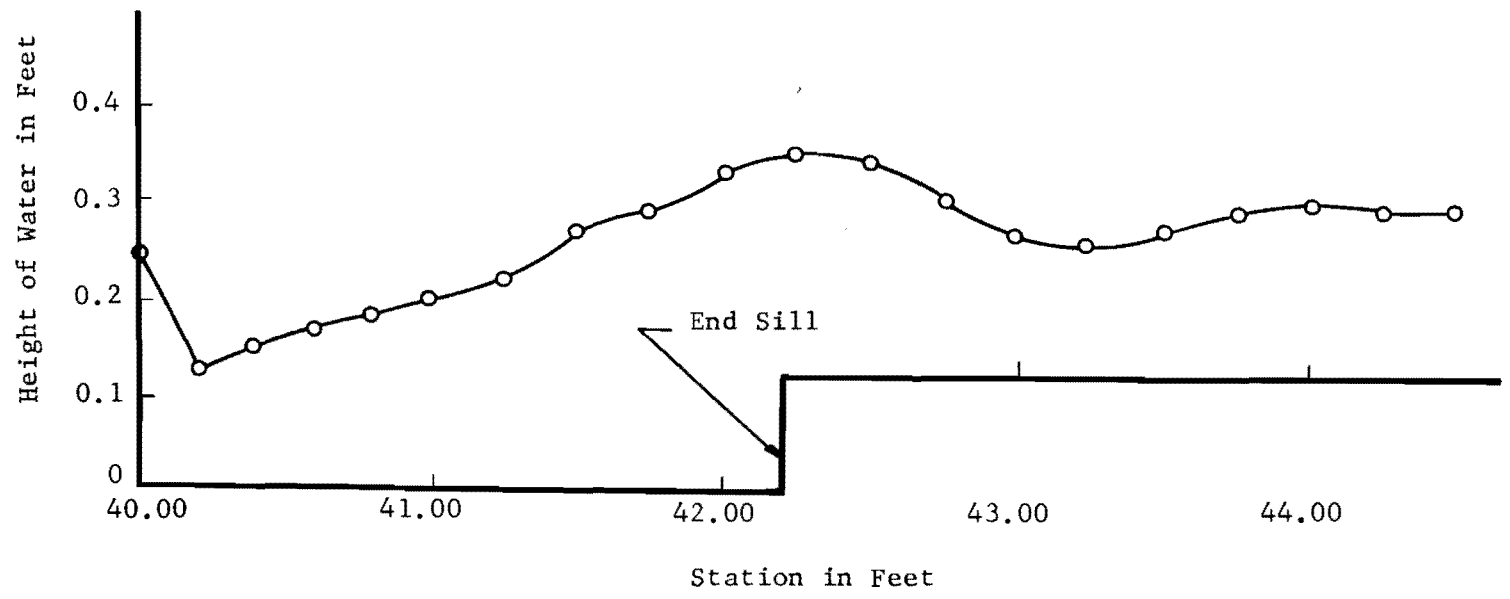


FIG. 3-31 WATER SURFACE PROFILE OF FLOW ALONG THE q_c OF TRAPEZOIDAL DOWNSTREAM CHANNEL

y_2 did not affect the position of the jump. When the tailwater depth became lower than y_2 , supercritical flow in the downstream channel resulted with a Froude number close to unity. However, since the downstream Froude number was close to unity, there would be no danger of scouring damage in the immediate vicinity of the basin within the downstream channel. When the tailwater depth was increased to a value greater than y_2 , the jump was moved upstream and finally became submerged.

In the discussion of the stability of the hydraulic jump for a rectangular downstream channel the effectiveness of the radial flow basin was pointed out. This effectiveness was especially apparent in TRAP arrangements when the jump was formed within the radial flow basin. Since in arrangements TRAP 2, 4, and 5 it was impossible for the jump to leave the basin and move into the downstream channel, the stabilizing effects of the radial flow basin were always present. The effect of F_t on the position of the hydraulic jump is shown in Figure 3-30. The water surface profiles indicating the jump positions for F_t of 1.86 and 2.56 in arrangement TRAP 4 are shown in this figure. The jump position for F_t of 2.56 was more upstream than that of F_t equal to 1.86. This indicated that as F_t decreased from its limiting value, the jump position moved downstream within the basin. The limiting value of F_t was previously defined as the Froude number at which the free fall flow would take place.

Comparison of Figures 3-30 and 3-31 showed that an increase in the height of drop of entrance channel (Z) placed the leading edge of the jump farther upstream in the basin. This behavior was attributed to the fact that when F_t was constant, an increase in Z increased the Froude number at

the beginning of the flared wingwalls because of the increased kinetic energy at this section.

Another factor in locating the position of the jump was the combined contraction influence of the converging walls and the abrupt rise in the flow. Contraction influence was defined as the ability of flow to be converged when the fluid advanced through the transition zone in the basin. The contraction influence was a function of B/b , c/b , ss , θ , and H_s . An increase in the contraction influence moved the jump upstream. This effect is observed in the position of the jump in Figures 3-29 and 3-30. The effect of B/b on the jump position was hence apparent from its effect on contraction influence. The smaller the ratio of B/b , the higher the contraction influence, thus the more upstream the jump position. For this reason the jump position was more upstream in arrangement TRAP 2 than arrangement TRAP 4 for the same F_t as indicated in Figures 3-29 and 3-30.

Velocity Distribution and Reduction: Velocity measurements were obtained at 0.03 foot, $0.4y_3$, and $0.8y_3$ from the channel bottom in trapezoidal channel. It is noteworthy that the depth y_3 was not necessarily the same as the sequent depth, y_2 , of the hydraulic jump. The procedure followed in obtaining the velocity measurements was essentially the same as the procedure used for the rectangular channel section. All velocity measurements were made under the condition of no tailwater control. Three transverse sections were considered for velocity measurements. These sections were located at 2.0 , 3.0 , and 4.0 feet, along the centerline of the channel, from the beginning of the flared wingwalls. The relative velocity magnitudes of V/V_m in these sections are shown in Figures 3-32 through 3-36. Velocity measurements were obtained for F_t of 1.86 and 2.56

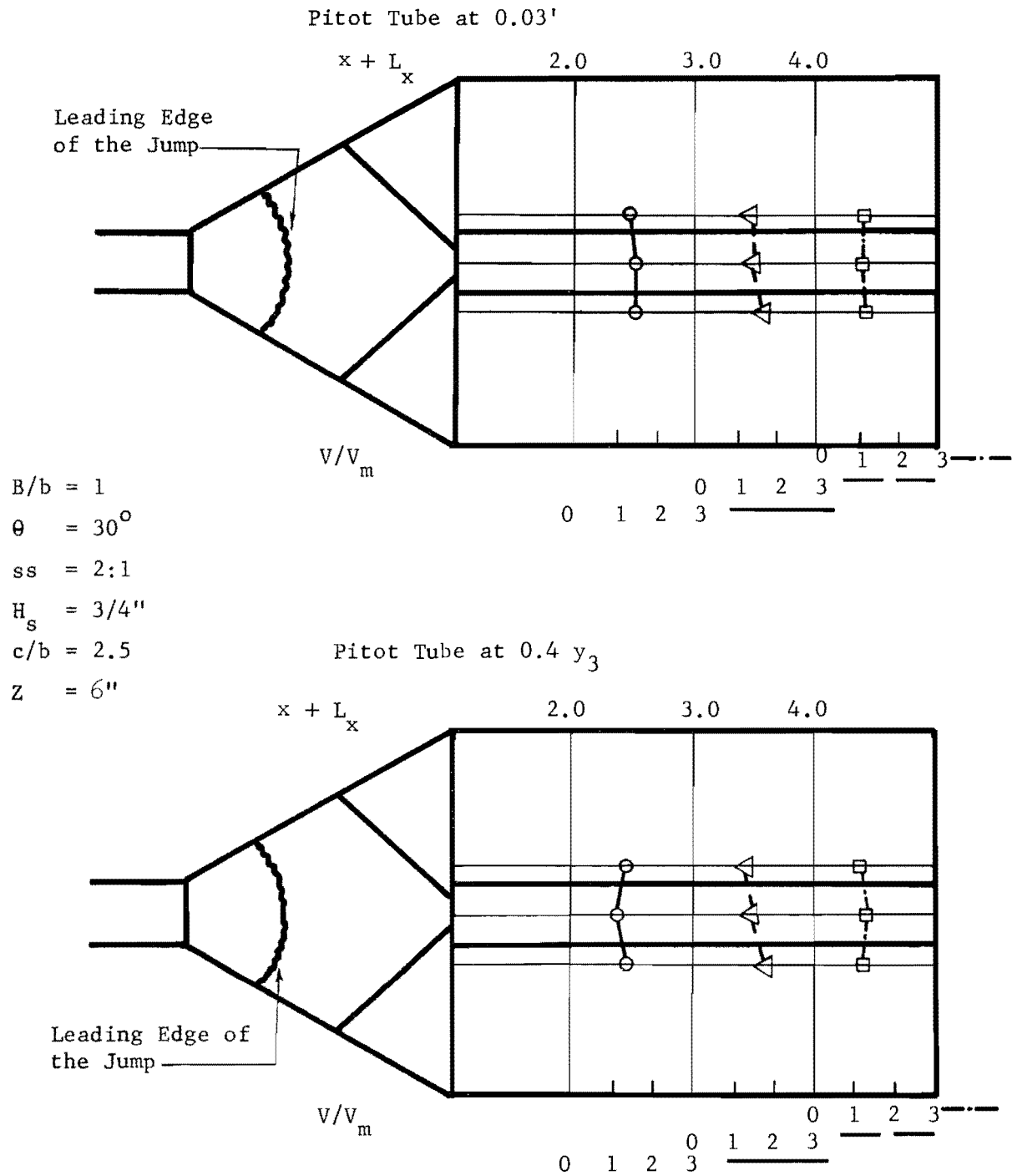


FIG. 3-32 VELOCITIES IN DOWNSTREAM CHANNEL FOR ARRANGEMENT TRAP2

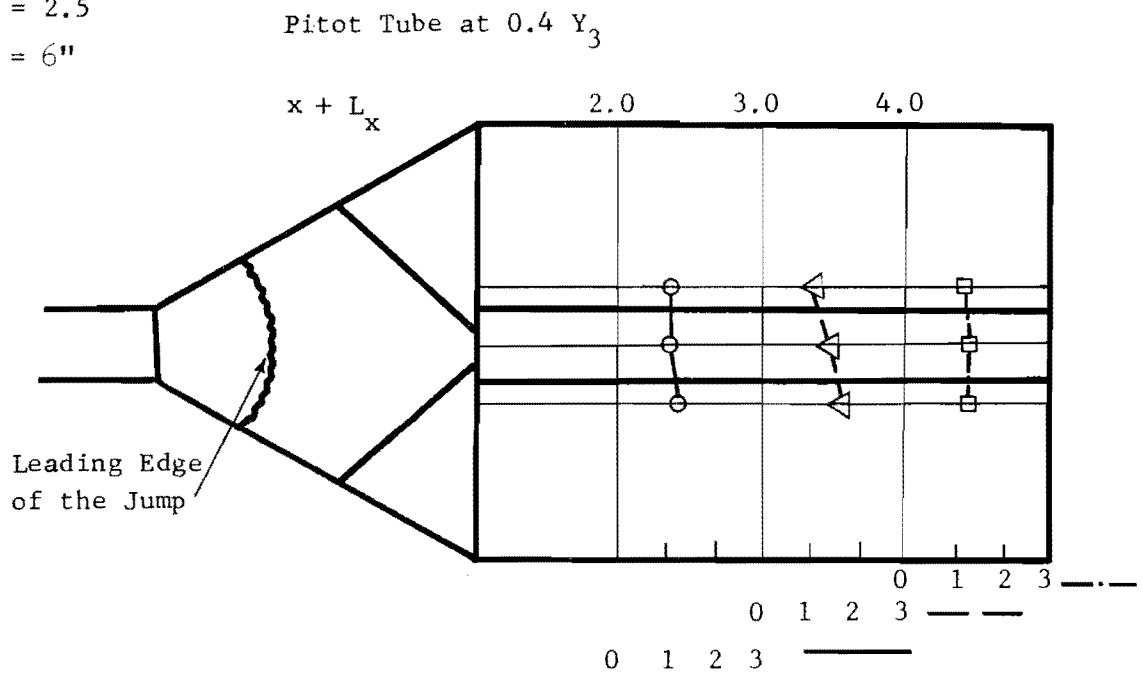
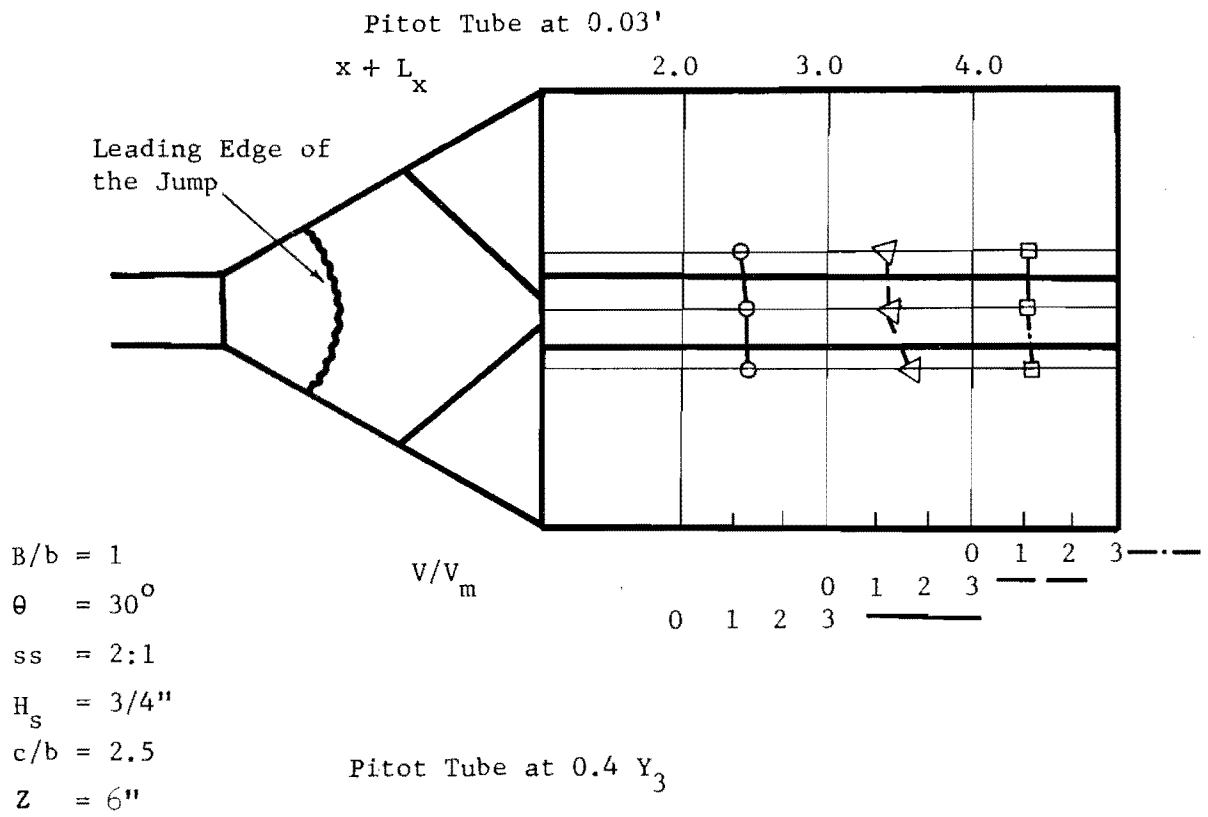


FIG. 3-33 VELOCITIES IN DOWNSTREAM CHANNEL FOR ARRANGEMENT TRAP2

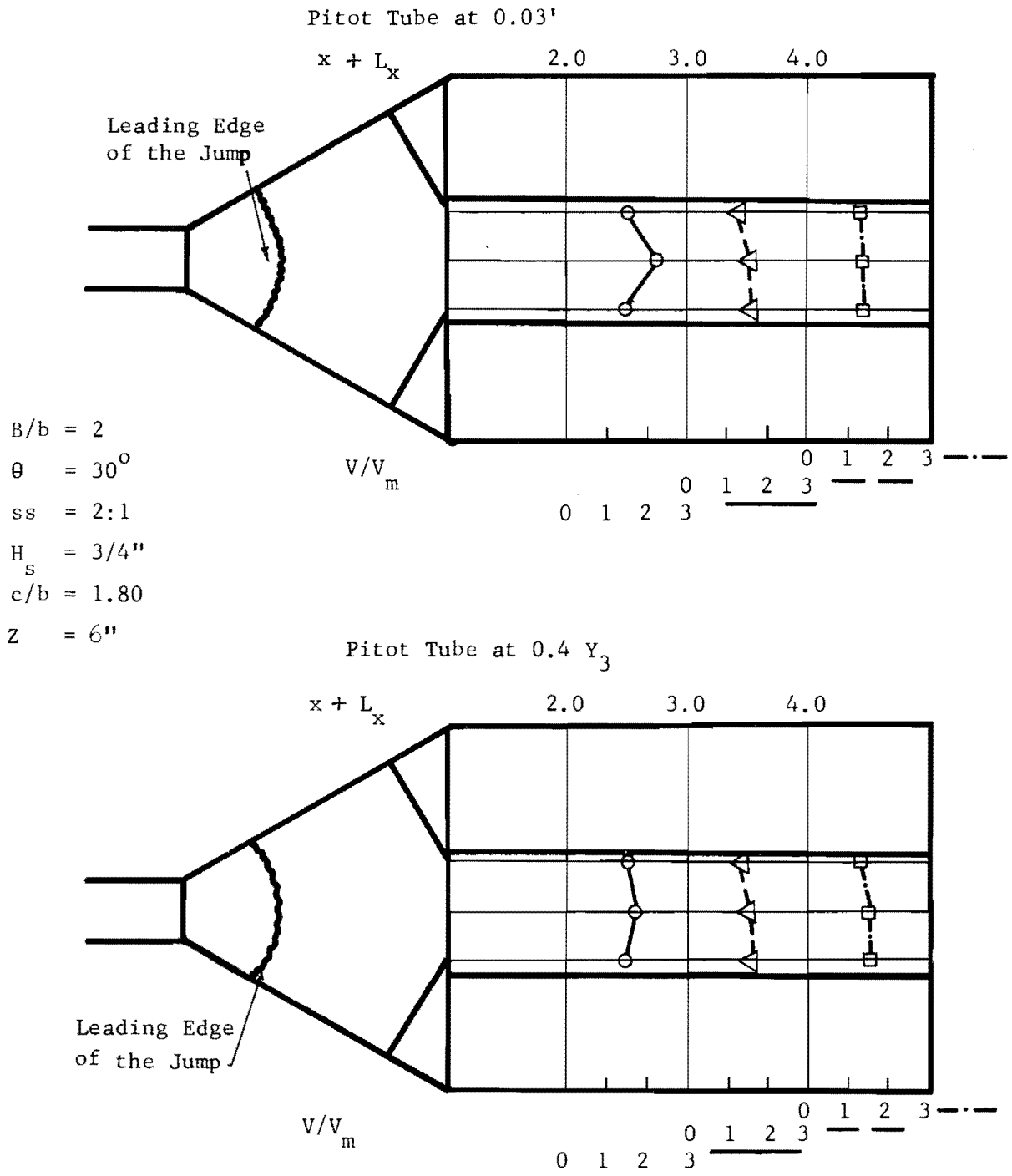


FIG. 3-34 VELOCITIES IN DOWNSTREAM CHANNEL FOR ARRANGEMENT TRAP4

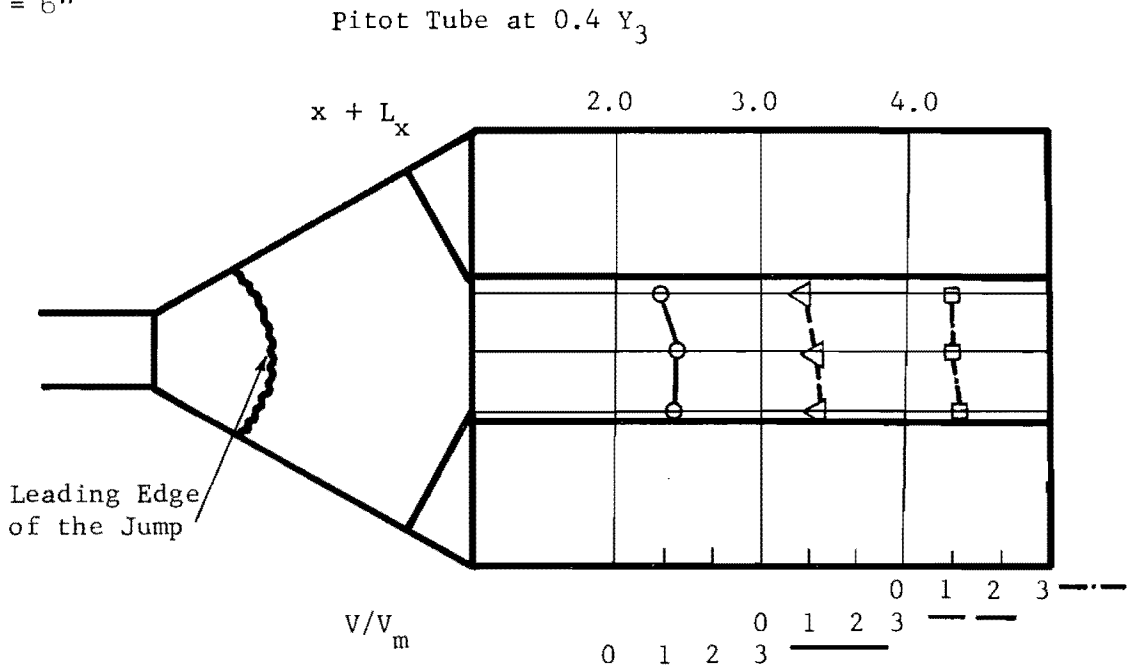
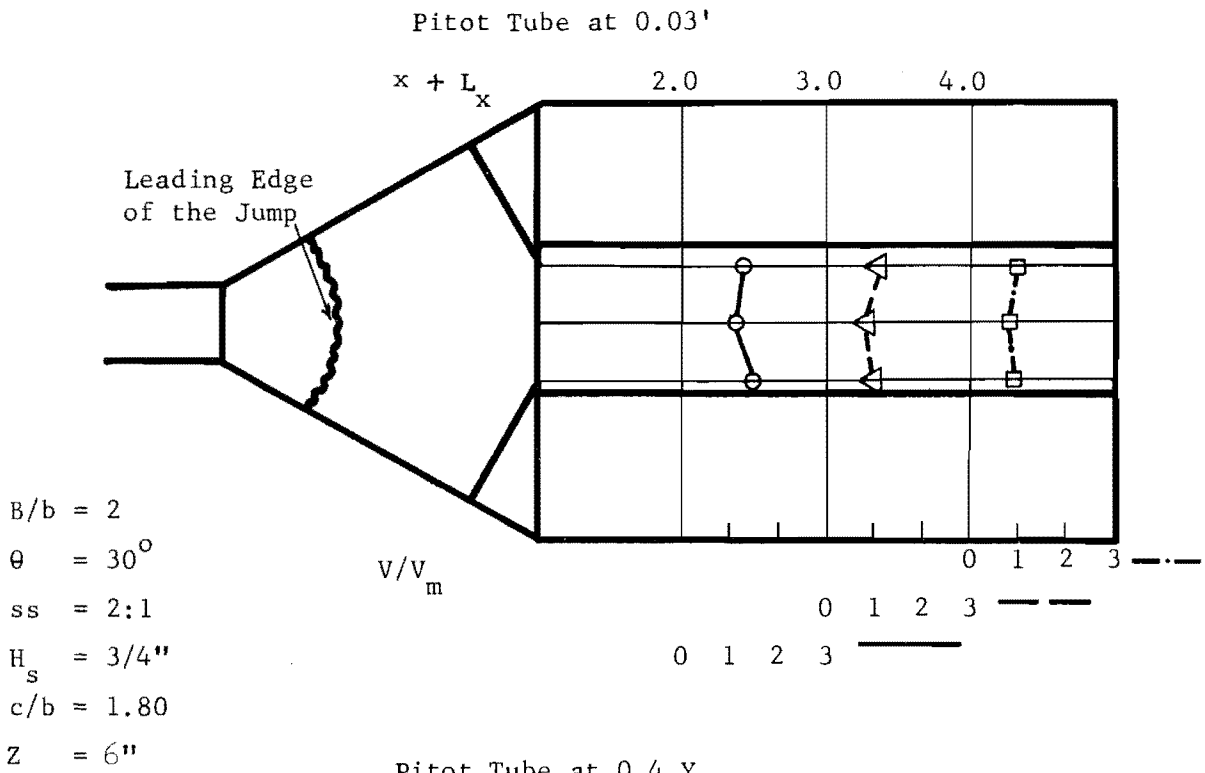


FIG. 3-35 VELOCITIES IN DOWNSTREAM CHANNEL FOR ARRANGEMENT TRAP4

in arrangements TRAP 2 and 4. In arrangement TRAP 5 the velocities were obtained only for F_t of 1.86 since F_t of 2.56 was out of the range of experimental validity. The uniformity of the velocity distribution in the downstream channel could be observed in Figures 3-32 to 3-36. Several interesting features of these figures are noteworthy. The velocity ratio V/V_m was fairly uniform in any transverse section for given hydraulic and geometric conditions. The velocity distributions for a given flow condition in the three transverse sections of the downstream channel were similar to each other. Furthermore, the velocity pattern and magnitude was almost the same for experimental results obtained at 0.03 ft., $0.4y_3$, and $0.8y_3$. This was an indication of the velocity uniformity in transverse, longitudinal, and vertical directions.

The effect of F_t on the velocity magnitude was rather small, especially in arrangement TRAP 2. When F_t was changed from 1.86 to 2.56, a noticeable velocity variation could not be detected in this arrangement. In arrangement TRAP 4, an increase in F_t decreased the magnitude of V/V_m slightly. This, of course, was due to the combined effect of the changes in V as well as V_m when F_t was varied. The effect of F_t on V/V_m in trapezoidal channel was opposite to that indicated by the performance of the rectangular downstream channel. In the rectangular downstream channel, an increase in F_t increased V/V_m . Comparison of Figures 3-34 to 3-36 showed a close agreement in the velocity distributions and magnitudes of V/V_m between arrangements TRAP 4 and 5. This agreement became more pronounced as the flow advanced downstream.

A relatively high degree of velocity reduction was observed in all experiments. The downstream channel velocities varied within a small range

in all geometric configurations. However, the velocities upstream from the jump varied considerably from arrangements TRAP 2 and 4 to arrangement TRAP 5 for the same F_t . The velocity upstream from the jump was much higher in arrangement TRAP 5 than that of TRAP 2 and 4. Hence the best velocity reduction was observed in arrangement TRAP 5.

The velocity distribution and uniformity of arrangements TRAP 2, 4, and 5 indicated a satisfactory performance on each of these three basins. Depending on the availability of geometric dimensions either one of these basins could be used efficiently.

Water Surface Profile: The general appearance of water surface profile along the channel centerline for arrangements TRAP 2, 4, and 5 are shown in Figures 3-29, 3-30, and 3-31 respectively. The hydraulic jump was followed by a critical section created over the crest of the abrupt rise. Under the condition of no tailwater control, the depth of flow in the downstream channel was close to the critical depth. The critical depth represents the state of flow at which the specific energy is minimum for a given discharge. Since a supercritical flow could not occur immediately downstream from the dissipating structure, a severe scour and erosion potential would not be anticipated.

The effect of F_t on the water surface profile is shown in Figure 3-30. An increase in F_t caused a decrease in the depth of water. Of course, this type of variation is apparent from the energy relationships within the flow median. The water surface profile was rather uniform in all experiments.

The purpose of this type of stilling basin was to allow the uniform spreading of water before the jump occurs. Hence, the length of the basin

had to be such that the water spread uniformly upstream from the jump. The closer the leading edge of the jump to the vertical face of the abrupt rise, the more efficient the performance of the basin. The situation would also allow satisfactory performance of the basin when the tailwater depth was higher than the sequent depth y_2 . Of course, the economic consideration was also a controlling factor in selecting the length of the basin. No attempt was made in this investigative work to test the effect of the basin length in the hydraulic performance of the structure. However, it is anticipated that the longest possible length within the region of wingwalls would have the best performance. The reason being the full development of radial flow within the region of flared wingwalls.

The depth of water in the trapezoidal section, when F_t equaled 2.56, was highest in arrangement TRAP 2 and lowest in arrangement TRAP 5. According to the results obtained and analyzed in this report, the general performance of the trapezoidal basin was preferred to that of a rectangular downstream channel basin. This evaluation was based on the tailwater requirements, the velocity reduction, and the jump stability. Besides these advantages, the trapezoidal downstream channel basin could be effectively operated on a larger range of discharges. The basin for trapezoidal downstream channel is self cleaning and there would be no danger of debris accumulation within it. The high turbulence within the basin carries any debris or sediment material into the downstream channel.

CHAPTER 4

DESIGN PROCEDURE FOR PROTOTYPE RADIAL FLOW DISSIPATORS

Extensive experimental investigations by Aguirre (12), Wear (13), Moore and Meshgin (14), and as reported in the previous chapter of this report all indicated the effectiveness of radial flow energy dissipator for highway culverts in reducing the energy of high-velocity flow, and stabilizing the jump within the basin permitting it to function satisfactorily over a considerable range of tailwater levels. Satisfactory performance of varying degrees over the conventional methods of energy dissipation was observed for a wide range of variables investigated. Other potential applications of radial flow energy dissipator may be anticipated at the: Outlet of multiple barrel culverts; reservoir outlet works; and irrigation waterways. The construction advantages of this type of structure includes its simplicity of geometric arrangements, simple straight horizontal elements of the entrance channel, and the absence of baffle blocks, impact walls and other appurtenances, aside from an end sill.

The radial flow energy dissipator is expected to be especially useful in regions of moderately steep topography dealing with drainage culverts for which a major maintenance expense is anticipated due to frequent occurrence of scour and erosion in the vicinity of the culvert outlet. However, since the topography of the region, the expected floods, the geometry of the outlet channel, the side slopes of the highway embankment, and the available area in which a dissipating structure is needed vary from

one situation to another, a standardized design of radial flow energy dissipator may not be advisable. For this reason and based on experimental and analytical results a procedure is recommended in this chapter which helps the engineer in designing an effective radial flow energy dissipator under given set of field conditions.

When the existing field conditions, expected drainage, and the highway dimensions are known, and scour or erosion is anticipated, the engineer is faced with the selection of a proper culvert size and its slope, required height, width, and the radius of curvature of entrance channel, the angle and the height of the flaring wingwalls, the length of the basin, and a workable B/b ratio. Upon choosing the aforementioned dimensions a suitable transition from the stilling basin to the downstream channel such as an end sill for rectangular downstream channel and the triangular converging walls incorporating an end sill for trapezoidal downstream channel may be recommended to improve the performance of the basin and to make the proper connection between the stilling basin and the downstream section. In the following articles a systematic approach to the selection of these dimensional variables is discussed and analyzed.

Hydraulic Design of Culverts

The hydraulic of conventional culverts are thoroughly discussed in many hydraulic structure books and publications which include charts for selecting a culvert size at a given set of conditions. No attempt is made to cover all phases of culvert design in this section and the designer is referred to Chow (16) for detailed procedure in design of highway culverts. Since the inlet flow line elevation is fixed, the outlet flow line elevation

must be selected in such a manner that sufficient height of drop is provided. Any outlet flow line elevation above the minimum required elevation governed by the drop height is permissible provided that it is economically feasible. After choosing the culvert outlet flow line elevation for a given highway cross section, the slope and the required size of the culvert may be determined. Two types of slope, namely mild or steep, may result. If the selected slope of the culvert is mild, critical depth of flow may be assumed to exist at the outlet of the culvert. However, if the slope is steep and the culvert is long, a normal depth may be used as the depth of flow at the outlet of the culvert. For short culverts and steep slopes, one of the conventional methods of water surface profile determination must be followed to estimate the expected depth of flow at the top of the vertical drop.

Width, Height, and the Radius of Curvature of Entrance Channel

The selection of the size of the culvert would determine the width of the entrance channel. This width must be the same as the width of the box culvert or the diameter of the circular culvert used under the highway. If the circular culvert is recommended, then, the connection between the culvert and the entrance channel should be an abrupt expansion. The entrance channel must have a rectangular cross section at every transverse section having a height of side walls at least equal to the depth of flow plus an appropriate freeboard. The height of the side walls must also be such that the vertical distance from the surface of the embankment on the side slopes of the road to the top elevation of the side walls at any section does not exceed two feet. This is a general recommended limit by

Highway Departments and exceptions in exceeding this limit are permissible where existing conditions indicate another acceptable solution; however, any such exceptions should be based on the results of thorough engineering study. Figure 4-1 shows a typical culvert installation and the radial flow energy dissipating structure.

In choosing the height of drop of the entrance channel several factors are of primary importance. Some of these factors are: the shortest horizontal distance from the beginning of the entrance channel to the centerline of the highway; the extent that the highway fill can be excavated for placing the dissipating structure; the available distance from the highway centerline to the highway right-of-way line; and finally the outlet flow line elevation of the culvert and the elevation of the bottom of the basin. Furthermore, the height of drop should be sufficient to cause enough pressure build-up in the flow as it impinges on the stilling basin floor to cause the desired lateral spreading of the flow. Based on experimental results, a minimum height of one times the culvert width or diameter is recommended as the lower limit of drop height. The process of selecting a feasible drop height calls for a trial solution of the problem. Based on the given conditions, several drop heights must be chosen and examined at first to determine their economic and hydraulic feasibility. After comparing several workable solutions, the most advantageous one may be adapted. Since a wide range of the values of drop height could be used in this type of structure and still result in an effective energy dissipator, the choice of a suitable height can be determined by engineering judgment and economical considerations.

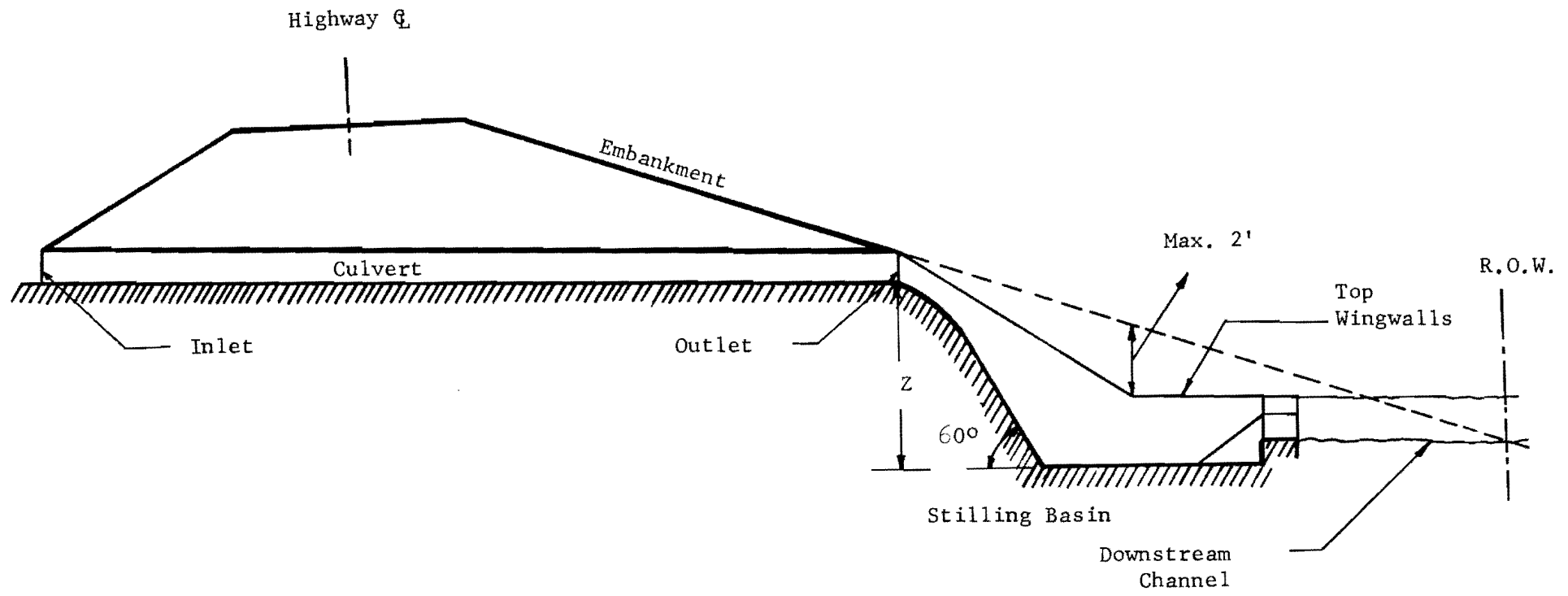


FIG. 4-1 SCHEMATIC REPRESENTATION OF CULVERT INSTALLATION AND DISSIPATING STRUCTURE

In design of a workable entrance channel the proper selection of the radius of vertical curvature for the drop is of primary importance. Too small a radius of curvature may cause excessive negative pressure on the bottom of the entrance channel or separation of the flow from the lower boundary, thus impairing the operation of the stilling basin. By limiting the negative pressure head to a minimum of approximately $-1.5y_t$, Aguirre (12) recommended a mathematical relationship shown in equation (4.1) for determination of the radius of curvature R of the vertical drop.

$$R = \frac{y_t F_t^2}{2.5} \quad (4.1)$$

He assumed that the top of the vertical drop is the critical section so far as negative pressure is concerned. Upon this basis, Aguirre recommended a radius of curvature for the model operating at a specific Froude number (F_t). However, the experimental results discussed in the previous chapter indicated that the circular culvert model could not be operated at this design F_t . At design F_t the free fall, or separation, of flow occurred and as indicated before, the limiting Froude number (F_t) was somewhat less than the design value. Application of equation (4.1) would result in the computation of a radius of curvature which is insufficient for proper hydraulic performance of the entrance channel. Because of the aforementioned reasons a curvature design procedure is recommended assuming that the critical section for the occurrence of maximum negative pressure is the lower portion of the vertical curve. It should be noted that these pressures cannot be accurately calculated by elementary means, but if the assumption of a free, or irrotational vortex is made a functional relationship may be obtained suggesting an approach to the evaluation of

pressure head on the curved channel bottom. This assumption is a reasonable one, since losses must be small over the short length of entrance channel, and the turbulent approaching flow usually has a uniform transverse velocity distribution which is the characteristic of irrotational flow. Considering the above assumptions, the derivation of the functional relationship expressing the pressure on the channel bottom (p_2) of the entrance channel is as follows: The simplified Euler's equation in polar coordinates applied to any element of fluid streamline may be represented by:

$$\frac{dh}{dr} = - \frac{a_r}{g} = \frac{V^2}{rg} \quad (4.2)$$

where r is the radius of curvature of the element of streamline, h is the piezometric head at r , a_r is the normal component of acceleration directed toward the center of curvature, and V is the mean velocity of flow. Integrating equation (4.2) between points 1 and 2 shown in Figure 4-2 the following would result:

$$\int_{h_2}^{h_1} dh = \int_R^{R+Y} \frac{V^2}{rg} dr \quad (4.3)$$

or

$$h_1 - h_2 = \frac{V^2}{g} \text{Log}_e \left(\frac{R+Y}{R} \right) \quad (4.4)$$

where R is the radius of curvature of entrance channel, and Y is the depth of flow on the entrance channel. Since,

$$h = \frac{p}{\gamma} + z \quad (4.5)$$

where z is the elevation of the point in question with respect to a

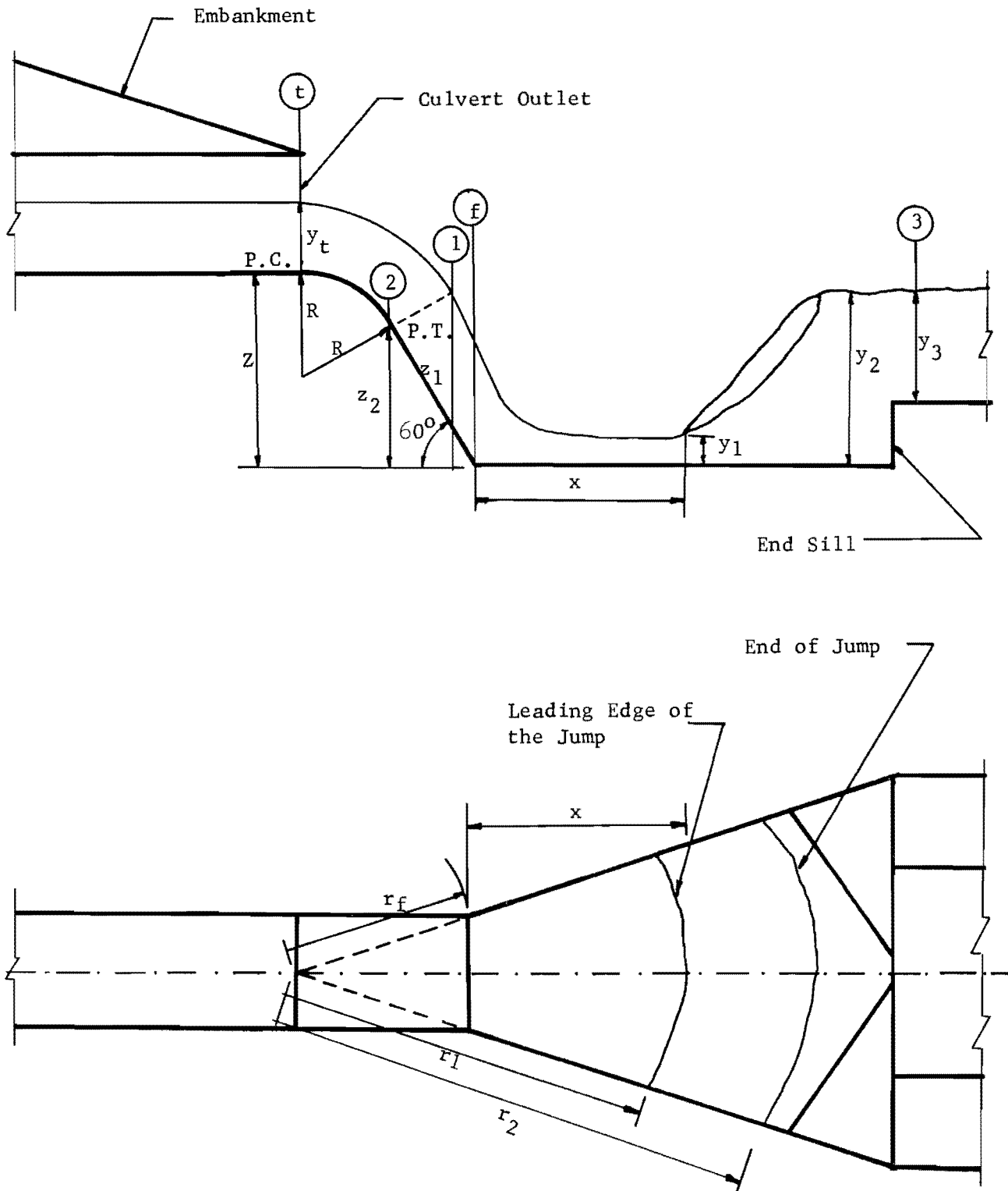


FIG. 4-2 A TYPICAL DISSIPATING STRUCTURE WITH TRAPEZOIDAL DOWNSTREAM CHANNEL INDICATING FLOW VARIABLES

reference plane, substitution of equation (4.5) into equation (4.4) gives,

$$\frac{p_1}{\gamma} + z_1 - \frac{p_2}{\gamma} - z_2 = \frac{V^2}{g} \text{Log}_e \left(\frac{R + Y}{R} \right) \quad (4.6)$$

where p_1 and p_2 are pressures at points 1 and 2 respectively. Since the pressure at point 1 is atmospheric, p_1/γ can be dropped from equation (4.6). Substitution of $(z_1 - z_2) = Y \text{Cos } 60^\circ = \frac{1}{2} Y$ into equation (4.6) results in:

$$\frac{Y}{2} - \frac{p_2}{\gamma} = \frac{V^2}{g} \text{Log}_e \left(\frac{R + Y}{R} \right) \quad (4.7)$$

or in dimensionless form:

$$\frac{Y/2 - p_2/\gamma}{V^2/g} = \text{Log}_e \left(\frac{R + Y}{R} \right) \quad (4.8)$$

The negative pressure head p_2/γ may be represented as:

$$\frac{p_2}{\gamma} = - c Y \quad (4.9)$$

where c is a constant. Substituting equation (4.9) into equation (4.8) it becomes:

$$\frac{(0.5 + c)Y}{V^2/g} = \text{Log}_e \left(\frac{R + Y}{R} \right) \quad (4.10)$$

or

$$\frac{0.5 + c}{F_{pt}^2} = \text{Log}_e \left(\frac{R + Y}{R} \right) \quad (4.11)$$

Where F_{pt} is the Froude number at the point of tangency of entrance channel and $F_{pt} \approx F_t$, $Y = y_t$, therefore:

$$\frac{0.5 + c}{F_t^2} = \text{Log}_e \left(\frac{R + y_t}{R} \right) \quad (4.12)$$

In order to estimate the approximate value of c , the limiting Froude number (F_t) from Figure 3 - 7, the corresponding flow depth, and the magnitude of the radius of curvature of entrance channel in the model were applied to equation (4.12). The value of c was hence determined to be unity. Substitution of numerical value of c in equation (4.12) results in:

$$\frac{1.5}{F_t^2} = \text{Log}_e \left(\frac{R + y_t}{R} \right) \quad (4.13)$$

Since F_t and y_t are known quantities, direct application of equation (4.13) results in the evaluation of the radius of curvature R . Values of F_t versus y_t/R computed from equation (4.13) are plotted in Figure 4 - 3 for a limited range of variables. Wherever applicable this graph may be used instead of equation (4.13) to simplify mathematical computations.

Experimental results showed that the most effective geometric configuration is the one in which the beginning of the vertical curve of the entrance channel is located at exactly the end of the culvert under the highway. Because of performance characteristics and ease of construction, therefore, the point of curvature of entrance channel must be tied to the outlet of the culvert. The vertical curve of the entrance channel must be connected to the bottom of the stilling basin by a short straight section which is tangent to the vertical curve and intersect the stilling basin bottom at an angle of 60° . The 60° angle was used in all the model studies and was chosen arbitrarily with consideration for the fact that it was

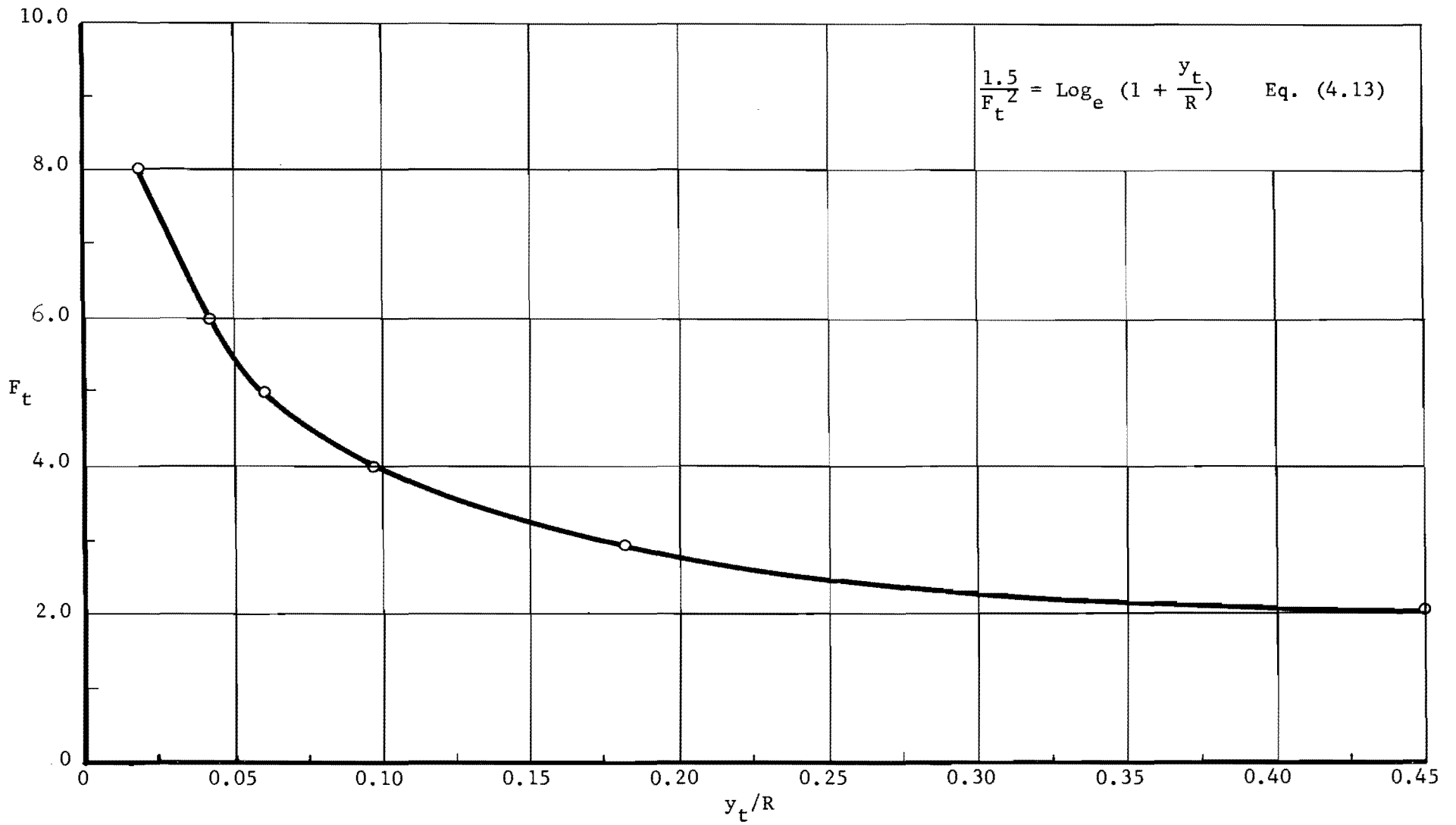


FIG. 4-3 GRAPH OF F_t vs. y_t/R

desirable to make the angle as large as possible to promote spreading action and avoid construction problems.

Stilling Basin Dimensions

Since the model studied in this investigation made use of a circular hydraulic jump, a review of this type of jump and its potential application is presented. The knowledge of functional relationships in this type of jump is an essential feature of proper stilling basin design. When supercritical flow spreads radially on a horizontal surface a circular hydraulic jump may occur. The theoretical analysis of circular hydraulic jump is based on the application of the continuity and momentum principles applied to a sector of the jump. The component parts of the circular jump along with the forces acting on a section of the jump confined by an angle $d\theta$ are shown in Figure 2-1. The variables used in the derivation of the sequent depth relationships are also shown in the same figure. The assumptions made in the derivation of circular jump equation as outlined in Chapter 2 are that: (1) the incompressible radial flow exists; (2) the friction shear along all solid boundaries in the jump region is negligible; (3) the energy and momentum coefficients are unity; (4) the hydrostatic pressure distribution prevails before and after the jump; (5) and the profile of the jump is a straight line. The derivation of the sequent depth equation is as follows:

$$\left| P_1 \right| = \frac{1}{2} \gamma y_1^2 r_1 d\theta \quad (4.14)$$

$$\left| P_2 \right| = \frac{1}{2} \gamma y_2^2 r_2 d\theta$$

$$\left| P_{s_1} \right| = \left| P_{s_2} \right| = \sqrt{\left(\frac{y_1 + y_2}{2}\right)^2} (r_2 - r_1) \left[\frac{y_1^2 + y_2^2 + y_1 y_2}{3(y_1 + y_2)} \right] \quad (4.15)$$

where P_1 , P_2 , P_{s_1} , and P_{s_2} are forces acting on the surfaces shown in Figure 2-1. Applying momentum principle,

$$P_1 - P_2 + 2P_{s_1} \sin\left(\frac{d\theta}{2}\right) = \rho V_2^2 r_2 y_2 d\theta - \rho V_1^2 r_1 y_1 d\theta \quad (4.16)$$

For small angles, $\sin\left(\frac{d\theta}{2}\right) = \frac{d\theta}{2}$.

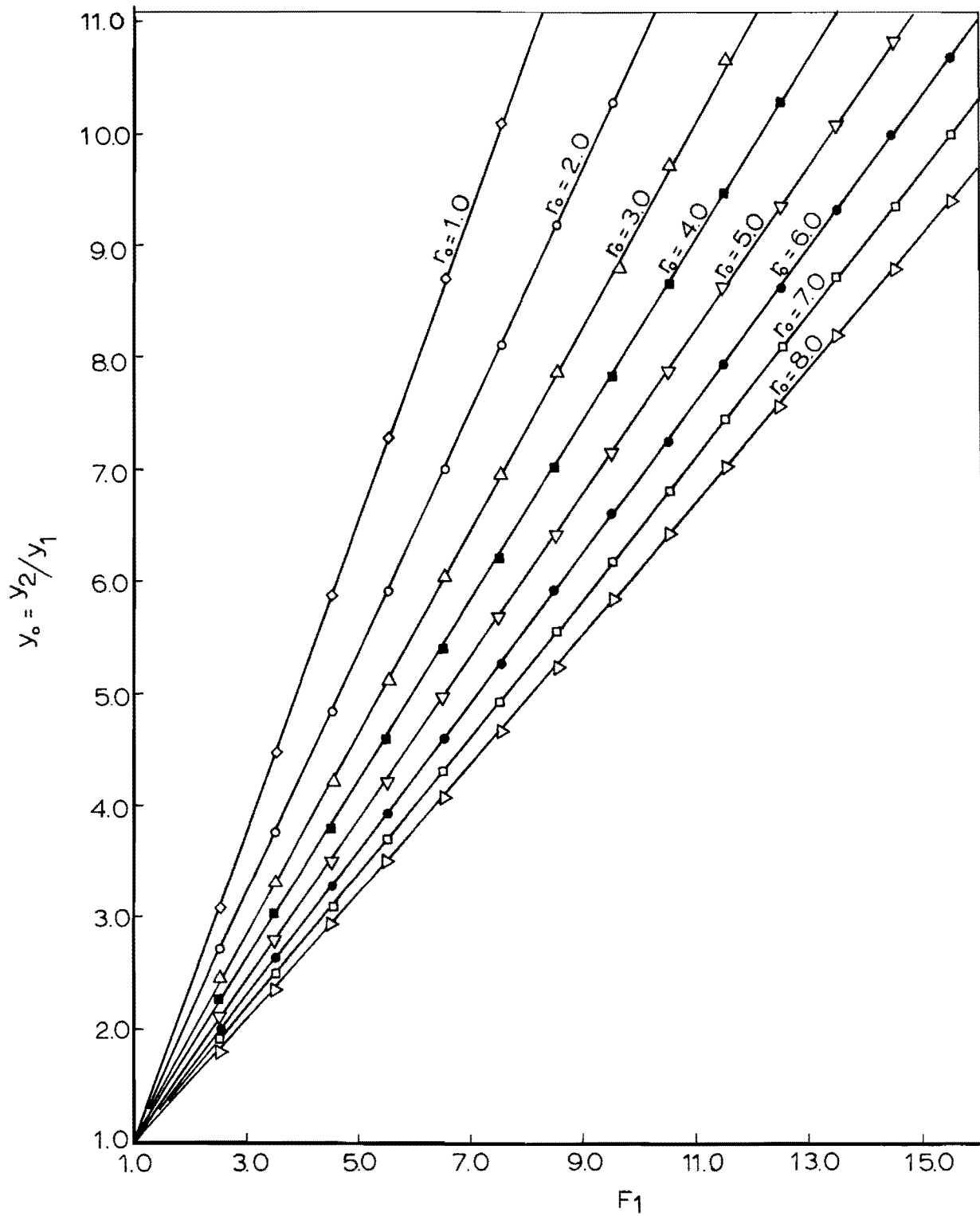
Direct substitution of continuity equation into equation (4.16) and its simplification results in:

$$1 - \frac{r_2}{r_1} \left(\frac{y_2}{y_1}\right)^2 + \left(\frac{1}{3}\right) \left(\frac{r_2}{r_1} - 1\right) \left[1 + \left(\frac{y_2}{y_1}\right)^2 + \frac{y_2}{y_1} \right] = \frac{2V_1^2}{gy_1} \left(\frac{r_1 y_1}{r_2 y_2} - 1\right) \quad (4.17)$$

Now letting, $y_o = y_2/y_1$, $r_o = r_2/r_1$, and $F_1 = V_1/\sqrt{gy_1}$ which is the Froude number upstream from the jump, and substituting them into equation (4.17) results in:

$$y_o^3 - \frac{r_o - 1}{2r_o + 1} y_o^2 - \frac{r_o + 6F_1^2 + 2}{2r_o + 1} y_o + \frac{6F_1^2}{r_o(2r_o + 1)} = 0 \quad (4.18)$$

It is desirable to obtain a simplified form of equation (4.18) so that it can be more readily applied to design situations. A simplified circular jump equation may be obtained by plotting numerous values of y_o and F_1 for different values of r_o . These values are determined for a practical range of variables by a FORTRAN IV computer algorithm run on CDC-6600 computer and plotted in Figure 4-4. The Newton-Raphson iterative technique was the basis for this computer solution. Other information concerning the computer program such as description of variables, flow chart, and program write-up are shown in Appendix A. Several features of Figure 4-4 are noteworthy and helpful in indicating that a simple

FIG. 4.4. PLOT OF y_0 VS. F_1

relationship between y_o , r_o , and F_1 exists for the range of variables of common interest. These features are that: (1) a linear functional relationship is present between y_o and F_1 for a specified r_o ; (2) the curves having r_o of 1.0 through 8.0 all intersect at a common point; and (3) the angle confined between any two consecutive r_o curves decreases in somewhat a uniform rate as r_o increases. Based on these indications, linear equations of a straight line of the form:

$$y_o = m F_1 + c \quad (4.19)$$

where m is the slope of the curve and c is the intercept of y_o axis are fitted to the curves of Figure 4-4. It is fortuitous that the following relationship holds true for the range of r_o under consideration:

$$m + c = 1.0 \quad (4.20)$$

The reason for validity of equation (4.20) is that the point of intersection of all curves coincide with a point having y_o and F_1 coordinates of 1, and 1. This condition, hence, suggests that:

$$y_o = m F_1 + 1 - m \quad (4.21)$$

or

$$y_o = 1 - m (1 - F_1) \quad (4.22)$$

Since the angle confined between any two consecutive r_o curves appears to change in a systematic manner, a relationship between r_o and m must exist. This relationship could be detected from the graph of m versus r_o . Therefore, values of m as a function of r_o are plotted in a

Log - Log graph paper as shown in Figure 4-5. The equation of the curve passing through the plotted points in Figure 4-5 is found to be:

$$m = 1.54 r_o^{-0.47} \quad (4.23)$$

Substitution of equation (4.23) into equation (4.22) results in the following simplified version of equation (4.18).

$$y_o = 1 - 1.54 r_o^{-0.47} (1 - F_1) \quad (4.24)$$

The error resulting in computation of y_o from equation (4.24) was less than 3% of that computed from equation (4.18) for the range of variables shown in Figure 4-4. This error is within the acceptable limits for hydraulic jump computations.

Through the application of equations (2.6) and (4.24), proper stilling basin dimensions such as the length, the flaring angle and the height of the wingwalls are determined. The flaring angle of wingwalls and the length of the basin are first selected in a trial process, with some controlling factors. These factors are as follows: The flaring angle θ must be within an effective range of 15° to 45° , which was determined experimentally, and the maximum allowable length of the basin is fixed by the geometry and properties of the area under consideration. With these limitations in mind, an arbitrary length is selected. Since B and b are known parameters, for a trial value of length, the angle θ could be computed from the geometry of the basin.

Upon selection of the first trial values of basin length (L) and the flaring angle θ , the values of y_f and V_f must be computed. y_f and V_f

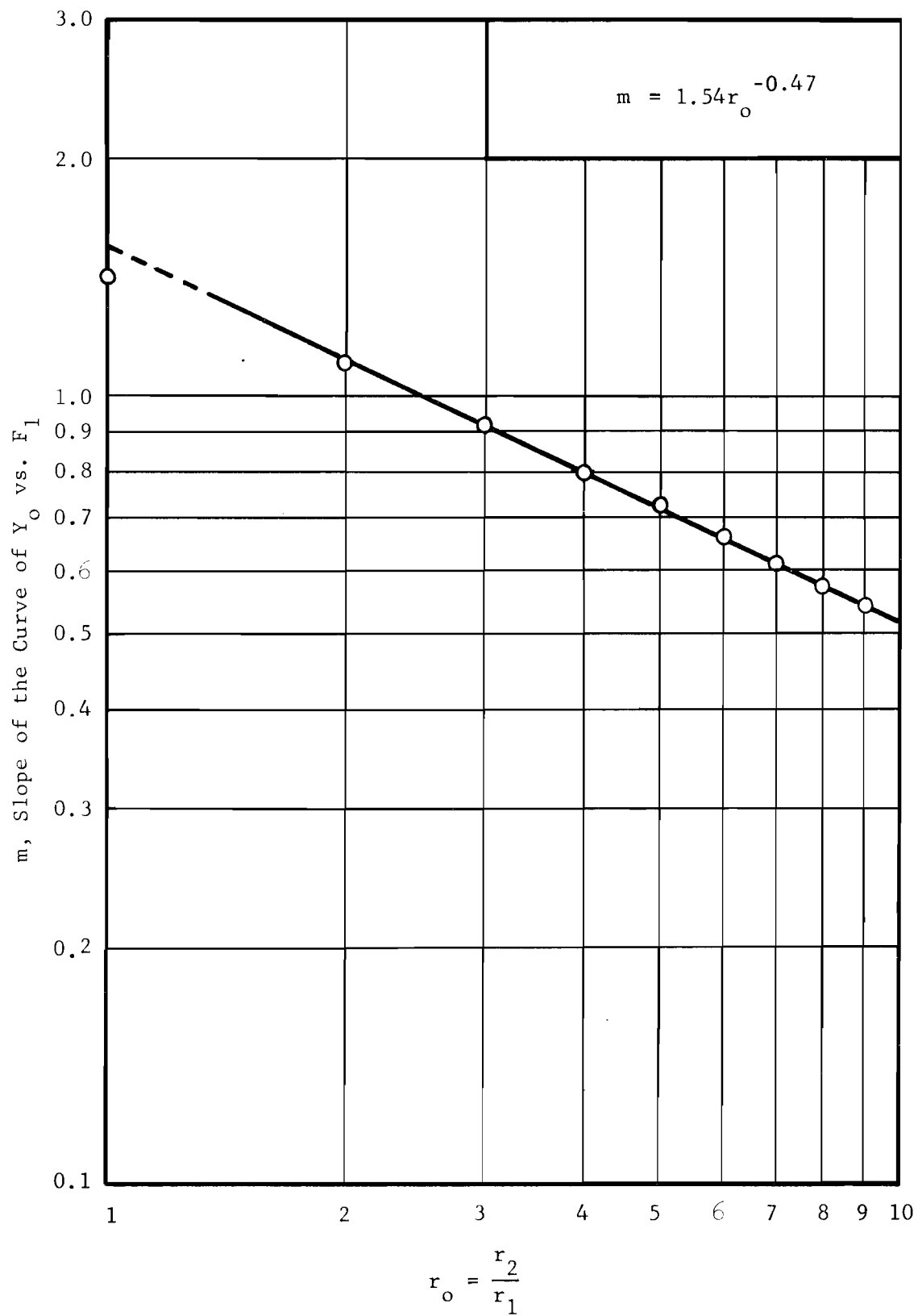


FIG. 4-5 GRAPH OF m vs. r_o

are the index depth and average flow velocity at the beginning of the basin. This information may be attained through the application of Bernoulli's and continuity equations. Bernoulli's equation is applied between the upstream end of the entrance channel (section t) and the beginning of the basin (section f), neglecting losses occurring in this channel segment. Sections t and f are shown in Figure 4-2. Since the pressure at both sections is atmospheric, P/γ terms are dropped from Bernoulli's equation resulting in:

$$\frac{V_t^2}{2g} + y_t + Z = \frac{V_f^2}{2g} + y_f = \frac{Q^2}{2g b^2 y_f^2} + y_f \quad (4.25)$$

where Z is the height of drop of entrance channel. All parameters in equation (4.25) are known quantities except y_f . This equation must, therefore, be solved in order that the numerical value of y_f may be determined. Applying the continuity equation,

$$Q = V_f y_f r_f \theta \quad (4.26)$$

the magnitude of V_f is evaluated. r_f is the radial distance from the intersection of flaring wingwalls to the beginning of the stilling basin.

The next step is to decide where the leading edge of the jump is to occur. The jump may at first be assumed to occur at $x = 0, y_f, 2y_f, 3y_f$, etc. It might be necessary to use different increments in variation of x instead of y_f . The incremental variation of y_f is merely a recommendation and need not be exactly followed. Intermediate values may be used for more accurate results if necessary. The computation starts by assuming that the leading edge of the jump is at the beginning of the basin

($x = 0$). Then, F_1 which is the Froude number upstream from the jump may be evaluated. Since F_1 , r_1 , y_1 are now known quantities, simultaneous solution of equations (2.6) and (4.24) results in values of y_2 and r_2 . Upon determination of the value of y_2 , the water surface elevation should be compared to that of the tailwater level. If close agreement is present between these two values, then, the assumed value of x indicates the true section at which the jump occurs, if the two values of depth do not compare closely then the next recommended value, i.e. $x = y_f$, should be tried. This process must continue until the intended agreement is attained between the sequent depth of hydraulic jump and available tailwater depth. It should be noted that when $x = 0$, then $y_f = y_1$ and $V_f = V_1$, which are already determined quantities. However, if $x > 0$ values of r_1 and y_1 should be determined prior to the simultaneous solution of equations (2.6) and (4.24). Equation (2.34) may be used for this purpose assuming that the boundary frictional losses of supercritical flow within the basin are negligible. This equation states that:

$$y_f r_f = y_1 r_1 \quad (4.27)$$

When the position of the jump is fixed at a specified distance x , r_1 could be determined from the geometry of structure and y_1 is evaluated from equation (4.27). Hence, the necessary information upstream from the jump is known and solution of equations (2.6) and (4.24) results in the values of y_2 and r_2 .

It should be recalled that the computations of basin dimensions so far are based on the first trial value of basin length. A check in the

validity of trial value of the length is therefore a necessity. The length of the basin may be computed mathematically from the following functional relationship:

$$L = x + r_2 - r_1 \quad (4.28)$$

It is not always necessary that the entire body of the jump be confined within the basin. For this reason a shorter length (L) may be recommended as computed by equation (4.29)

$$L = x + 0.8 (r_2 - r_1) \quad (4.29)$$

Equation (4.29) can be used as the lower limit of the basin's length. If the computed value of L agrees with the originally selected value, then the design is completed; if not, a new trial value of L must be selected, and the computations repeated until a satisfactory result is attained. When the final selection of L is made and basin computations are completed, y_2 plus an appropriate freeboard determines the minimum required height of the wingwalls. The freeboard of the basin is the vertical distance from the top of the flaring wingwalls to the water surface at design conditions. This distance should be sufficient to prevent waves or fluctuations in water surface from overflowing the sides. Since the height of freeboard will depend upon the design discharge, a general value may not be recommended. Chow (16) has recommended approximate rules for determining the freeboard and the height of bank for lined canals and the designer may refer to them in estimating appropriate freeboard heights.

When tailwater conditions are such that a hydraulic jump cannot be created within the basin, primarily due to the effects of tailwater depth,

an end sill or an abrupt rise must be incorporated into the structure. Experimental studies have shown that the end sill can force the jump to form within the basin and, furthermore, the height of the sill plays an important part in stabilizing the jump at a particular position. Bernoulli's equation may be used between the downstream end of the jump and the downstream channel to determine the feasibility of a recommended sill height.

The first step in carrying out the flow computations with regard to sill height is the determination of the critical depth of flow on the brink of the abrupt rise. The following equation may be used for this purpose

$$\frac{V_s^2}{2g} = \frac{D_s}{2} \quad (4.30)$$

where D_s and V_s are the hydraulic depth and the mean velocity on the sill respectively. In the case of rectangular channel section $D_s = y_s$, where y_s is the mean flow depth on the sill. Upon recommending a sill height, the computation of the actual depth of flow on the sill may be carried out through the application of Bernoulli's equation and consideration of the following assumptions: (1) the sequent depth of the hydraulic jump occurs upstream from the face of the sill, and (2) the losses due to the abrupt rise are equal to one approaching velocity head (i.e. $V_2^2/2g$). Bernoulli's equation used for this purpose has the form:

$$\frac{V_2^2}{2g} + y_2 = \frac{V_3^2}{2g} + y_3 + H_s + H_L \quad (4.31)$$

where y_3 and V_3 are the flow depth and velocity in the downstream channel,

H_s is the sill height, and H_L represents losses due to the abrupt rise. Substitution of the loss term into equation (4.31) and its simplification results in:

$$y_2 = \frac{v_3^2}{2g} + y_3 + H_s \quad (4.32)$$

Equation (4.32) must be solved for value of y_3 . If there is not any positive value of y_3 which satisfies equation (4.32) then the sill height is too large and a smaller trial value is selected and the computations repeated. This process continues until a desirable height of sill is attained. When y_3 is smaller than y_c the flow would go through the critical depth at the brink and the height of the downstream channel sides in the immediate vicinity of the sill should be equal to y_c plus an appropriate freeboard. If y_3 is larger than y_c , then the available depth of downstream channel must be y_3 plus the necessary freeboard.

The aforementioned design procedure is for rectangular downstream channel. The same procedure with certain modifications based on experimental observation is recommended for the design of a stilling basin with a trapezoidal downstream channel. The basic difference in the latter case is the design of a workable transition from the stilling basin to the trapezoidal downstream channel. It should be noted that in the design of stilling basin dimensions for rectangular channel, B was the bottom width of the channel. When encountering computations of the trapezoidal channel basin the bottom width of the trapezoidal channel could be used as B wherever applicable. The recommended transition from the stilling basin to the downstream channel is a pair of symmetrically placed triangular

converging walls and an end sill. The method for the computations of the height of sill should be similar to that outlined for rectangular channel.

The triangular converging walls must be located such that the apex of the triangular surface coincides with the point of intersection of the top of side slope of downstream channel with the plane of the flared wingwalls. One edge of the triangular wall, referred to as a' , should be placed along the side slope of the channel at the beginning of the trapezoidal section. This edge (a') must start at the apex of the triangular wall and terminate on the stilling basin bottom. The base of the triangular converging walls is set on the horizontal bottom of the stilling basin. It was experimentally determined that the performance of the basin was not too sensitive to this base length within the experimental range. For this reason a general rule is recommended for the selection of the magnitude of this dimension. This rule states that the base length of the converging walls should be approximately equal to the projected length of a' on a horizontal plane when the horizontal angle confined within them is less than or equal to 45° . If the magnitude of the angle exceeds this upper limit a shorter base length should be selected such that a 45° angle is maintained. The third edge of the triangular wall could easily be determined from the geometry of the basin, thus completing the selection of the dimensions of the transition segment. It is realized that this is a conservative design, however, in the absence of any other method it could be used with satisfactory results. The triangular walls are preferred to a sudden contraction between the stilling basin and the downstream channel for economy of construction.

The design procedure developed in this chapter is intended to help the engineer to undertake the design of an effective radial flow energy dissipator. Based on this procedure a prototype culvert installation and energy dissipating structure was designed for a set of field conditions which were provided by Texas Highway Department. A model of the energy dissipating structure having a scale ratio of 1:3 was constructed and tested at Balcones Research Center, The University of Texas at Austin. The details of this installation with the experimental results are shown in Appendix B.

CHAPTER 5
CONCLUSIONS

Laboratory experimental investigations showed the effectiveness of the radial flow energy dissipator in stabilizing the jump, reducing the energy of high-velocity flow, and spreading the flow within the basin for a range of F_t of less than or equal to approximately 2.6. It should be noted that higher values of F_t could be used effectively if the magnitude of the radius of the curvature of entrance channel is changed to suit the particular range of design Froude number. The sensitivity of the performance of the structure to such variables as the flaring angle of wingwalls, the ratio of the width of downstream channel to the culvert diameter, and the total height of the drop from the culvert outlet to the basin floor were explored. Also, the adaptability of the dissipator to rectangular and trapezoidal downstream channels was investigated. Three basic parameters were varied in constructing nine different configurations of the model. These parameters included the horizontal angles of wingwalls of 10° , 15° , 22.5° , and 30° ; the ratios of the width of the downstream channel to the diameter of the culvert of 1, 2, and 4; and the ratios of the height of drop, from the culvert outlet to basin floor, to the culvert diameter of 1 and 3.

Experimental information on the effective range of variables for satisfactory performance of the basin together with a semi-analytical treatment of the hydraulic characteristics of the radial flow basin led to the development of a design procedure which may be used for the selection

of the important dimensions of a radial flow dissipator under a given set of field conditions.

The comparison of the relative jump stability characteristic of the various structures showed that the trapezoidal downstream arrangements TRAP 2, TRAP 4, TRAP 5 performed with satisfactory results. The hydraulic jump was formed in each of these structures independent of tailwater requirements within the experimental range of F_t . In structures with a rectangular downstream channel, arrangement REC 3 appeared to be the most effective basin followed by arrangement REC 4. Arrangement REC 1 was not particularly suitable for radial flow energy dissipation as it did not provide sufficient expansion of flaring wingwalls for full radial flow development.

From the point of view of velocity reduction and uniformity of distribution in the downstream channel, all of the TRAP arrangements exhibited a high degree of velocity reduction and uniformity. The downstream channel velocities varied within a small range in all TRAP geometric configurations. However, the velocities upstream from the jump varied considerably from arrangement TRAP 2, 3, and 4 to arrangement TRAP 5 for the same F_t . So far as the rectangular downstream channel structures were concerned, the best basins were arrangements REC 4 followed by REC 3 for reducing the velocity and yet maintaining a fairly uniform velocity distribution in the downstream channel. The effectiveness and efficiency in velocity reduction and distribution of arrangement REC 1 was considered to be unsatisfactory.

Generally speaking, the radial flow basins maintained a fairly uniform spreading of the flow except for a high wave and spray formation

near the upstream portion of the flaring wingwalls. Experiments indicated that the best spreading action with continuous decrease in the flow depth along the radial lines, the best symmetry of flow profile about the centerline, and the smallest depth of waves adjacent to the flaring side walls were provided by arrangement REC 2. Other arrangements also performed satisfactorily in this respect and the observed difference in performance between the various structural configurations were relatively small. The depth of water in the REC arrangements were measured along radial lines while in the TRAP arrangements were only measured along the basin centerline since the hydraulic jump was always formed automatically and independent of tailwater requirements within the basin.

The overall comparison of the performance of various geometric arrangements indicated that the radial flow energy dissipator could be effectively utilized for a range of flaring angle of wingwalls between 15° to 45° , the B/b ratios of 2 to 4, and the height of drop of entrance channel in excess of one culvert diameter or width. Experiments showed that the structures having the transition section between the basin and the trapezoidal downstream channel which consisted of a pair of triangular converging walls and an end sill performed satisfactorily. Furthermore, the basin performance was not too sensitive to the size of the triangular converging walls within the range of the experimental investigation. The trapezoidal channel basin could not operate efficiently without an end sill.

According to the results obtained and analyzed, the general performance of the basins with trapezoidal downstream channel was preferred to that of rectangular downstream section. This evaluation was based on the tailwater requirements, the velocity reduction, and the jump stability.

The stilling basin for trapezoidal channel is self-cleaning and there would be no danger of ordinary debris accumulating within it.

Since model simulation proved the effectiveness of a radial flow basin, a design procedure was developed for the selection of the dimensions of such structure for a prototype energy dissipator. Due to the fact that the model used in this investigation made use of a circular hydraulic jump, the theoretical analysis of this type of jump was undertaken and a circular jump equation was derived. The development of the circular hydraulic jump equation was based on the application of the continuity and momentum principles applied to a sector of the jump. A simplified form of this equation was obtained through graphical and mathematical analyses. The application of this equation was the basis for the design procedure.

A trial and error process was followed in the design of various dimensions of a prototype basin. The design outline gave consideration to the selection of culvert size and slope, entrance channel dimensions, stilling basin components, and downstream channel improvements. A theoretical equation was presented for the determination of the vertical radius of curvature of the entrance channel. This equation results in the evaluation of a radius of curvature for an entrance channel with minimum undesirable characteristics due to the negative pressure head on the channel bed.

BIBLIOGRAPHY

1. Silvester, R., "Hydraulic Jump in all Shapes of Horizontal Channels," Proceedings, ASCE, Journal Hydraulic Division, Vol. 90, No. HY 1, January 1964.
2. U. S. Bureau of Reclamation, Progress Report II, "Research Study on Stilling Basins, Energy Dissipators, and Associated Appurtenances," Hydraulic Laboratory Report Hyd. - 399, June 1955.
3. Argyropoulos, P. A., "Theoretical and Experimental Analysis of the Hydraulic Jump in Parabolic Flume," Seventh Conference, I.A.H.R. Paper D12, Vol. ii, 1957.
4. Kindsvater, C. E., "Hydraulic Jump in Enclosed Conduits," M. S. Thesis, State University of Iowa, 1936.
5. Rajaratnam, N., "Profile of the Hydraulic Jump," Proceedings, ASCE, Journal Hydraulic Division, Vol. 94, No. HY 3, May 1968.
6. Sadler, C. D. and M. S. Higgins, "Radial Free Surface Flow," M. S. Thesis, Massachusetts Institute of Technology 1963.
7. Koloseus, H. J. and D. Ahmad, "Circular Hydraulic Jump," Proceedings, ASCE, Journal Hydraulic Division, Vol. 95, No. HY 1, January 1969.
8. Rand, W., "Flow Geometry at Straight Drop Spillways," Proceedings, ASCE, September 1955.
9. Bradly, J. N. and A. J. Peterka, "Hydraulic Design of Stilling Basins," Proceedings, ASCE, Journal Hydraulic Division, Vol. 83, No. HY 5, October 1957.
10. Keim, D. R., "The Contra-Costa Energy Dissipator," Proceedings, ASCE, Journal Hydraulic Division, Vol. 88, No. HY 2, March 1962.
11. Elevatorski, E. A., Hydraulic Energy Dissipators, McGraw-Hill Book Co., New York, 1959.
12. Aguirre, R. G., "Radial Flow Energy Dissipator for Culvert Outlets," Ph. D. Dissertation, The University of Texas at Austin, January 1968.
13. Wear, R. R., "Culvert Outlet Energy Dissipator Incorporating Radial Flow and a Transverse Sill," M. S. Thesis, The University of Texas at Austin, January 1968.

14. Moore, W. L. and K. Meshgin, "Adaptation of Radial Flow Energy Dissipator for Use with Circular or Box Culverts," Center for Highway Research, The University of Texas at Austin, December 1969.
15. Davis, W. B., "Transition Phenomena in Radial Free Surface Flow," M. S. Thesis, Massachusetts Institute of Technology 1958.
16. Chow, V. T., Open-Channel Hydraulics, Mc-Graw Hill Book Co., New York, 1959.

APPENDICES

APPENDIX A

DESCRIPTION OF PROGRAM CUBE

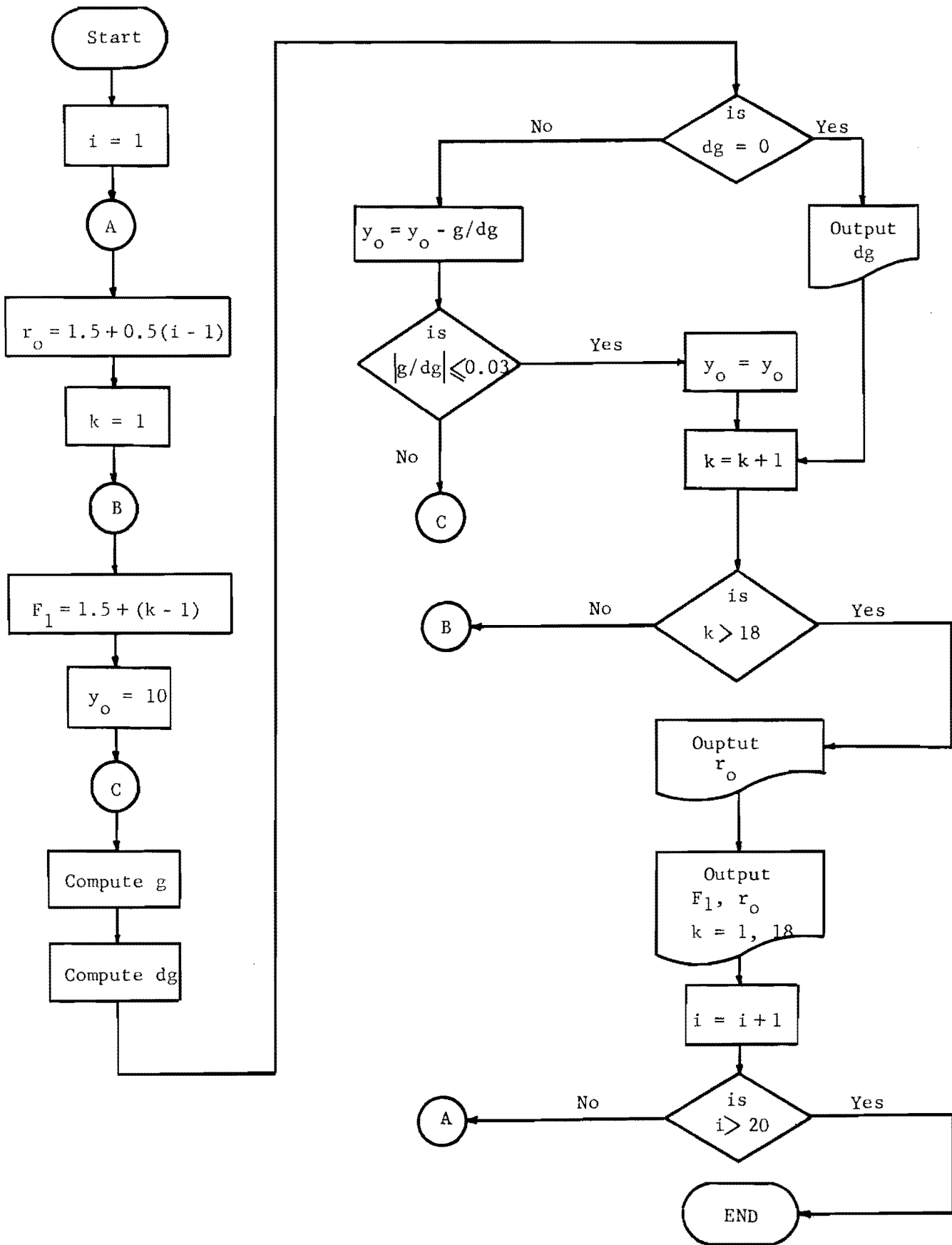
Program CUBE, written in FORTRAN IV, is an algorithm for the solution of the circular hydraulic jump cubic equation (4.18). The Newton-Raphson iterative technique is the basis for this computer solution. Notation and description of variables, the flow chart, and the program write-up are shown in this appendix.

NOTATION AND DESCRIPTION OF VARIABLES - PROGRAM CUBE

Input Parameters

<u>FORTTRAN</u> <u>Notations</u>	<u>General</u> <u>Notations</u>	<u>Description</u>
R(I)	r_o	Ratio of the radial distance from the intersection of flared wingwalls to the end of the jump to the radial distance to beginning of jump.
F(K)	F_1	Froude number upstream from the jump.
I		Integer indicating the range of variation of r_o .
K		Integer indicating the range of variation of F_1 .
Y	y_o	Ratio of the depth of flow after the jump to depth fo flow before the jump.
G	g	Equation (4.18).
DG	dg	First derivative of equation (4.18).

FIG. 1A - FLOW CHART FOR PROGRAM CUBE



PROGRAM CUBE (INPUT, OUTPUT)	1
DIMENSION R(50),F(50),Y(50)	2
PRINT 6	3
6 FORMAT(1H1)	4
DO 10 I = 1,20	5
R(I) = 1.5+(I-1)*0.5	6
DO 20 K = 1,18	7
F(K) = 1.5+(K-1)	8
Y=10.0	9
4 G = (2.0*R(I)+1.0)*Y**3-(R(I)-1.0)*Y**2-(R(I)	10
1+6.0*F(K)**2+2.0)*Y+6.0*F(K)**2/R(I)	11
DG=3.0*(2.0*R(I)+1.0)*Y**2-2.0*(R(I)-1.0)*Y	12
1-(R(I)+6.0*F(K)**2+2.0)	13
IF(DG.EQ.0.0) GO TO 120	14
Y=Y-G/DG	15
IF(ABS(G/DG)-0.03) 2,2,4	16
2 Y(K)=Y	17
GO TO 20	18
120 PRINT 121,DG	19
121 FORMAT(50X,F5.2)	20
20 CONTINUE	21
PRINT 35,R(I)	22
35 FORMAT(4X,*R =*,F4.1,//)	23
PRINT 15,(Y(K),K = 1,18)	24
15 FORMAT(2X,18(X,F6.2),//)	25
PRINT 25,(F(K),K = 1,18)	26
25 FORMAT(7X,18(X,F5.2),//)	27
10 CONTINUE	28
END	29

APPENDIX B
DESIGN AND EXPERIMENTAL RESULTS OF A TYPICAL
CULVERT AND ENERGY DISSIPATOR INSTALLATION

In order to investigate the validity and workability of the design procedure outlined in Chapter 4, several dimensional configurations for two prototype structures were selected based on a set of existing field conditions provided by Texas Highway Department. The information supplied by the above agency included such features as the topography of the area, road dimensions of highway crossing, design discharge, and the available headwater depth at culvert inlet. The recommended design details of one of these structures is outlined herein to serve as a guide to those using the design procedure described in Chapter 4.

Statement of the Problem

A design discharge of 120 cfs is delivered to a highway crossing. The highway dimensions, culvert inlet elevation, downstream natural channel elevation, and the available headwater depth are shown in Figure 1B. The natural channel had a trapezoidal cross section with 1.5:1 side slopes. Design a culvert and a radial flow energy dissipator at the culvert outlet. As shown in Figure 1B:

Inlet Flow Line Elevation = 87.0'

Road Surface Elevation = 100.0'

Downstream Flow Line Elevation = 82.3'

Available Headwater Depth = 5.0'

Available Tailwater Depth = 1.5'

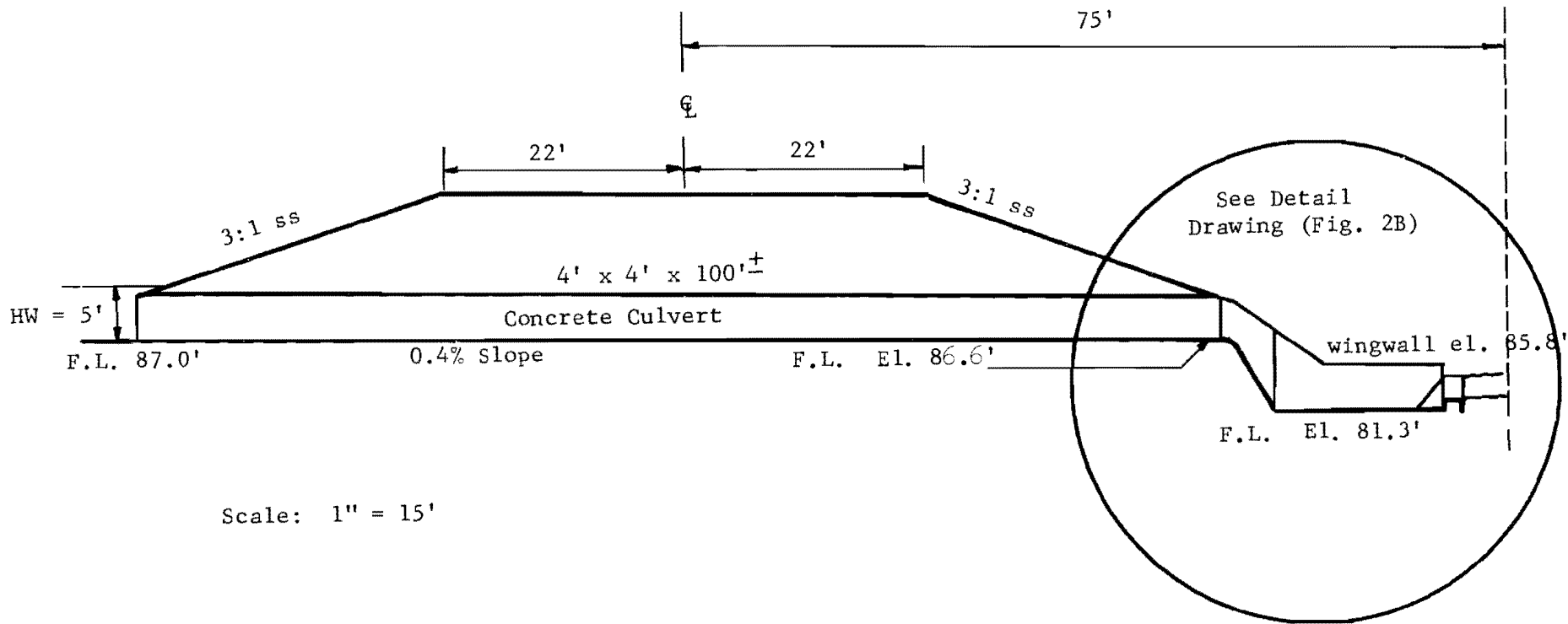


FIG. 1B TYPICAL HIGHWAY CULVERT INSTALLATION AND ENERGY DISSIPATOR

Design Procedure

Stepwise method of computations includes (I) design of culvert dimensions, (II) design of entrance channel components, (III) selection of stilling basin dimensions, and (IV) design of transition section from the stilling basin to the trapezoidal downstream channel. Detail computations of each step is as follows:

Step I - Culvert Design: Assume the first trial value of a box culvert having square-edged entrance and:

$$b = 4' \quad \text{Culvert width}$$

$$d = 4' \quad \text{Culvert height}$$

$$\frac{Q}{b} = \frac{120}{4} = 30$$

From chart 17-29, page 498, Chow (16), $H/d = 1.25$, where H is the headwater depth. Therefore,

$$H = 1.25d = 1.25 (4) = 5.0'$$

Since the computed headwater depth is equal to the available headwater depth, the trial box size of 4' x 4' is recommended as the actual culvert size to be used. Computing the critical depth within the box culvert results:

$$y_c = \sqrt[3]{\frac{Q^2}{b^2 g}} = \sqrt[3]{\frac{(120)^2}{(4)^2 (32.2)}} = 3.0' \quad \text{critical depth of flow in culvert}$$

$$A_c = by_c = 4 \times 3 = 12 \text{ ft.}^2 \quad \text{critical area in culvert}$$

$$R_c = \frac{A_c}{p} = \frac{12.0}{10.0} = 1.2' \quad \text{critical hydraulic radius}$$

$n = 0.012$ Manning roughness coefficient for concrete pipe

$$S_c = \left(\frac{Q n}{1.49 A_c R_c^{2/3}} \right)^2 \quad \text{Manning equation - critical slope of flow}$$

$$S_c = \left[\frac{120 (.012)}{1.49 (12) (1.2)^{2/3}} \right]^2 = 0.0049 \text{ or } 0.49\%$$

Assume $S_o = 0.4\%$ Slope of the culvert

$$\frac{AR^{2/3}}{b^{8/3}} = \frac{Q n}{1.49 (S_o)^{1/2} (b)^{8/3}} = \frac{120 (.012)}{1.49 (.0063) (40)} = 0.38$$

From charts in page 130 Chow (16), $\frac{y_n}{b} = 0.82$

$y_n = 0.82 (4) = 3.28'$ Normal depth of flow in culvert

Since $S_o < S_c$, Critical depth of flow occurs at the outlet of culvert just upstream of entrance channel.

Final culvert design details are:

Culvert Inlet F. L. Elevation = 87.0'

Culvert Outlet F. L. Elevation = 86.6'

Culvert Size = 4' x 4' x 100'

Slope of Culvert (Mild) = 0.4%

Flow Depth at Culvert Outlet = 3.0'

Step II - Entrance Channel Components: Assume the maximum allowable negative pressure head on the curved section (p_2/γ) to be $-y_t$, and the point of curvature of the entrance channel vertical curve start at exactly the outlet of the culvert, then:

$$F_t = 1.0 \quad \text{and} \quad y_t = 3.0 \text{ feet}$$

Determine the magnitude of the radius of curvature (R) from equation (4.13) as follows:

$$\frac{1.5}{1} = \text{Log}_e \left(1 + \frac{3}{R} \right)$$

$$R = 0.86 \text{ ft.}$$

Note that the minimum required radius is 0.86 ft.; however, the geometry of the area requires a larger radius. Thus a radius of 3.5 ft. is recommended.

$$\text{Use } R = 3.5'$$

$$\alpha = 60^\circ$$

Deflection angle between the tangent section to the downstream end of entrance channel vertical curve and horizontal stilling basin bottom.

The height of the wingwalls and the width of the entrance channel along with other pertinent information are shown in Figures 2B and 3B.

Step III - Stilling Basin Design: The beginning width of the basin is set as the width of entrance channel which is 4' while the end width of the basin is fixed by the geometry of the area to be 11.8' which is the top width of the downstream channel. Select the first trial value of basin length (L) along the centerline by letting $L = 12.0'$. From the basin's geometry compute,

$$\tan \theta = \frac{3.9}{12} = 0.325$$

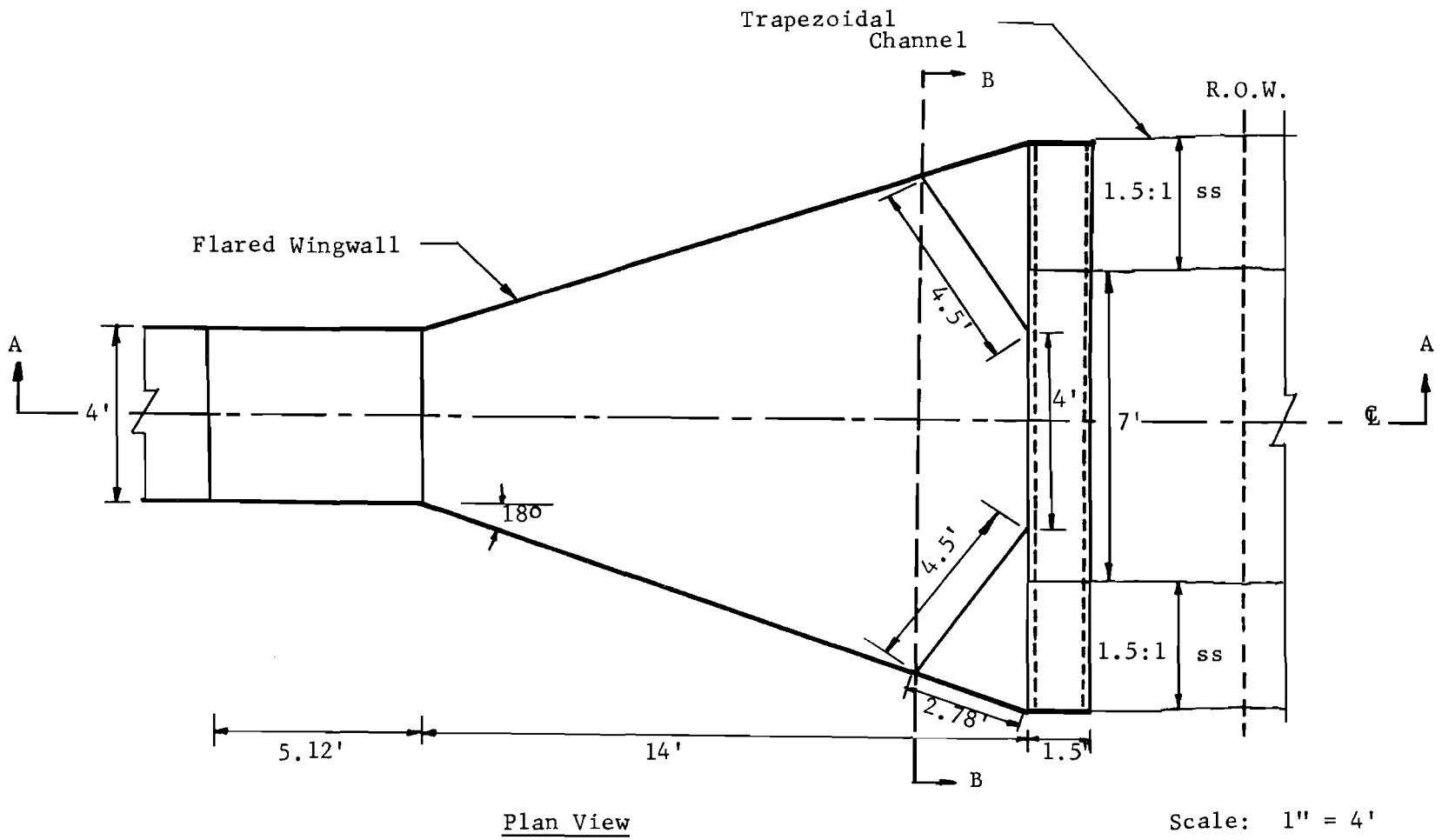
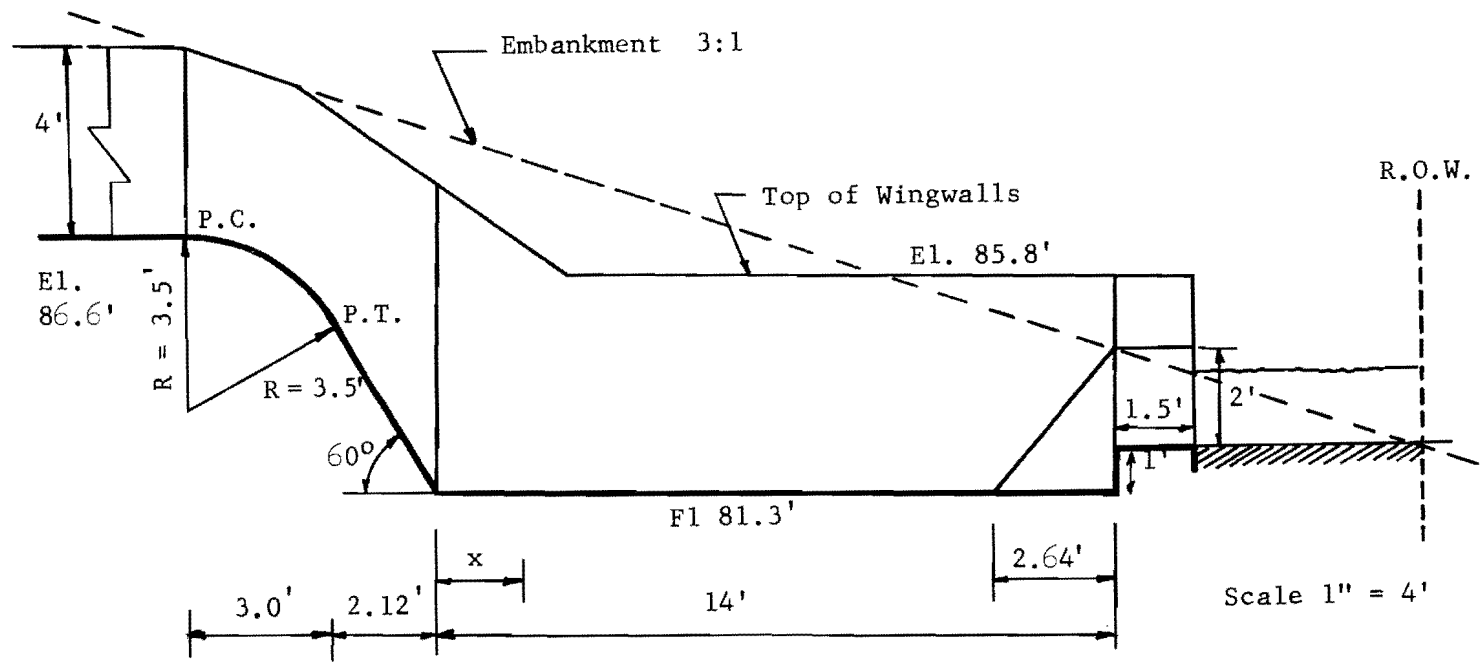


FIG. 2B RADIAL FLOW STILLING BASIN



Elevation View-Section AA

FIG. 3B RADIAL FLOW STILLING BASIN

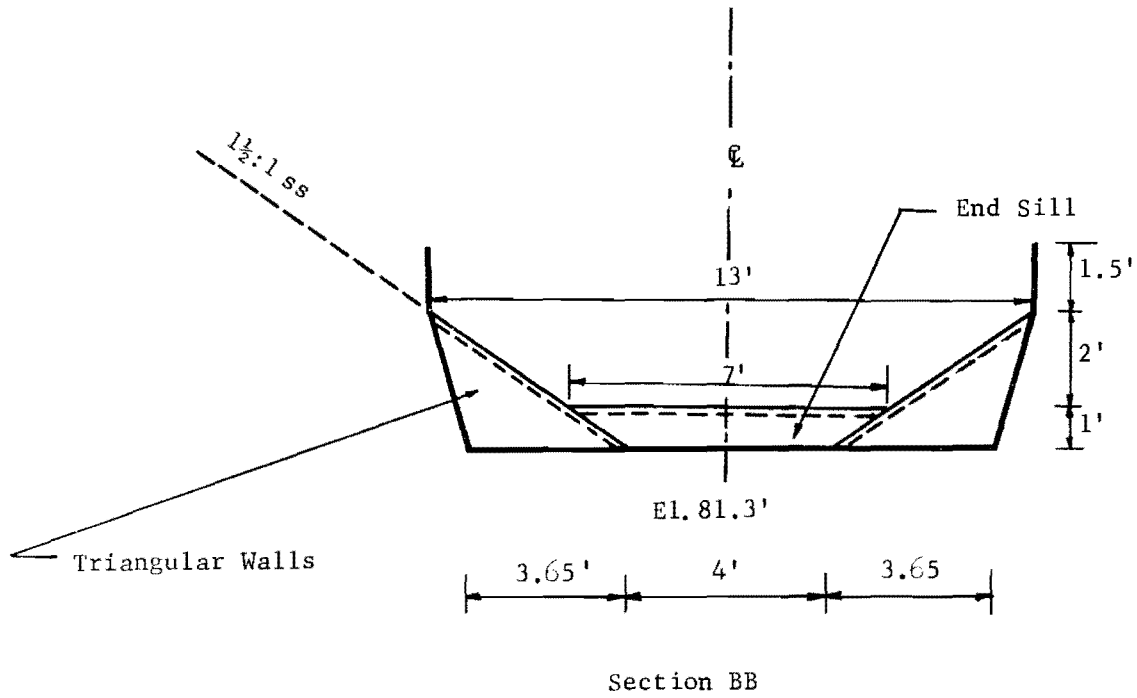


FIG. 4B VIEW OF THE TRANSITIONAL SECTION AND THE END SILL

$$\theta = 18^{\circ}$$

Flared angle of wingwalls

Set the elevation of the horizontal bottom of stilling basin at 81.3' to account for a 1' end sill. Now the index depth at the beginning of the basin could be determined by using Bernoulli's equation between this section and the outlet of culvert, neglecting frictional losses, as follows:

$$\frac{v_c^2}{2g} + y_c + Z = \frac{(Q/by_f)^2}{2g} + y_f$$

$$\frac{(10)^2}{2g} + 3.0 + 5.3 = \frac{900}{2g y_f^2} + y_f$$

Solving for y_f results:

$$y_f = 1.28'$$

The index depth at the beginning of basin

From the geometry of the basin:

$$r_f = \frac{b}{2 \sin \theta}$$

Radial distance from the intersection of the flared wingwalls to the beginning of basin.

$$r_f = \frac{4.0}{2 \sin 18^{\circ}} = 6.5'$$

Assuming negligible boundary friction for supercritical flow equation

(4.27) may be evaluated as follows:

$$r_1 y_1 = r_f y_f$$

$$r_1 y_1 = 6.5(1.28) = 8.31 \quad \text{constant}$$

Using equation (4.26):

$$V_f = \frac{(360)Q}{2\pi(2\theta)r_1 y_1} = \frac{360(120)}{2\pi(36)8.31} = 22.9 \text{ fps} \quad \text{Supercritical velocity at the beginning of basin.}$$

Since x is the distance along the centerline from the beginning of the basin to the leading edge of the jump, then

$$r_1 = x + r_f$$

Assume $x = 0$, and $2y_f$, where $y_f = 1.28$, and compute the sequent depth of the hydraulic jump (y_2) and the radial distance to the end of the jump (r_2) through the simultaneous solution of equations (2.6) and (4.24) as follows:

Case 1: When $x = 0$

$$y_1 = y_f = 1.28'$$

$$r_1 = r_f = 6.5'$$

$$V_1 = V_f = 22.9 \text{ fps}$$

$$F_1 = \frac{V_1}{\sqrt{gy_1}} = \frac{22.9}{\sqrt{32.2(1.28)}} = 3.57 \quad \text{Froude number upstream from the jump.}$$

Substituting above numerical values and simplifying equations (4.24) and (2.6) one gets:

$$\left\{ \begin{array}{l} y_2 = 1.28 + \frac{12.2}{r_2} \quad \text{From equation (4.24)} \\ y_2 = -0.35 + \frac{r_2}{4} \quad \text{From equation (2.6)} \end{array} \right.$$

Solving for r_2 and y_2 .

$$r_2 = 18.8'$$

$$y_2 = 4.35'$$

$$L_j = r_2 - r_1 = 18.8 - 6.5 = 12.3' \quad \text{Jump length}$$

Case II: When $x = 2y_f = 2.56'$

$$r_1 = r_f + x = 6.5' + 2.56' = 9.06'$$

$$y_1 = \frac{r_f y_f}{r_1} = \frac{8.31}{9.06} = 0.92'$$

$$v_1 = 22.9 \text{ fps}$$

$$F_1 = \frac{22.9}{\sqrt{32.2 (0.92)}} = 4.2$$

Substituting above numerical values and simplifying equations (4.24) and (2.6) results in:

$$\begin{cases} y_2 = 0.92 + \frac{12.48}{r_2} & \text{From equation (4.24)} \\ y_2 = -1.34 + \frac{r_2}{4} & \text{From equation (2.6)} \end{cases}$$

Solving r_2 and y_2 ,

$$r_2 = 21.2'$$

$$y_2 = 3.94'$$

$$L_j = r_2 - r_1 = 21.3 - 9.06 = 11.24'$$

The assumed length of the basin of 12' would be small if the jump had to

occur downstream from $x = 2y_f$. In order to accommodate the transition section and also provide a factor of safety for jump confinement within the basin, total basin length of 14' is recommended. Figures 2B, 3B, and 4B show the details of basin dimensions. Step III computation indicate the approximate position of the leading edge of the jump. As shown in these figures:

$$L = 14'$$

$$\theta = 18^\circ$$

$$\text{Height of Wingwalls} = 4.5'$$

The recommended height of the wingwall would provide sufficient freeboard for safe operation of the basin.

Step IV - Design of the Transition Section and the End Sill: It should be noted that so far the computations were conducted on the basis of a rectangular downstream channel. The selection of the dimensions of converging triangular walls is based on the recommendations outlined in Chapter 4. The base length of the triangular wall is 4.5' which is equal to the projected length of the edge of the triangular surface along the side slope of the downstream channel on the bottom of the basin. The apex of the triangular wall is set at elevation 84.3' which is the point of intersection of the flared wingwalls and the side slope of trapezoidal downstream channel. The details of the transition section are shown in Figures 2B, 3B, and 4B.

The height of the sill (H_s) was previously assumed to be 1.0' in order that the elevation of the bottom of stilling basin could be computed. The workability of the assumed height must now be checked. Application of

equation (4.32) determines the depth of flow on the sill as follows:

$$y_2 = \frac{V_3^2}{2g} + y_3 + H_s \quad \text{Equation (4.32)}$$

$$V_3 = \frac{Q}{(7 + 1.5y_3) y_3} \quad \text{Average velocity on the sill}$$

When the leading edge of the jump is at $x = 2y_f$, calculations showed that $y_2 = 3.94'$ and hence,

$$3.94 = \frac{(120)^2}{2g [(7 + 1.5 y_3) y_3]^2} + y_3 + H_s$$

Above relationship results in $y_3 = 1.35'$ when the height of the sill is 1.0'. Thus, the recommended height of the sill is:

$$H_s = 1.0' \quad \text{Sill height}$$

The critical depth of flow on the sill is calculated as follows:

$$D = \frac{y_{cs} (7 + 1.5 y_{cs})}{7 + 3 y_{cs}} \quad \text{Critical hydraulic depth on sill}$$

$$V_{cs} = \frac{Q}{A} = \frac{120}{y_c (7 + 1.5 y_c)} \quad \text{Critical velocity on sill}$$

$$\frac{V_{cs}^2}{2g} = \frac{D}{2}$$

$$\frac{(120)^2}{2g y_{cs} [(7 + 1.5 y_{cs})]^2} = \frac{y_{cs} (7 + 1.5 y_{cs})}{2 (7 + 3 y_{cs})}$$

y_{cs} could be solved by trial and error to be:

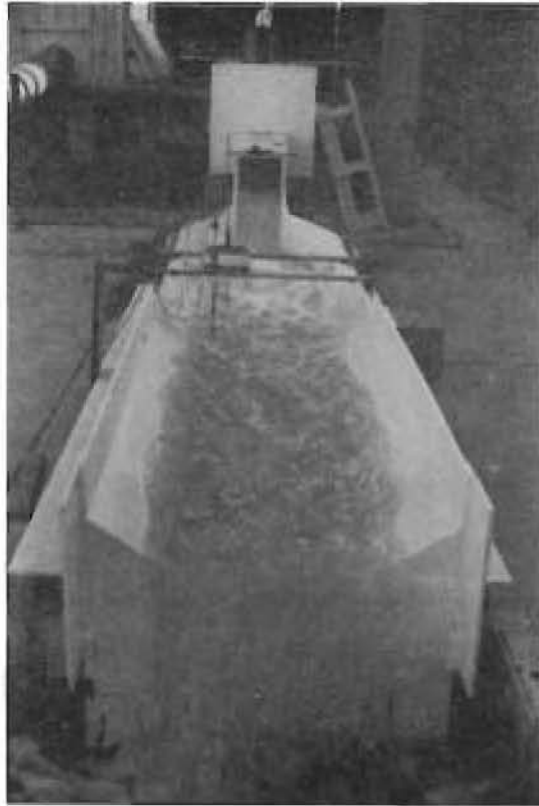
$$y_{cs} = 1.8' \quad \text{Critical depth of flow on sill}$$

Since $y_{cs} > y_3$ the flow would go through critical depth at the brink and the depth of downstream channel in the vicinity of the stilling basin should be 2.5' to provide sufficient depth for flow plus freeboard. Since the allowable tailwater depth is only 1.5', an improvement in the downstream trapezoidal channel is recommended to maintain the required height plus freeboard as shown in Figures 2B and 3B.

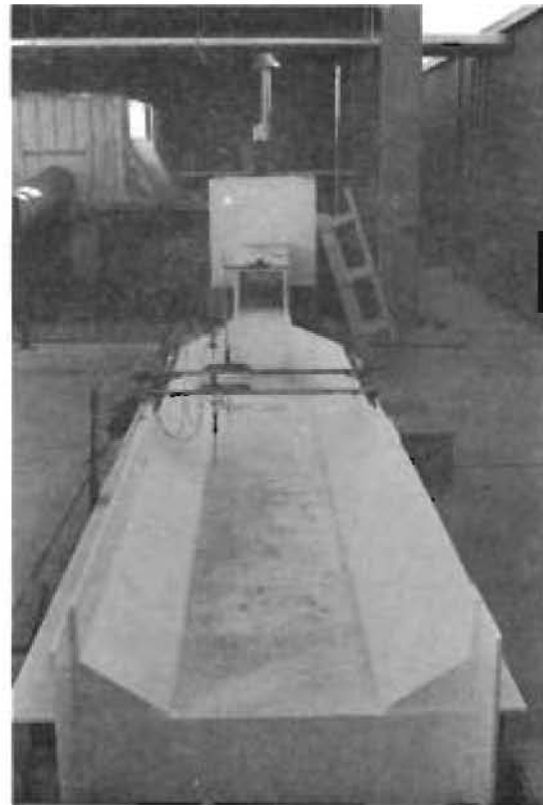
Experimental Results

In order to determine the effectiveness and performance characteristics of the recommended structure, a model of this energy dissipator having a scale ratio of 1:3 was constructed and tested at Balcones Research Center, The University of Texas at Austin. A photographic view of the model with and without flow is shown in Figure 5B. The discharge was delivered to a stilling tank from a 6" diameter supply pipe and was measured by a sharp crested weir after it left the dissipating structure. The stilling tank was 4' x 4' x 8' having a transverse screen within it to damp out the flow disturbance. A horizontal box culvert 8.0' long conveyed the flow from the tank to the entrance channel. All entrance channel, stilling basin, and downstream cross section dimensions were 1/3 of the ones recommended in the design section. A 16' horizontal trapezoidal downstream channel was constructed to minimize the downstream effects on the performance of the dissipating structure.

The experimental procedure included the measurements of the depth of flow at the outlet of the box culvert, the position of the leading edge of the jump, the sequent depths of the hydraulic jump, the depth of flow in the downstream channel, and the velocities in transverse as well as



(a) With Flow



(b) Without Flow

FIG. 5B PHOTOGRAPHIC VIEW OF THE MODEL AT BALCONES CENTER

longitudinal sections of the downstream channel. Although it was desirable to have a discharge of 7.5 cfs; however, the pumps and the piping arrangements limited the flow delivery to maximum of 5.0 cfs. Hence, the experiments were conducted within the available range of discharge.

Satisfactory performance was observed for the range of flow variables tested as shown in Table 1B. The hydraulic jump was formed within the basin as anticipated. Froude numbers F_t in excess of design values were provided to test the effective performance of the dissipator. As shown in Table 1B, F_t of 1.71 resulted in satisfactory performance.

Velocity measurements were obtained at 0.03 foot and at $0.4y_3$ from the channel bottom in the downstream channel to determine the transverse velocity distribution and the degree of velocity reduction within the basin. The relative velocity ratio V/V_m at each section is shown in Figure 6B. The velocity ratio V/V_m was fairly uniform in any transverse section for a given set of hydraulic conditions. A relatively high degree of velocity reduction was observed in all experiments. Analyses of velocity profiles showed that for sections farthest downstream the velocities were reduced to an approximate range of 25 to 65 percent of V_t . The general performance of the structure was satisfactory as a radial flow energy dissipator.

TABLE 1B

Design Data	Experimental Results			
Q = 7.5 cfs	Q = 4.8 cfs	Q = 4.8 cfs	Q = 4.0 cfs	Q = 4.0 cfs
$F_t = 1.0$	$F_t = 1.08$	$F_t = 1.71$	$F_t = 1.05$	$F_t = 1.57$
$y_t = 1.0'$	$y_t = 0.70'$	$y_t = 0.517'$	$y_t = 0.64'$	$y_t = 0.48'$
$x = 0.9'$	$x = 1.5'$	$x = 1.9'$	$x = 1.50'$	$x = 1.6'$
$y_1 = 0.2'$	$y_1 = 0.23'$	$y_1 = 0.22'$	$y_1 = 0.23'$	$y_1 = 0.19'$
$y_2 = 1.3'$	$y_2 = 0.89'$	$y_2 = 0.95'$	$y_2 = 0.83'$	$y_2 = 0.89'$
$y_3 = 0.45'$	$y_3 = 0.51'$	$y_3 = 0.53'$	$y_3 = 0.40'$	$y_3 = 0.40'$
$y_s = 0.6'$	$y_s = 0.56'$	$y_s = 0.61'$	$y_s = 0.49'$	$y_s = 0.57'$

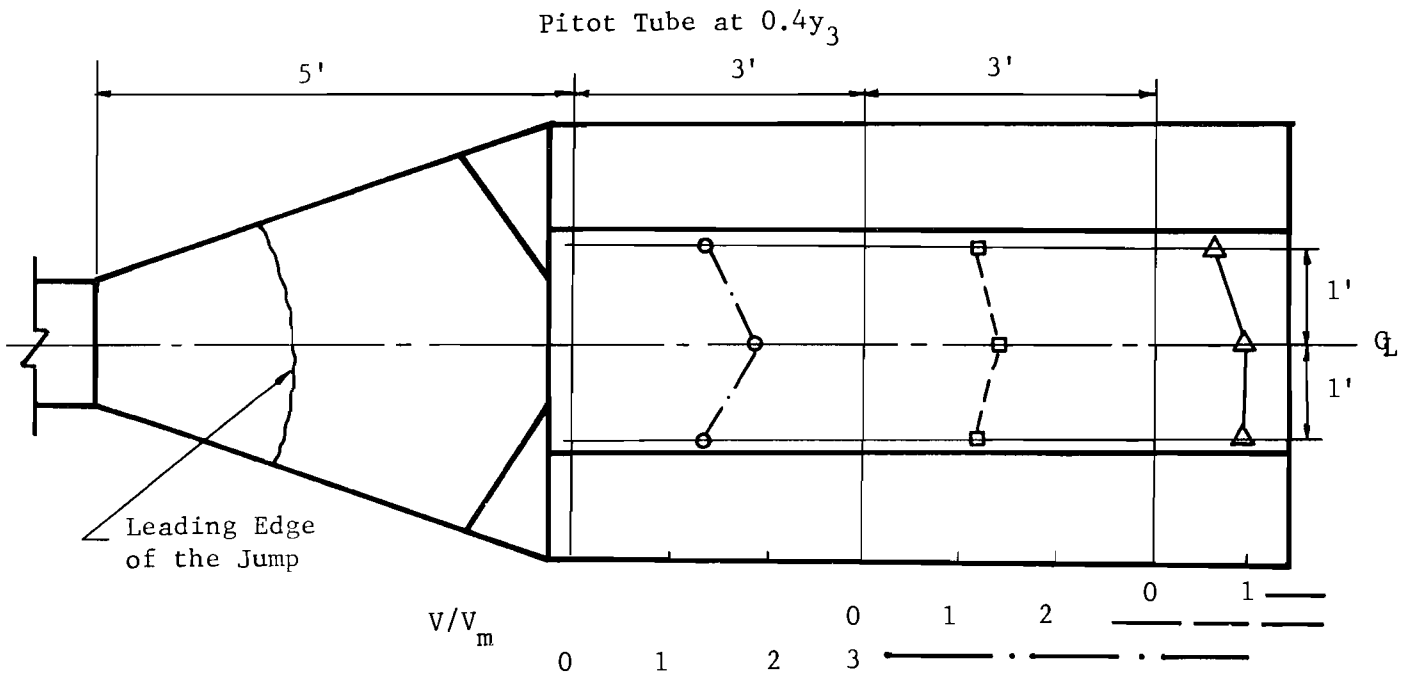
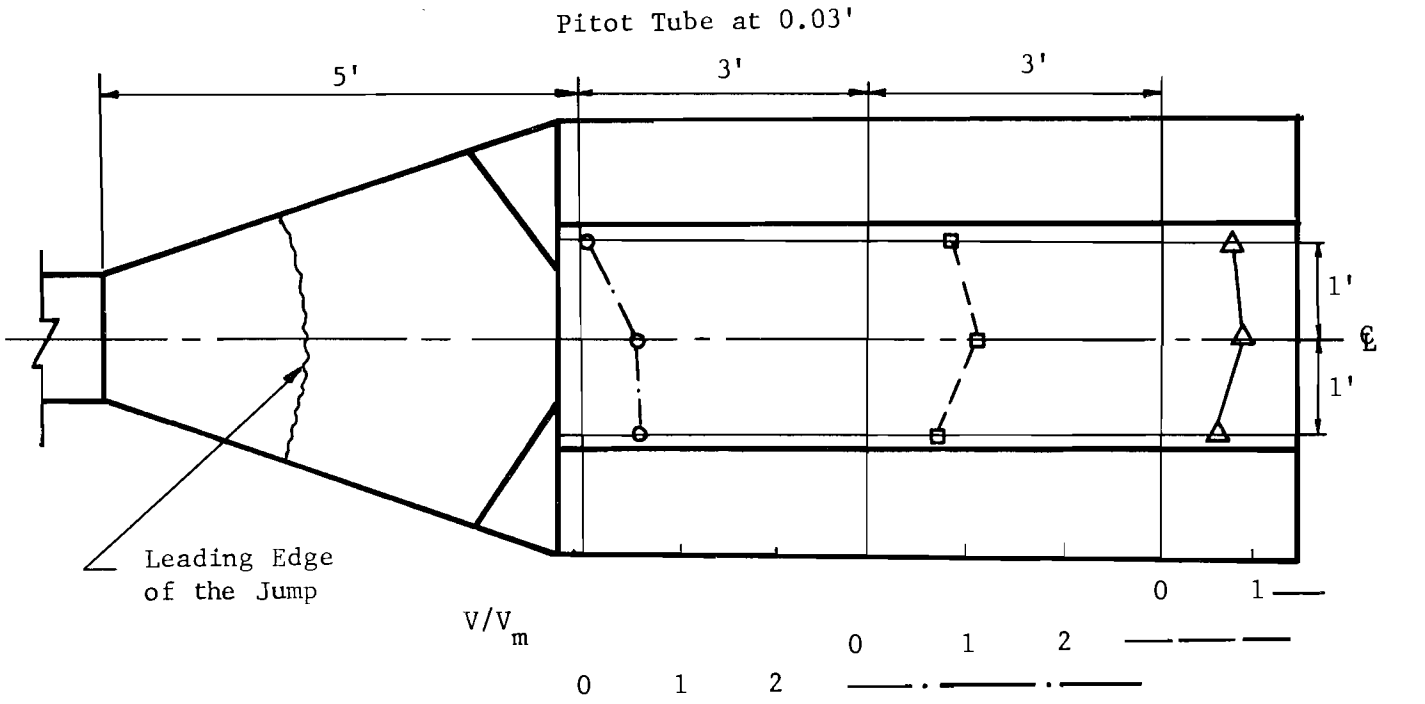


FIG. 6B RELATIVE VELOCITY PATTERN IN DOWNSTREAM CHANNEL